THE MICROWAVE SPECTRA OF TERTIARY BUTYL CHLORIDE AND TERTIARY BUTYL BROMIDE

ARTHUR G. EARLE

THE MICROWAVE SPECTRA OF TERTIARY BUTYL CHLORIDE AND TERTIARY BUTYL BROMIDE

By

© Arthur G. Earle, B.Sc.

A THESIS SUBMITTED IN PARTIAL FULFILLMENT
OF THE REQUIREMENTS FOR THE DEGREE OF
MASTER OF SCIENCE

Department of Physics
Memorial University of Newfoundland

December 1974

St. John's Newfoundland

ABSTRACT

The microwave spectra of tertiary butyl chloride and tertiary butyl bromide were observed in the 8 to 12.4 GHz region using a Stark effect spectrometer with a 100 KHz square wave modulation. The absorption cell was a ten-foot section of S-band wave guide with a flat Stark electrode in the center of the guide and parallel to the broad side.

All rotational transitions took place at the dry-ice temperature with the ground vibrational state being most dominant. From a partial resolution of the nuclear quadrupole hyperfine structure the rotational constant B_0 and quadrupole coupling constant eQq were calculated for the two dominant species of each molecule. The centrifugal distortion constants were shown to be very small and no attempt was made to evaluate them.

The rotational constants B_0 and quadrupole coupling constants eQq were obtained for the four species $(C^{12}H_3)_3C^{12}X$, where X was Cl^{35}, Cl^{37}, Br^{79}, and Br^{81}. The value eQq = -52.28 ± 1.25 MHz for the case where X was Cl^{37} is a new result. The remaining constants were found to be in good agreement with the values obtained previously by Lide and Jen[1], and Zeil, Winnewisser and Huttner[6]. The transitions in this work involved lower J numbers and frequencies than were used previously, that is, the J=1 → 2 and J=2 → 3 transitions.

ACKNOWLEDGEMENTS

The author wishes to thank the following individuals for their assistance in the preparation of this thesis from the research stage to its final form:

- My supervisor, Professor P.D.P. Smith for his assistance and guidance throughout;

- Mr. Ray Penney who worked as a summer assistant in the Microwave Spectroscopy Lab, and later as an instrument technician in the department Electronic Shop;

- Mr. Alex McCloy, senior instrument technician in the department Electronic Shop;

- Mr. Ralph Alexander, the department photographer;

- Mr. Russ Tucker, the department draftsman;

- Mr. Terry White and other staff members of the department Machine Shop;

- Mr. Paul Gillard, a fellow graduate student, who did the original computer programming for the section on ammonia. This was later expanded, particularly by Professor Smith, to the results as given in this thesis; and

- Special thanks to Miss Deanna Janes who typed this thesis.

This research was supported in part by a Provincial Government Fellowship which the author held for a period of twenty months.

TABLE OF CONTENTS

LIST OF TABLES

LIST OF FIGURES

*abbreviated title

*abbreviated title

CHAPTER 1

INTRODUCTION

Microwave spectroscopy is that branch of spectroscopy which employs electromagnetic radiation in the sub-millimeter to centimeter range - that is, wavelengths from about 0.3 mm to about 30 cm or frequencies of 1 gigahertz to 1000 gigahertz (a gigahertz is 10^9 cycles per second, and is commonly used in microwave spectroscopy). The absorption of such radiation by moderate-sized polar molecules at pressures of a few hundredths of a torr can be observed and accurately measured by equipment, largely electronic in nature. The outstanding features of microwave spectroscopy, from an experimental point of view, are the ease with which frequencies can be measured to an accuracy of better than one part in a million and the effectiveness with which adjacent absorption frequencies can be resolved, even though they may be separated by a mere fraction of a megahertz - that is to say, by less than 1/30,000 of a wavenumber. Furthermore, a very small amount of material, of the order of a microgram, is required.

In nearly all cases the absorption of the electromagnetic radiation produces a change of rotational energy in the free gas molecule. This rotation is quantized and governed by well-known quantum mechanical formulae. To a first and very good approximation, a rigid rotating body with three principal mechanical moments of inertia serves as an adequate molecular model for many of the observations.

A number of types of information about individual molecules can be obtained by means of microwave spectroscopy, including very accurate

molecular structures, dipole moments, nuclear quadrupole coupling constants, magnetic coupling constants, low-lying vibrational frequencies, conformations and energy differences of rotational isomers, to name a few.

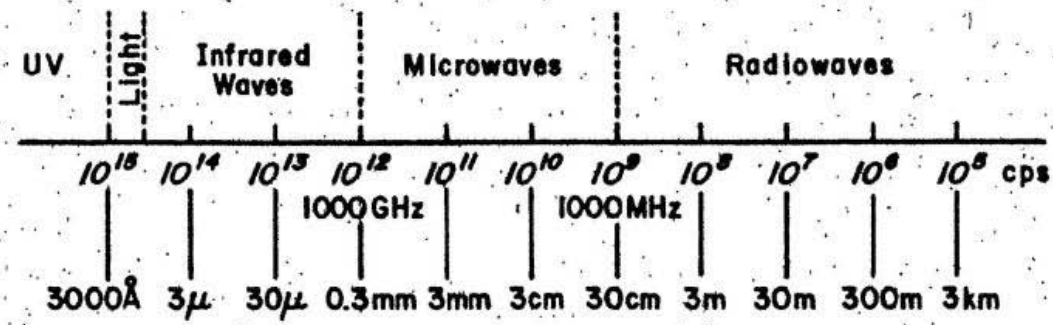

Fig. 1.1 Chart showing the extent of the microwave region of the electromagnetic spectrum (from Gordy and Cook, Chapter 1).

1.1 The Chemical Compounds Used in this Experiment

The spectra of tertiary butyl chloride (both $(C^{12}H_3)_3C^{12}Cl^{35}$ and $(C^{12}H_3)_3C^{12}Cl^{37}$) and tertiary butyl bromide (both $(C^{12}H_3)_3C^{12}Br^{79}$ and $(C^{12}H_3)_3C^{12}Br^{81}$) were observed in this experiment.

Tertiary butyl chloride (2-chloro-2-methylpropane) is an organic compound, liquid at room temperature, with a molecular weight of 92.57, a melting point of $-25.4^{\circ}C$, a boiling point of $52^{\circ}C$, and a density of $0.8420\ gm/cm^3$.

Tertiary butyl bromide (2-bromo-2-methylpropane) is an organic compound, liquid at room temperature, with a molecular weight of 137.03, a melting point of $-16.2^{\circ}C$, a boiling point of $73.25^{\circ}C$, and a density of $1.2209\ gm/cm^3$.

Both tertiary butyl chloride and tertiary butyl bromide belong to a class of molecules called symmetric tops, with the chlorine (or bromine) nucleus lying on the symmetry axis. The chlorine and bromine nuclei each have a nuclear spin of 3/2 and hence they act as quadrupole coupling nuclei. Thus the rotational spectrum is no longer simple but is split into many components of various intensities due to the nuclear quadrupole coupling effect. This theory is covered in Chapter 2.

1.2.a Previous Work on Tertiary Butyl Chloride

The most recent published work on tertiary butyl chloride was that of Lide and Jen[1]. From the unresolved J = 4 → 5 and the J = 5 → 6 rotational transitions it was found that the effective B value was 3017.69 ± 0.02 MHz for the $(C^{12}H_3)_3C^{12}Cl^{35}$ species and 2953.54 ± 0.02 MHz for the $(C^{12}H_3)_3C^{12}Cl^{37}$ species. A partial resolution of the hyperfine structure of the J = 2 → 3 transition of the Cl^{35} species was achieved, which led to B_o = 3017.72 ± 0.02 MHz and a quadrupole coupling constant, eQq, of -66.9 ± 1.5 MHz.

The spectrum of tertiary butyl chloride was first reported by Williams and Gordy[2], and structural parameters were calculated subject to several assumptions. Previous to the work of Lide and Jen[1], an investigation of the compound was carried out by Muller, Winnewisser, and Zeil[3], but the information available was insufficient for a reliable determination of structures.

In none of the previous work was the quadrupole hyperfine spectrum resolved, with the exception of the partial resolution achieved by Lide and Jen[1]. As well, the quadrupole coupling constant was measured for the Cl^{35} isotope only, and then only from a partially resolved transition.

A thorough search of the literature revealed no data on this molecule at frequencies below 18 GHz.

A more complete tabulation of microwave spectral constants up to 1967 may be found in Molecular Constants from Microwave Spectroscopy by Stark (Vol. 4, Group II, Landolt-Bornstein, Numerical Data and Functional Relationships in Science and Technology)[4], or Microwave Spectral Tables (National Bureau of Standards, Monograph 70, Vols. I-V)[5].

1.2.b Previous Work on Tertiary Butyl Bromide

The most recent published work on the microwave spectrum of tertiary butyl boomide was that of Zeil, Winnewisser, and Huttner[6]. From the J = 4 → 5 rotational transitions and the resolvable hyperfine spectrum, it was found for the $(C^{12}H_3)_3C^{12}Br^{79}$ species B = 2044.2 ± 0.05 MHz and eQq = 511.6 ± 5 MHz, and for the $(C^{12}H_3)_3C^{12}Br^{81}$ species B = 2028.3 ± 0.05 MHz and eQq = 427.4 ± 5 MHz.

A thorough search of the literature revealed no data on this molecule at frequencies below 20 GHz.

For complete tabulation on this molecule up to 1967 one may refer to the references[4,5].

1.3 The Present Study of the Microwave Spectrum of Tertiary Butyl Chloride and Tertiary Butyl Bromide

Both spectra were observed in the 8.0 to 12.4 GHz region using a Stark Effect Spectrometer with a 100 KHz square wave modulation. The sample vapor pressure was in the range 0.040 to 0.050 torr. All spectra were recorded at the dry-ice temperature.

Only four species were detected in natural abundance - $(C^{12}H_3)_3C^{12}Cl^{35}$, $(C^{12}H_3)_3C^{12}Cl^{37}$, $(C^{12}H_3)_3C^{12}Br^{79}$, and $(C^{12}H_3)_3C^{12}Br^{81}$. No attempt was made to identify the less abundant species*.

In all cases the quadrupole hyperfine structure was partially observed and analyzed, thus leading to accurate values for B_o and eQq. The parameters thus found were compared with those previously published, except for the $(C^{12}H_3)_3C^{12}Cl^{37}$ species for which no eQq was previously determined by microwave spectroscopy.

1.4 Method of Searching for Spectrum

Using the values of B_o and eQq previously published as a first approximation, a theoretical spectrum was generated. This spectrum was then used as a basis for the experimental work. Then, having found the required spectrum, new values of B_o and eQq were evaluated. The agreement between our values of the molecular parameters and those previously published was found to be good.

The $(C^{12}H_3)_3C^{12}Cl^{37}$ species had to be treated differently. In this case only B_o was known to a first approximation, as eQq had not been previously determined. Hence from a knowledge of the ratio of the nuclear moments of Cl^{35} and Cl^{37} a value of the eQq of Cl^{37} was estimated and used to generate a theoretical spectrum. This method proved acceptable.

---

*Throughout this thesis wherever the carbon atom is referred to as C, the C^{12} isotope is implied. No experimental work was performed on any compounds containing other carbon isotopes.

CHAPTER 2

MOLECULAR THEORY

In this chapter, only those aspects of the theory needed in the main body of this thesis are given, and hence discussion is generally limited to symmetric-top molecules. There is no attempt to reproduce derivations; in most cases only the appropriate formulae are given.

Most of the material in this chapter was condensed from the many standard microwave spectroscopy texts, particularly Gordy and Cook[7], but also including Gordy, Smith and Trambarulo[8], Townes and Schawlow[9], Wollrab[10], and Sugden and Kenney[11].

2.1 Symmetric-Top Molecules

A molecule in which two of the principal moments of inertia are equal is a symmetric top. In general this condition is met when the molecule has an axis of symmetry which is trigonal or greater[12,13]. A linear molecule is equivalent to the case of a symmetric top in which the angular momentum about the symmetry axis is zero.

2.1.a The Rigid Rotor Approximation

Let the three principal moments of inertia be I_a, I_b, and I_c. The principal moments of inertia which have their axes perpendicular to the symmetry axis are equal. The molecule is a prolate symmetric top if 'a', the axis of least moment of inertia ($I_a < I_b = I_c$), lies along the symmetry axis. The molecule is an oblate symmetric top if 'c', the axis of greatest moment of inertia ($I_a = I_b < I_c$), lies along the symmetry axis.

Most of the symmetric-top molecules observed in the microwave region are prolate.

If the 'a' axis is chosen along the symmetry axis ($I_c = I_b$) and with $P^2 = P_a^2 + P_b^2 + P_c^2$, where P is the total angular momentum, the Hamiltonian operator of the rotational energy may be expressed as

$$H_r = \frac{P^2}{2I_b} + \frac{1}{2}\left(\frac{1}{I_a} - \frac{1}{I_b}\right)P_a^2 \qquad (2.1)$$

The eigenvalues of the Hamiltonian of Eq. 2.1 are the quantized rotational energies of the rigid prolate symmetric top, i.e.,

$$E_{J,K} = h[BJ(J+1) - (A-B)K^2] \qquad (2.2)$$

where

$$A = h/8\pi^2 I_a$$

$$B = h/8\pi^2 I_b$$

$$J = 0, 1, 2, 3, \ldots$$

$$K = 0, \pm 1, \pm 2, \pm 3, \ldots, \pm J$$

The magnetic quantum number M takes the values $0, \pm 1, \pm 2, \ldots, \pm J$ but in the field-free rotor the rotational energies do not depend on M.

The selection rules for the field-free rotor are

$$\Delta J = 0, \pm 1 \qquad \Delta K = 0$$

which leads to the rule corresponding to absorption of radiation

$$J \rightarrow J+1 \qquad K \rightarrow K .$$

Applying these rules to Eq. 2.2 gives the formula for the absorption frequencies for the rigid symmetric top

$$\nu = 2B(J+1) \qquad (2.3)$$

which is the same as that of the linear molecule.

2.1.b The Non-rigid Rotor

Centrifugal stretching is treated as a perturbation of H_r. After performing the appropriate quantum mechanical calculations, one arrives at the energy perturbation due to centrifugal distortion (to a first-order approximation) as

$$E_d^{(1)} = -h[D_J J^2(J+1)^2 + D_{JK} J(J+1)^2 K^2 + D_K K^4] \qquad (2.4)$$

in which D_J, D_{JK}, and D_K are the usual first-order centrifugal stretching constants of the symmetric-top molecule expressed in frequency units.

Addition of Eq. 2.2 and Eq. 2.4 gives the expression for the rotational energy of the non-rigid prolate symmetric-top molecules as

$$E_{JK} = h[BJ(J+1) - (A-B)K^2 - D_J J^2(J+1)^2 - D_{JK}(J+1)K^2 - D_K K^4] \qquad (2.5)$$

For the oblate symmetric top, (A-B) in Eq. 2.5 becomes (C-B). Applying the absorption selection rules $J \rightarrow J+1$ and $K \rightarrow K$ one gets the rotational frequencies

$$\nu = 2B(J+1) - 4D_J(J+1)^3 - 2D_{JK}(J+1)K^2 \qquad (2.6)$$

2.1.c Line Intensities

From Gordy and Cook[7], p. 155, one has a formula for the absorption coefficient α_{max} at the center of the resonance corresponding to the frequency $\nu = \nu_o$, for which the maximum absorption occurs. In the special case where $J\nu_o << T$ and $(A-B)K^2 << T$, as is true for relatively low J transitions

$$\alpha_{max} = X\nu_0^3 \left[1 - \frac{K^2}{(J+1)^3}\right] \qquad (2.7)$$

where

$$X = \frac{6.11 \times 10^{-4} \; F_v i_c \mu^2 \sigma g_I g_K \sqrt{A^{\frac{1}{2}}}}{(\Delta\nu)_1 \; T^{5/2}}$$

and F_v = fraction of molecules in the particular state observed

i_c = fractional concentration of the isotopic species observed

T = temperature of observation in absolute scale

μ = molecular dipole moment in Debye units

$(\Delta\nu)_1$ = line breadth in MHz for a pressure of 1 mm of Hg when $T = 300^oK$

A,B = spectral constants in GHz units

g_K = 1 for K=0; = 2 for K > 0

ν_o = resonance frequency in GHz units

σ = symmetry number

g_I = reduced nuclear statistical weight factor.

2.1.d Optimum Region for Detection of Rotational Spectra

By equating the derivative of α_{max} with respect to J to zero and by solving for J_{opt} one can predict the spectral region where the rotational absorption lines of symmetric-top molecules are strongest. The

calculation is further simplified by setting K=0, since one is only interested in the general spectral region, and thus the problem is reduced to that of a linear molecule. From Gordy and Cook[7] one has

$$J_{opt} \approx 5.5(T/B)^{\frac{1}{2}} \tag{2.8}$$

$$\nu_{opt} \text{ (in GHz)} \simeq 2B + 11(BT)^{\frac{1}{2}} \tag{2.9}$$

where B is in GHz and T is in ^{o}K. The optimum wavelength in millimeters is

$$\lambda_{opt} \text{ (in mm)} \simeq \frac{300}{2B + 11(BT)^{\frac{1}{2}}} \tag{2.10}$$

2.2 Symmetric-Top Molecules with Nuclear Hyperfine Structure

Nuclei possess a spin angular momentum $\vec{I}$ which is represented by an integral or half-integral quantum number I whose value is dependent on the composition and structure of the nucleus. Under proper conditions the nuclear spin angular momentum can couple with the rotational angular momentum to produce a hyperfine structure in the rotational spectrum. This coupling may be magnetic, or electric, or both. The most important is electric, that is, the electric interaction of the molecular fields with the nuclear moments.

For a quadrupole interaction it is necessary that the nucleus possesses a nonvanishing quadrupole moment which results from a nonspherical charge distribution in the nucleus. Such a charge distribution is found in nuclei with a spin angular momentum greater than $\frac{1}{2}\hbar$. The interaction between the nuclear quadrupole moment Q and the electric field gradient of the molecule at the quadrupole nucleus provides a mechanism through which $\vec{I}$ and $\vec{J}$ can couple. Q can be either positive or negative, depending on charge distribution.

Molecules in the ground state have singlet Σ electronic states. All their electrons are paired so that to a first-order approximation their electronic magnetism, whether from electron spin or orbital motion, is cancelled. When the molecules are not rotating, the molecular magnetism is cancelled even in higher orders of approximation. However, the end-over-end rotation of the molecule generates weak magnetic fields which can interact with the nuclear magnetic moments to produce a slight magnetic splitting or displacement of the lines. This magnetic displacement is usually one or two orders of magnitude less than the splitting caused by the quadrupole coupling. Hence we shall concern ourselves with the nuclear quadrupole coupling hyperfine structure only.

2.2.a Quadrupole Interactions by a Single Coupling Nucleus

For an external-field-free molecule the nuclear spin $\vec{I}$ is coupled to the molecular rotational angular momentum $\vec{J}$ to form a resultant $\vec{F}$. In the first-order treatment, $\vec{J}^2$ is still a constant of the motion. The good quantum numbers are now F, M_F, J, and I.

$$\begin{aligned} F &= J+I,\ J+I-1,\ J+I-2,\ \ldots,\ |J-I| \\ M_F &= F,\ F-1,\ F-2,\ \ldots,\ -F \\ J &= 0,\ 1,\ 2,\ 3,\ \ldots \end{aligned} \qquad (2.11)$$

From quantum mechanical considerations we arrive at a first-order approximation for the energy due to nuclear quadrupole coupling in a rotating molecule

$$E_Q^{(1)} = \frac{eQq_J}{2J(2J-1)I(2I-1)} [3/4\ C(C+1) - J(J+1)I(I+1)] \qquad (2.12)$$

where

$$C = F(F+1) - J(J+1) - I(I+1) \qquad (2.13)$$

e is the electronic charge

Q is the nuclear quadrupole moment

and q_J is the average of the field gradient (the second-order partial derivative of the potential at the nucleus in question) in a space-fixed axis.

Q is a measure of the deviation of the nuclear shape from spherical symmetry. A positive Q indicates that the nucleus is elongated along the spin axis, and is prolate; a negative Q indicates that the nucleus is flattened along the spin axis, and is oblate. For a spherical nucleus, Q vanishes.

2.2.b Nuclear Quadrupole Coupling in Symmetric-Top Molecules

The most common case arises from a single coupling nucleus on the symmetry axis. The appropriate formulae follow:

$$q_J = q \frac{J}{2J+3} \left[\frac{3K^2}{J(J+1)} - 1 \right] \qquad (2,14)$$

where q_J is the field gradient along the symmetry axis. The resulting first-order quadrupole energy of the symmetric top is, from Eq. 2.12,

$$E_Q^{(1)} = eQq \left[\frac{3K^2}{J(J+1)} - 1 \right] Y(J,I,F) \qquad (2.15)$$

where

$$Y(J,I,F) = \frac{3/4\ C(C+1) - I(I+1)(J(J+1)}{2(2J-1)(2J+3)I(2I-1)} \qquad (2.16)$$

and eQq is generally referred to as the nuclear quadrupole coupling constant.

Selection rules for hyperfine transitions in rotation absorption are

$$J \to J+1 \qquad F \to F \qquad F \to F\pm 1 \qquad I \to I \ .$$

Hence the rotational frequencies perturbed by quadrupole coupling are

$$\nu = \nu_0 + eQq \left[\frac{3K^2}{J(J+1)} - 1\right][Y(J+1,I,F') - Y(J,I,F)] \qquad (2.17)$$

where $F' = F, F\pm 1$. ν_0 is the "unperturbed" rotational frequency which would be observed if there were no quadrupole coupling.

Appendix B contains numerical tabulations of $Y(J,I,F)$ for various values of J, I, and F as well as the relative intensities of the individual hyperfine components.

2.2.c Second-Order Effects in Nuclear Quadrupole Interactions

The first-order treatment outlined above accounts very satisfactorily for the quadrupole hyperfine structure when the spacings of the rotational energy levels are large compared with the quadrupole splitting. In this experiment it was found necessary to apply second-order corrections. For the symmetric-top molecule the expression for the second-order quadrupole energy is rather complicated and will not be reproduced here.

Appendix C contains a tabulation of the second-order quadrupole energies for the linear and symmetric-top molecule for various values of J, I, and F. Further information may be found in references 7 to 11.

2.2.d Relative Intensities of Hyperfine Components

The relative intensities of the components of a hyperfine multiplet of a particular rotational transition are given by the following

formulae abstracted from Gordy and Cook[7]:

For J-1 → J

F-1 → F

$$\frac{B(J+F+I+1)(J+F+I)(J+F-I)J+F-I-1)}{F} \qquad (2.18)$$

F → F

$$\frac{B(J+F+I+1)(J+F-I)(J-F+I)(J-F-I-1)(2F+1)}{F(F+1)} \qquad (2.19)$$

F+1 → F

$$\frac{B(J-F+I)(J-F+I-1)(J-F-I-1)(J-F-I-2)}{F+1} \qquad (2.20)$$

where B is a constant which depends on the strength of the unsplit line. Appendix B contains a tabulation of these relative intensities.

2.3 Symmetric-Top Molecules and Applied Electric Fields

One of the basic requirements for the existence of a pure rotational transition in a molecular spectrum is the presence of a permanent or induced dipole moment. This permanent dipole moment may be represented by a vector $\vec{\mu}$ whose magnitude is measured by the distribution of charge in the molecule and the distance between the centers of charge. This may be expressed as

$$\vec{\mu} = \sum_i e_i \vec{r}_i$$

where e_i is the charge of the ith particle and $\vec{r}$ is the vector distance of that ith particle from the origin of a coordinate system fixed in the molecule. The summation is over all the nuclei and electrons in the molecule.

Existence of a dipole moment causes an interaction between a rotating molecule and a static electric field. The rotational energy levels of the molecule are perturbed by the external field through this interaction, which is called the Stark Effect. From the Stark effect the most accurate evaluation of electric dipole moments of gaseous molecules can be made. It is also useful in the identification of pure rotational transitions and is widely used as an aid in the detection of spectral lines.

2.3.a Symmetric-Top Molecules without Nuclear Quadrupole Coupling

In microwave spectroscopy the Stark energies can be evaluated with significant accuracy from perturbation theory. Linear and symmetric-top molecules have a dipole moment only along the symmetry axis. The first-order Stark energy is simply the average of the Hamiltonian due to the electric field $\vec{\varepsilon}$ over the unperturbed rotational state. For the symmetric-top molecule one has

$$E_S^{(1)} = -\frac{\mu\varepsilon K M_J}{J(J+1)} \qquad (2.22)$$

where $M_J = -J, -J+1, -J+2, \ldots, J$.

For a rotational transition $J \rightarrow J+1$ with the microwave electric vector parallel to the Stark field ε as is the usual experimental case, the selection rules are $K \rightarrow K$ and $M_J \rightarrow M_J$. These conditions yield the frequency displacement from the unperturbed rotational line frequency as

$$\Delta\nu^{(1)} = 2\left(\frac{\mu\varepsilon}{h}\right)\frac{K M_J}{J(J+1)(J+2)} \qquad (2.23)$$

The first-order Stark Effect was derived on the assumption that the dipole moment $\vec{\mu}$ is independent of the electric field $\vec{\varepsilon}$. Actually, the

electric field perturbs the rotational motion, giving rise to an additional component of dipole moment proportional to the electric field. Thus one may compute the second-order Stark energy and arrive at the expression below for the symmetric-top molecule

$$E_S^{(2)} = \frac{\mu^2\varepsilon^2}{2hB}\left\{\frac{(J^2-K^2)(J^2-M_J^2)}{J^3(2J-1)(2J+1)} - \frac{[(J+1)^2-K^2][(J+1)^2-M_J^2]}{(J+1)^3(2J+1)(2J+3)}\right\} \qquad (2.24)$$

2.3.b Symmetric-Top Molecules with Nuclear Quadrupole Coupling

The theory involved in treating the effects of applied electric fields on symmetric-top molecules with nuclear quadrupole interactions is complex and only a brief outline will be given here.

In finding the characteristic energies, it is convenient to consider three cases separately: the weak-field case, the intermediate-field case, and the strong-field case. The weak- and strong-field cases are considerably simpler than the intermediate-field case, and the greatest number of measurements involving the Stark effect have been made involving those simpler cases. Perturbation theory allows the derivation of closed formulae for the weak- and strong-field cases; for the intermediate-field case a secular equation must be solved.

The weak-field case: $\mu\varepsilon \ll eQq$

The Stark interaction can be treated as a perturbation on the hyperfine state. The first-order Stark energy of a symmetric-top molecule is

$$E_S^{(1)} = -\frac{\mu\varepsilon KM_F[F(F+1)+J(J+1) - I(I+1)]}{2J(J+1)F(F+1)} \qquad (2.25)$$

The second-order Stark energy of a symmetric-top molecule is normally only needed when the first-order vanishes. Thus for K = 0

$$E_S^{(2)}\ (K=0) = -\frac{\mu^2\varepsilon^2[3M_F^2 - F(F+1)][3D(D-1) - 4F(F+1)J(J+1)]}{2hBJ(J+1)(2J-1)(2J+3)2F(F+1)(2F-1)(2F+3)} \qquad (2.26)$$

where

$$D = F(F+1) - I(I+1) + J(J+1) \ . \qquad (2.27)$$

The strong-field case: $\mu\varepsilon >> eQq$

In the strong-field case the applied electric field is sufficiently strong to break down the nuclear coupling between I and J but not large enough to perturb significantly the rotational state. For the symmetric-top molecule in the strong-field case the Stark energies are

$$E_Q = \frac{eQq}{4(2J-1)(2J+3)I(2I-1)}\left[\frac{3K^2}{J(J+1)} - 1\right]$$

$$\times\ [3M_J^2 - J(J+1)][3M_I^2 - I(I+1)] \qquad (2.28)$$

where

$$M_J = -J, -J+1, -J+2, \ldots, +J$$

and

$$M_I = -I, -I+1, -I+2, \ldots, +I \ .$$

The intermediate-field case:

The theory concerning the intermediate-field case is complex but essentially involves a combination of the weak- and strong-field cases. Each individual problem must be solved separately and computers are necessary to perform the calculations. It suffices to say that M_J and M_I cease to be good quantum numbers and that the selection rules for M are

$\Delta M = 0, \pm 1$. The formulae will not be reproduced here, but further information may be found in references 7 to 11.

2.3.c Relative Intensities of the Stark Components

The actual intensities are proportional to the square of the dipole moment matrix elements. For no near degeneracies, the intensities are very weak functions of the field, and the appropriate relative intensities are:

Without hyperfine structure:

$$\text{Intensity } (\Delta J=0) \propto M^2 \tag{2.29}$$

$$\text{Intensity } (|\Delta J|=1) \propto (J'^2 - M^2) \tag{2.30}$$

where J' represents the larger of the two J values.

With hyperfine structure:

The intensities can be determined by a consideration of the weak- and strong-field limiting cases. Only the selection rule $\Delta M=0$ is considered. In the limiting weak-field case the relative intensities are

$$\text{Intensity } (\Delta F=0) \propto M_F^2 \tag{2.31}$$

$$\text{Intensity } (|\Delta F|=1) \propto (F'^2 - M_F^2) \tag{2.32}$$

where F' is the larger of the two F values. In the strong-field limit Eqs. 2.28 and 2.29 hold since J and M_J are the good quantum numbers. Relative intensities in the intermediate case where the Stark and quadrupole perturbations are similar in magnitude are more difficult to obtain. It is possible to find an approximate solution by interpolating between the weak- and strong-field intensities.

CHAPTER 3

EXPERIMENTAL APPARATUS AND TECHNIQUE

The essential features of any microwave spectrometer are a source of monochromatic radiation with the proper frequency range, a sample cell, a detection system, and a method for spectral presentation. These features are similar for any absorption spectrometer, e.g. infrared or optical, except that monochromatic radiation is not always used.

Microwave oscillators are essentially monochromatic, unlike the conventional thermal sources for the infrared which produce a continuous output spectrum governed by the black body distribution curve, and hence require a dispersive prism or grating. At normal temperatures for a thermal source ($\sim 1500^{\circ}K$) the radiation peaks in the vicinity of 3.5 microns and decreases rapidly with increasing wavelength. Hence, at microwave frequencies the intensity is so low that electronic sources must be used.

The electromagnetic radiation produced by the microwave oscillator is transmitted through a conducting metal tube called a wave guide to the sample cell and the detector. The cut-off frequencies and modes of the wave guide are governed by boundary conditions specified at the wave guide walls. The sample cell must also act as a wave guide, while at the same time performing other special functions such as the application of external electric or magnetic fields to the sample and amplitude modulation of the microwave signal.

Detection is normally by crystal detector, and amplification is generally achieved by either a wide-band or narrow-band system using

varying degrees of frequency or amplitude modulation. The absorption lines are displayed on an oscilloscope or chart recorder along with a set of frequency markers produced by mixing a sample of the microwave radiation with a known reference frequency.

Part A: Experimental Apparatus

3.1 The Stark-Modulation Microwave Spectrograph - An Introduction

To provide greater sensitivity and to aid in the identification of spectral lines, a system making use of the Stark effect was used in this experiment. It is usually referred to as the Stark-modulation method and the technique is widely used in microwave spectroscopy.

Briefly, the Stark-modulation scheme makes use of the change in the absorption frequency of a molecule when the molecular energy levels are perturbed by an external electric field, i.e. the so-called Stark effect. The basic principle used is the modulation of the absorption of the gas at a low radiofrequency (100 KHz) by the application of a square wave voltage to an electrode in the wave guide, thus creating a time-dependent alternating Stark effect.

Referring to Fig. 3.1, microwave energy from the source is passed through the gas to be studied which is confined in a wave guide cell by transparent mica (or Mylar) windows at each end. If the source is tuned to an absorption frequency there is a diminished amount of power received at the crystal detector. The absorption frequency of the gas is being alternately switched between two frequencies corresponding to the peaks and troughs of a 100 KHz square wave electric field based on zero voltage. Hence the signal reaching the crystal detector is amplitude-modulated at a

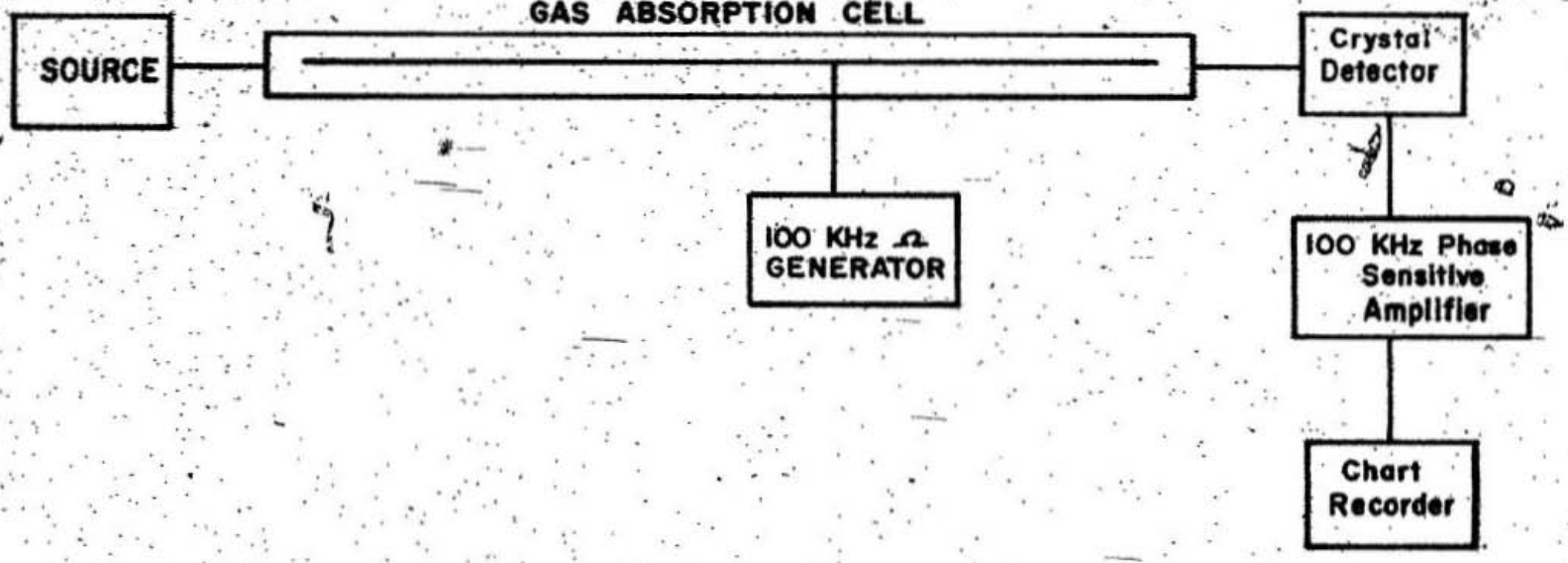

Fig. 3.1. Simplified block diagram of a Stark-modulated spectrograph.

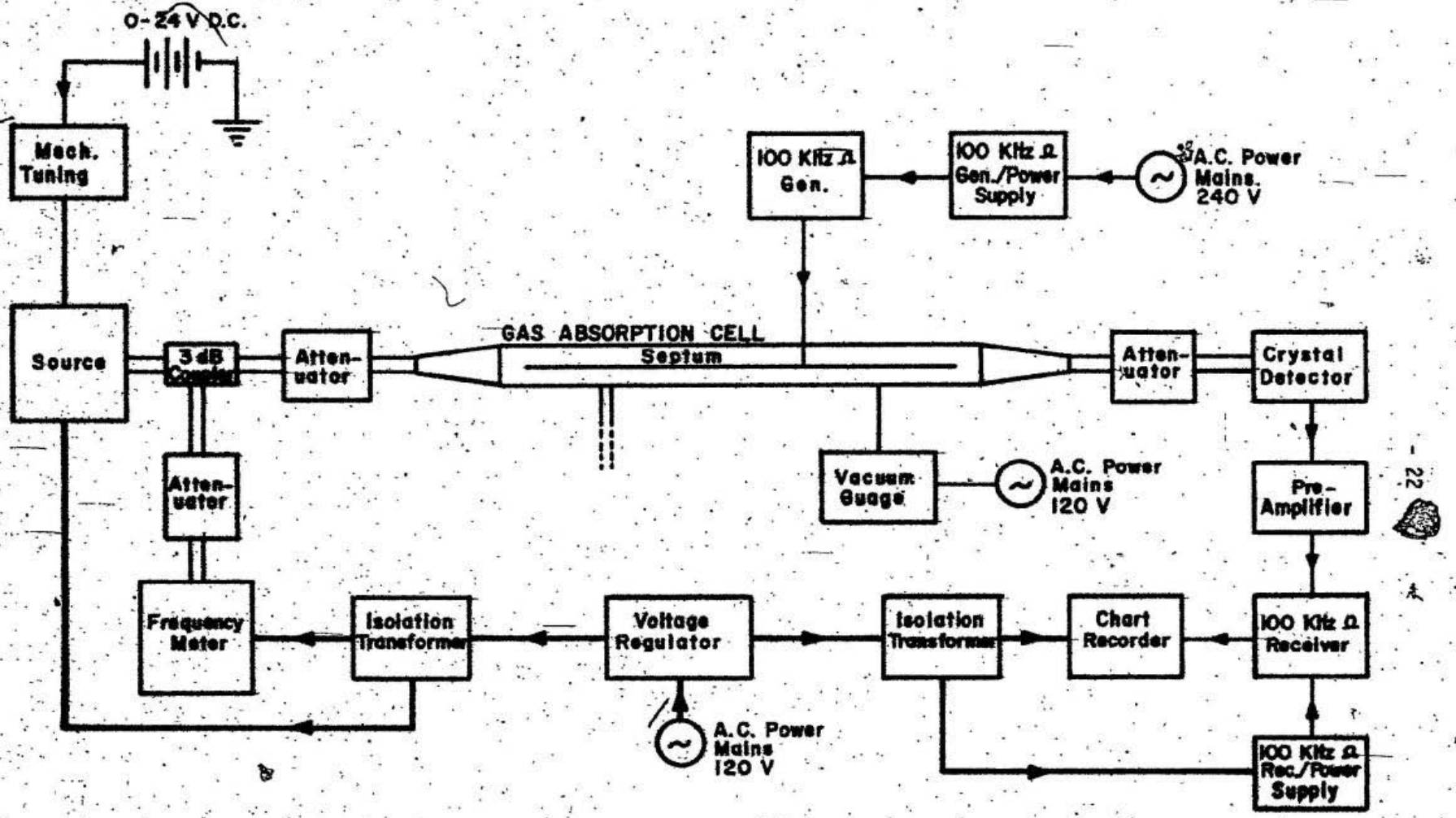

Fig. 3.2. Complete block diagram of the Stark-modulated microwave spectrometer electronic gear.

100 KHz rate and may be amplified and presented on an oscilloscope or chart recorder. Fig. 3.2 shows a complete block diagram of the system used. The components will be discussed later.

The spectrum observed using the Stark-Modulation Spectrograph is considerably more complicated than that given by the simpler spectrograph, but on the other hand, correspondingly more information is displayed.

The optimum Stark-modulation frequency is somewhere in the neighbourhood of 100 KHz. This is seen after considering the following factors: (1) by detecting and amplifying at a frequency of 100 KHz, one avoids the lower frequency region where there is a high crystal and source noise; (2) at higher frequencies the capacitive reactance of the wave guide cell becomes so low that it is difficult to obtain a good amplitude square wave modulation voltage; (3) if one uses modulation frequencies higher than about 100 KHz, the true absorption line shape becomes distorted.

The main advantages of this system over straight detection and amplification at audiofrequencies without any Stark-modulation are: (1) greater sensitivity and hence more successful in detecting weak absorption lines; (2) there are readily available commercial receivers and amplifiers in the 100 KHz region; (3) spurious responses caused by standing waves and other frequency sensitive devices in the wave guide system are eliminated; (4) a 100 KHz response is obtained only when one tunes the source through an absorption line; and (5) the Stark pattern of the absorption lines is present and is often useful in identifying the transition and for measuring the dipole moments.

3.2 Description and Discussion of Components

Sources: The microwave radiation sources were two Watkins-Johnson Backward-Wave Oscillators, Models WJ-2020-2 and WJ-2019-1, called X and J bands, respectively. The X band has an absolute frequency range of 8.0 to 12.4 GHz and the J band has an absolute frequency range of 4.0 to 8.0 GHz. Power output from both these oscillators is in the range 50 to 100 milliwatts.

The appropriate Backward-Wave Oscillator tube was mounted in the Hewlett-Packard Sweep Oscillator, Model 8690A. The capabilities of the 8690A are too numerous to mention and we only availed of a few of its features. The BWO tube, when mounted in the HP Sweep Oscillator, is tuned by a continuously variable ramp voltage which is swept by a single turn 500 K-ohm potentiometer. The maximum sweeping time provided is 100 seconds and the frequency region being swept can vary from the full range of the BWO tube (about 4 GHz) to about 5 MHz. Hence the slowest sweeping rate available on the unmodified Sweep Oscillator would be about 3 MHz per minute. This was found to be unsuitable for this experiment for a variety of reasons to be discussed later. As a result a slight modification in the sweeping circuit was made. The 500 K-ohm potentiometer was removed and replaced by a resistance consisting of a 220 K-ohm resistor followed by a 50 K-ohm ten-turn potentiometer and then another 220 K-ohm resistor, all in series. The 50 K-ohm ten-turn potentiometer was then connected to the shaft of a 4 to 24 Volt D.C. synchronous motor. By varying the driving voltage of the motor it was possible to obtain a wide variety of slow sweep rates. Precautions were taken to shield this motor drive device from the other electronic equipment.

Frequency measurement: The microwave energy output of the BWO, via the HP 8690A, was fed through a 3 db coupler with one portion of the electromagnetic energy going to the absorption cell and the other portion going to the frequency measuring device, via a variable attenuator. The frequencies were measured on a Hewlett-Packard Electronic Counter, Model 5245L equipped with the Hewlett-Packard Frequency Converter 3 to 12.4 GHz, Model 5255A. The unit was calibrated in the laboratory using the rotational absorption lines of carbonyl sulfide.

The absorption cell: Referring to Fig. 3.3, the absorption cell was made of a ten-foot piece of S-band wave guide, interior dimensions 2.840 inches by 1.340 inches. The ends of the cell were vacuum sealed with mica or Mylar windows utilizing the appropriate O rings and vacuum grease. The ends also had flanges, on to which tapered sections of wave guide could be attached to facilitate the further attachment of the appropriate X- and J-band equipment. The interior dimensions of the X- and J-band wave guide are 0.900 inches by 0.400 inches and 1.372 inches by 0.622 inches, respectively. The cut-off frequencies for the cominant TE_{10} mode for the S, J, and X wave guides are 2.078 GHz, 4.301 GHz, and 6.557 GHz, respectively.

The microwave radiation passes through a series of wave guide sections and then into the absorption cell which holds a small amount of sample vapor. The radiation is linearly polarized and used in the dominant TE_{10} mode for the rectangular wave guide.

The TE_{10} mode is the mode for which the lowest frequency of propagation is possible. This TE or transverse electric wave is

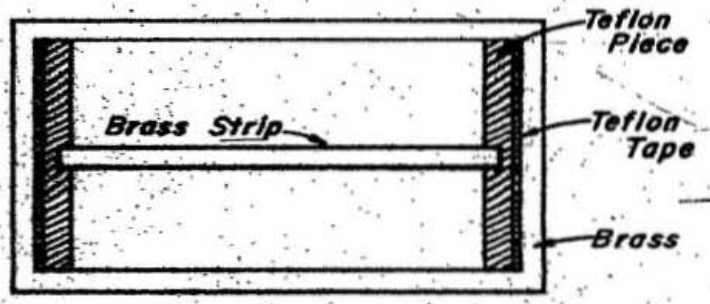

(a) Wave guide cross section.

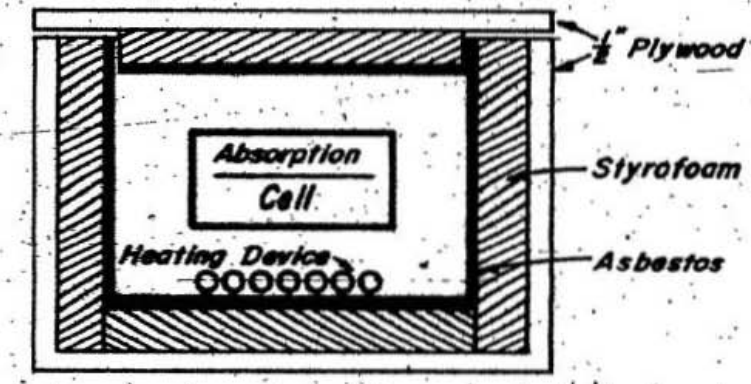

(b) Absorption cell enclosure.

(c) Transformer sections, etc.

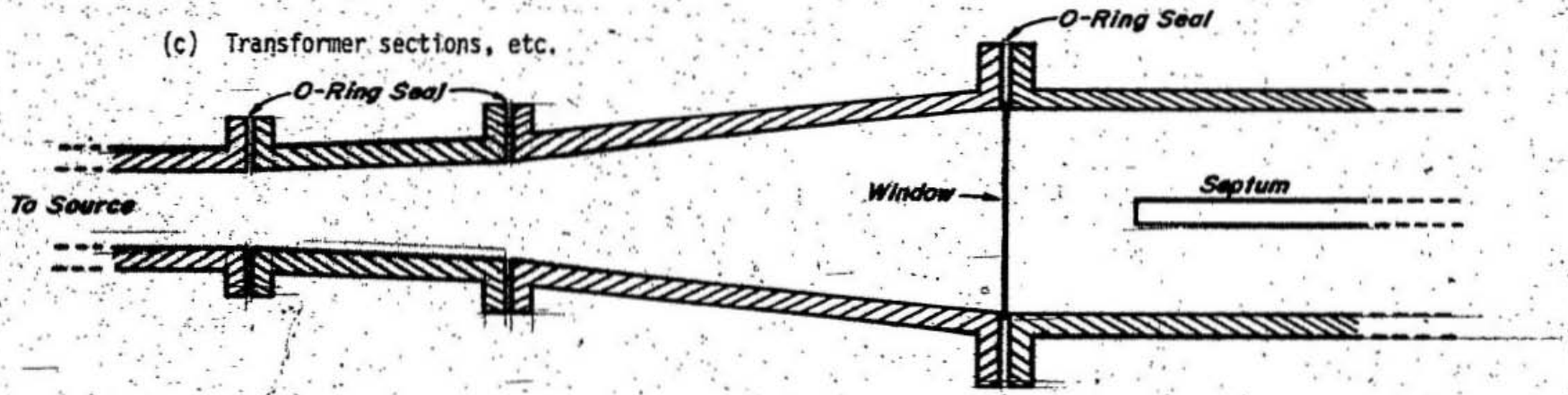

Fig. 3.3. Some details of the absorption cell.

characterized by a transverse electric field component with no axial electric field. The electric field vector is normally oriented parallel to the short side of the wave guide. However, since electromagnetic theory requires that the field strength approach zero at the guide walls, if they are considered perfect conductors, the maximum field strength is placed at the center of the wave guide. The magnetic field forms closed loops whose planes are parallel to the wide side of the wave guide.

The cell is directly connected to a vacuum system and is sealed from the atmosphere by transmitting windows. The windows in our particular cell were originally made from thin sheets of mica, but after some consideration and testing it was decided to replace the mica with Mylar of about 0.5 mil thickness. It was found that Mylar caused little if any reflections and had no significant absorption band in our region of interest. In addition it was considerably tougher and more flexible than mica for this experiment.

A thin (about 1/8 inch thick) brass septum, insulated from the wave guide and parallel to the wider edge, ran almost the entire length of the cell. Insulation was provided by machined strips of Teflon extending the length of the wave guide. A slot of appropriate thickness was machined into the insulator to rigidly hold the septum at the center of the cell. The septum and insulator strips were tapered near the ends of the cell to reduce unwanted reflections.

The function of the septum is to introduce modulation onto the microwave energy passing through the cell. When the vapor is exposed to an electric field, a splitting of the energy levels (Stark effect) occurs. The Stark effect leads to the measurement of dipole moments and serves as

a means of identifying rotational transitions. About two-thirds along the length of the septum an insulated lead was taken from the side of the septum and through the shorter wave guide wall and thence to the 100 KHz square wave generator.

The wave guide absorption cell was enclosed by a wooden box (made of one-half inch plywood and insulated with one-inch styro-foam) to house dry ice refrigerant. The box terminated about 6 inches from the cell windows. This arrangement allowed one to chill the sample to near a dry ice temperature by one daily filling of crushed dry ice. Asbestos, about one-sixteenth of an inch thick, was fastened (by glue and staples) to the styro-foam. A heating wire enclosed in glass tubing ran several lengths along the bottom of the box. This allowed one to raise the temperature of the sample gas to 100 C.

The entire absorption cell was connected to a vacuum system by an outlet through the broad side of the wave guide about one-third along its length.

Signal modulation: The signal was amplitude modulated by a zero-biased 100 KHz square wave generator purchased from Industrial Components Incorporated. The voltage was continuously variable up to 2000 volts.

Zero-biased square wave modulation is convenient for the study of rotational spectra because this technique allows the absorption line as well as its Stark components (M-degeneracy) to be observed simultaneously. When the electric field is absent, the unperturbed absorption line is detected; when the electric field is present, Stark components of the transition are observed. The two sets of lines can be presented with

opposite phases, allowing the Stark components to be easily distinguished from the zero-field lines. Introduction of modulation increases the sensitivity of the spectrometer with respect to video operation by allowing relatively narrow-band amplification and phase-sensitive detection.

Detection: The output signal from the sample cell was detected by a Hewlett-Packard Crystal Detector Model #X424A (negative biased). The detector element was supplied with the unit. The output of the crystal detector was fed into a preamplifier (purchased from Industrial Components Incorporated) and thence to the 100 KHz square wave receiver (also purchased from Industrial Components Incorporated).

A microammeter connected to the crystal terminals was used to give a measure of the average current through the crystal and also served as a means of monitoring the power passing through the absorption cell. The signal strength depends roughly on the first power of this current. From the pre-amplifier the signal was fed to a 100 KHz amplifier equipped with phase-sensitive detection or more specifically the above mentioned 100 KHz Receiver. This receiver had a number of bandwidth selections ranging from 1 'cycle' to 100 'cycles'. An additional two bandwidths were added, 0.1 'cycle' and 0.025 'cycle', by suitably modifying the internal circuitry of the receiver.

Display: The output signal from the 100 KHz receiver was displayed on a Hewlett-Packard Model 7100B Strip Chart Recorder. Frequency markings were periodically and randomly made on the same tracing by comparison with the frequency meter reading. The paper speed was normally 0.2 inches per

minute while the voltage scale was usually operated at 1 volt full scale deflection.

Pressure measurement: At first the pressure in the absorption cell was measured by a simple mercury manometer located in the glassware portion of the spectrometer. However, it was soon found that greater accuracy in the pressure measurement was required and thus an ionization-type vacuum gauge was connected to the absorption cell (the cell was provided with two suitable designed inlets/outlets, one of which was used to pump out the cell and admit the sample, the other was connected to the vacuum gauge). In this experiment the Hastings Vacuum Gauge Model SV1 was used.

Vacuum system: A block diagram of the vacuum system is shown in Fig. 3.4. The manifold is equipped with a number of stopcocks and test tubes for maximum convenience in handling the gases. The vacuum system is connected to the absorption cell via a suitably machined valve in the broad side of the wave guide. The diagram is essentially self-explanatory. The vacuum system and absorption cell were first evacuated by a roughing pump (Welch Scientific Model 1402) and then a higher vacuum was attained using a mercury diffusion pump. A liquid nitrogen trap condensed most vapors before they reached the pumps.

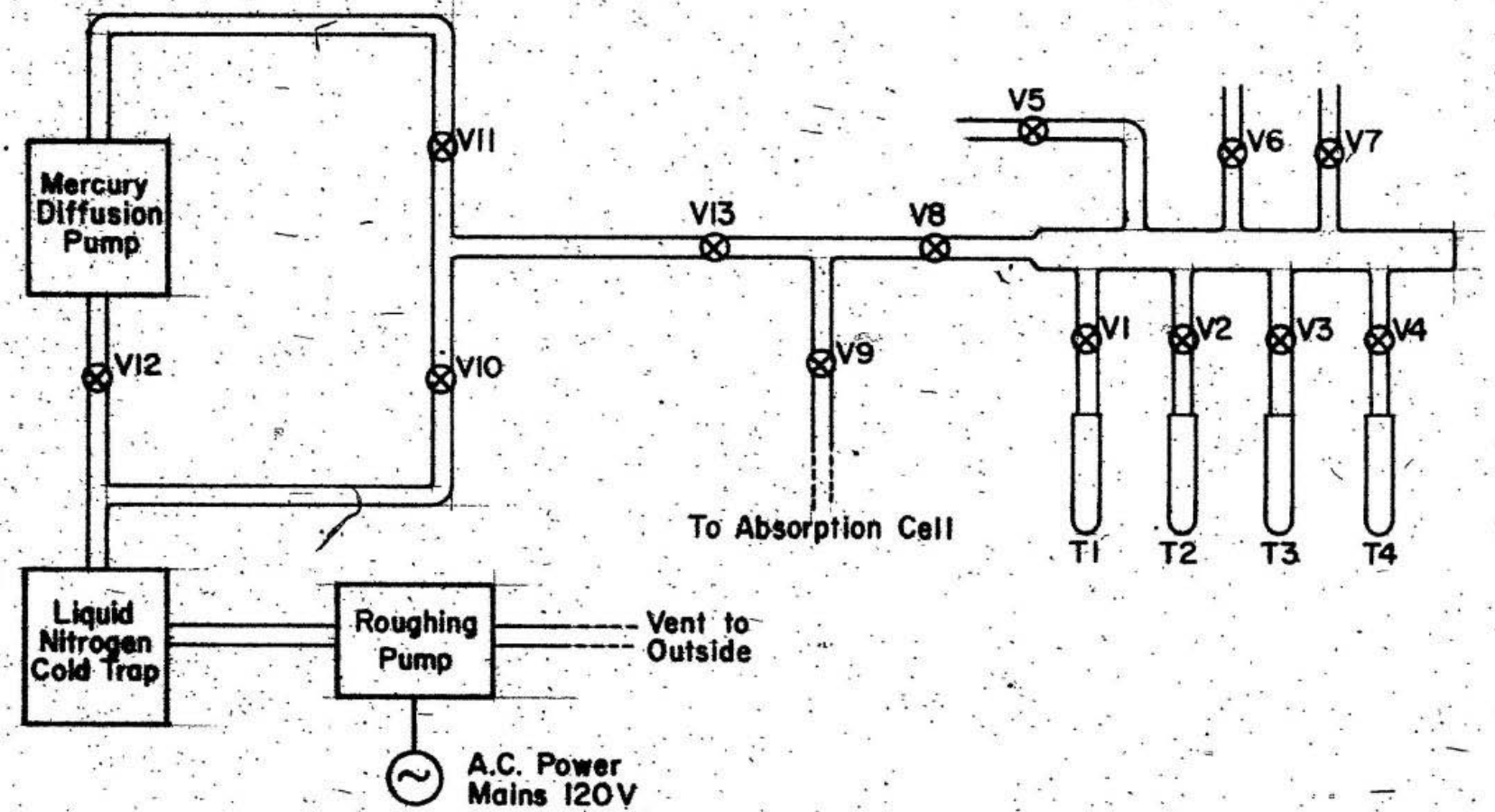

Fig. 3.4. Block diagram of the vacuum system.

Part B: Experimental Technique

Throughout the course of the experimental portion of this thesis a number of chemical compounds were used, namely, tertiary butyl chloride, tertiary butyl bromide, ammonia, trimethyl tin bromide, Freon 11, methyl alcohol, and carbonyl sulfide. The main body of experimental work concerned tertiary butyl chloride and tertiary butyl bromide. Work on one or two of the other compounds is reported in the latter part of Chapter 4.

3.3 Preparation of the Sample for Analysis

Tertiary butyl chloride and tertiary butyl bromide were both handled in much the same manner for this experiment. The step-by-step procedure follows:

The small bottle of compound was taken to the chemical preparation room. Utilizing the fume hood a small amount (about 5 ml) was placed in a test tube using a medicine dropper. The test tube containing the compound was then placed in a bath of liquid nitrogen contained in a Dewar flask. This combination was then removed from the fume hood and taken to the microwave spectroscopy laboratory.

The test tube (still in the bath of liquid nitrogen) was placed on the glassware system, say at position T2. Previous to this the absorption cell and glassware had been evacuated using the roughing pump and mercury diffusion pump to a pressure of 0.001 to 0.005 torr (a lower pressure was difficult to obtain with such a large volume absorption cell). Valves V1 to V10, inclusive, are closed, valves V11 to V13 are open. It should be noted that the mercury diffusion pump was not placed in operation

when the pressure exceeded about 0.100 torr as it is basically ineffective at those higher pressures as well as being harmful to the pump. In those cases where pressures were above 0.100 torr, the pressure was reduced by closing valves V11 and V12 and opening valve V10. When the pressure had reached a suitable level to use the mercury diffusion pump, valve V10 was closed and valves V11 and V12 opened. Note that the mercury diffusion pump is never used alone but always in conjunction with the roughing pump. Valves V2 and V8 were opened and all non-condensible vapors pumped off. Valves V2 and V8 were then closed and the compound allowed to 'thaw' by removal of the liquid nitrogen bath. It was then refrozen and the pumping procedure repeated. This 'freezing followed by pumping' sequence was repeated several times to eliminate as much foreign material as possible (it must be remembered that contaminants do not affect the spectrum of the compound being studied, but contribute a partial pressure making absolute pressure measurements impossible). After a final re-thawing, the sample was in the liquid form and ready for introduction of its vapor into the absorption cell.

Valve V13 is closed, effectively isolating the system from the vacuum pumps. Valves V2, V8 and V9 were opened and enough vapor was allowed to enter the absorption cell to maintain a pressure of 0.040 to 0.050 torr. Valves V2 and V9 were then closed. The sample is now ready for analysis. Previous to this last step it was found advisable to flush the cell several times with the sample vapor, and this was accomplished by allowing vapor to enter the cell until equilibrium was reached between the cell and test tube vapor pressures and then pumping out the cell to a vacuum of 0.001 to 0.005 torr. Then the sample vapor to be analyzed was used.

3.4 Optimum Sample Vapor Pressure for Analysis

In section 3.3 it was mentioned that a sample vapor pressure of 0.040 to 0.050 torr was used for analysis. This pressure range was decided upon after considerable experimentation to observe line shapes and the effects due to pressure broadening, power saturation, etc.

The figures on the following pages are copies of the actual experimental tracings of an absorption line of tertiary butyl chloride. The rotational transition shown is the J=1, K=1, F=5/2 to J=2, K=1, F=7/2 of $(C^{12}H_3)_3C^{12}Cl^{35}$. The line frequency was approximately 12075 MHz and has a theoretical intensity of 40.000% for that particular K level. The Stark voltage was 100 volts zero-based square wave. The time constant was 40 seconds. Such a large time constant eliminated most noise and other fast responses and consequently considerably smoothens the tracing, but however is adequate for the purpose needed here. In addition, the larger time constant causes an apparent frequency shift of the absorption line depending on the rate of sweep. The sweep rate was approximately 0.7 MHz per minute.

The unbiased crystal current can be considered as a measurement of the microwave power level in the cell. The crystal current varied from 25 micro-amps to 150 micro-amps and the sample vapor pressure varied from about 0.030 torr to about 0.085 torr. From the results of these tracings and other considerations it was decided to perform the analysis at 50 to 100 micro-amps crystal current and about 0.050 torr sample vapor pressure.

Fig. 3.5. Trace of the (2,1,7/2) → (1,1, 5/2) quadrupole component of tertiary butyl chloride--$(C^{12}H_3)_3C^{12}Cl^{35}$ - at various cell vapor pressures, p, and microwave power levels (measures as rectified crystal current), I. The transition was swept at a rate of about 0.7 MHz per minute using a forty-second time constant. The horizontal scale is frequency in MHz with a spot frequency indicated by the vertical 'up' arrow. The direction of increasing frequency is indicated by the horizontal arrow. The frequency marks occur every 2.0 MHz. The Stark voltage was 100 volts. The cell pressure, p, and microwave power level, I, are indicated on each individual figure. A vertical scale in milli-volts is shown on each figure to aid in the comparison of intensities.

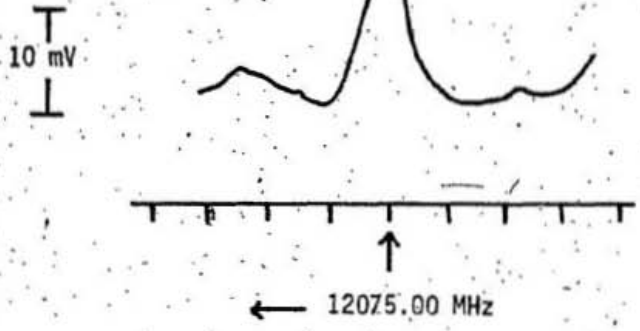

Fig. 3.5 (a)

p = 0.050 torr

I = 25 micro-amps

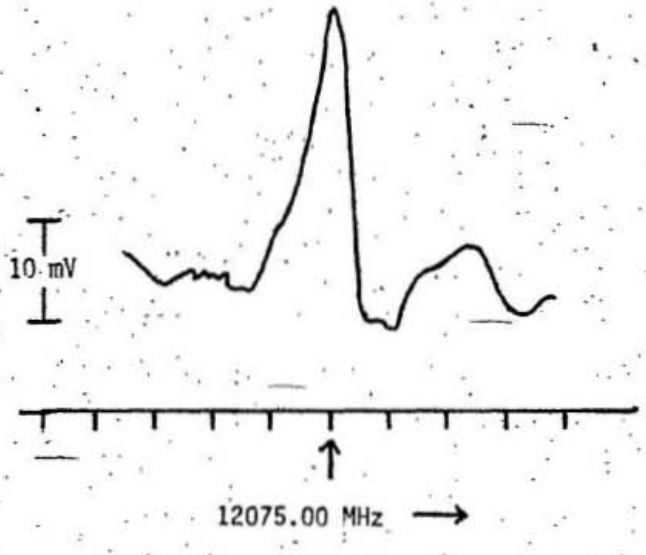

Fig. 3.5 (b)

p = 0.031 torr

I = 50 micro-amps

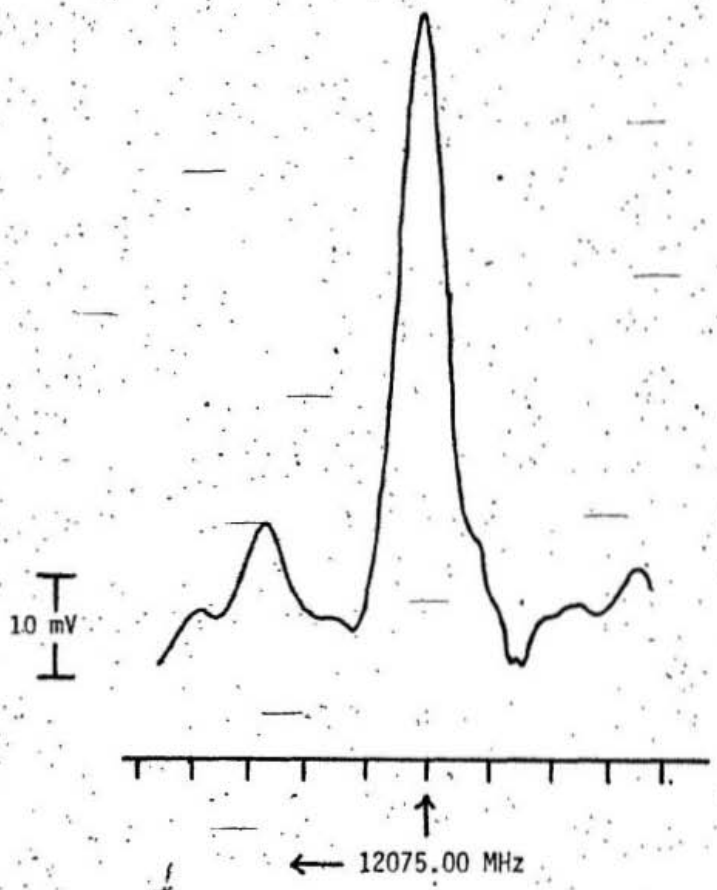

Fig. 3.5 (c)

p = 0.082 torr

I = 100 micro-amps

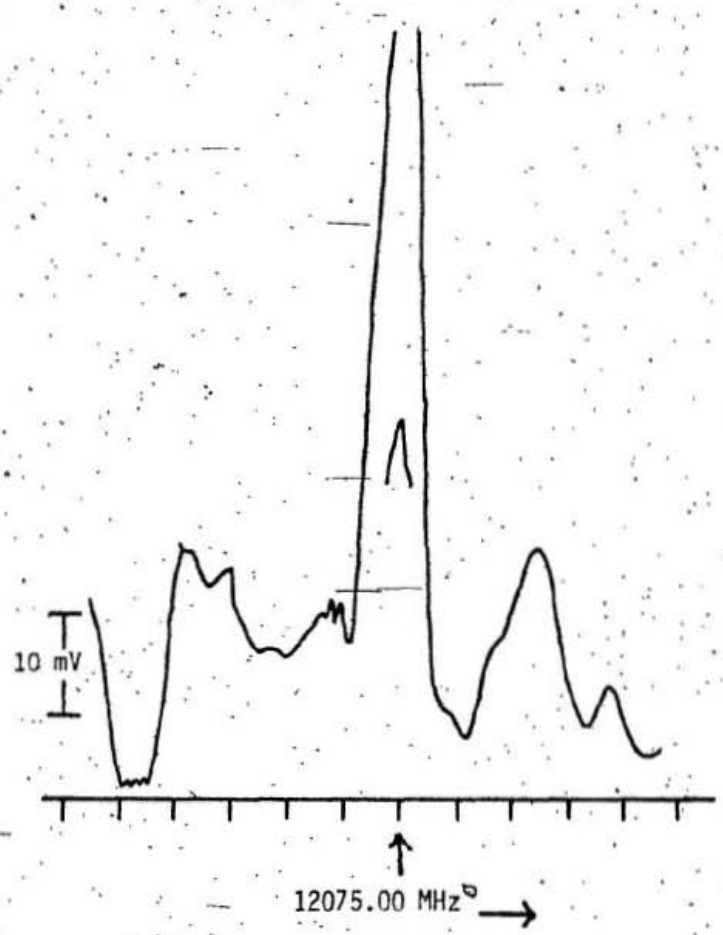

Fig. 3.5 (d)

p = 0.033 torr

I = 150 micro-amps

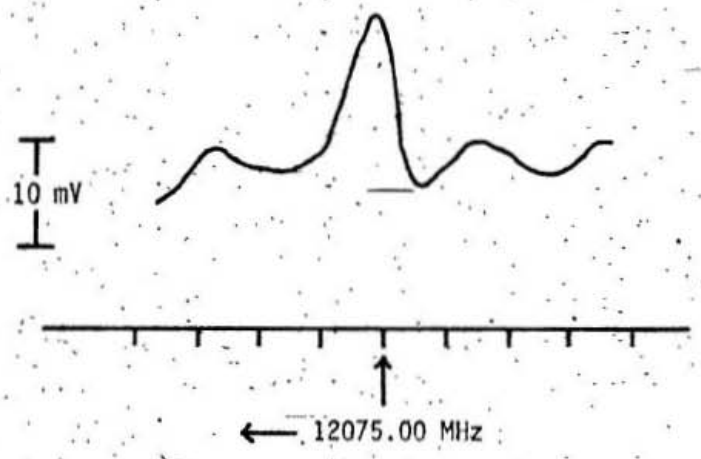

Fig. 3.5 (e)

p = 0.050 torr

I = 25 micro-amps

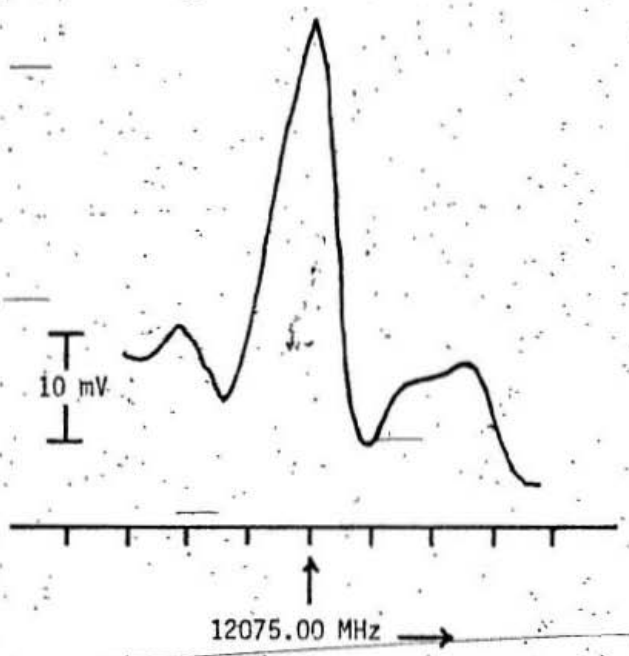

Fig. 3.5 (f)

p = 0.050 torr

I = 50 micro-amps

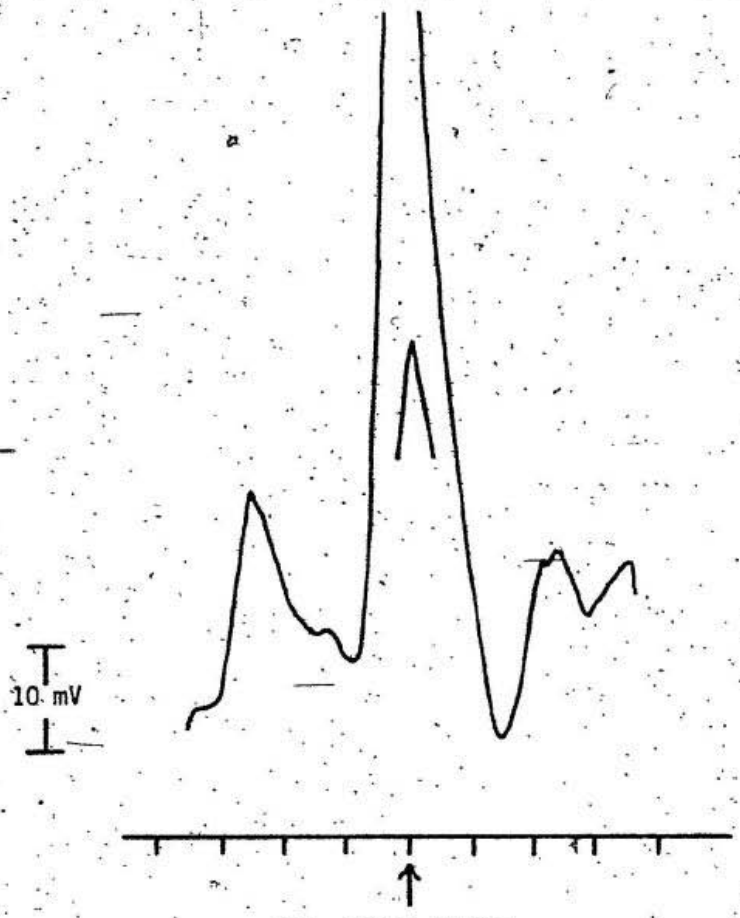

Fig. 3.5 (g)

p = 0.50 torr

I = 100 micro-amps

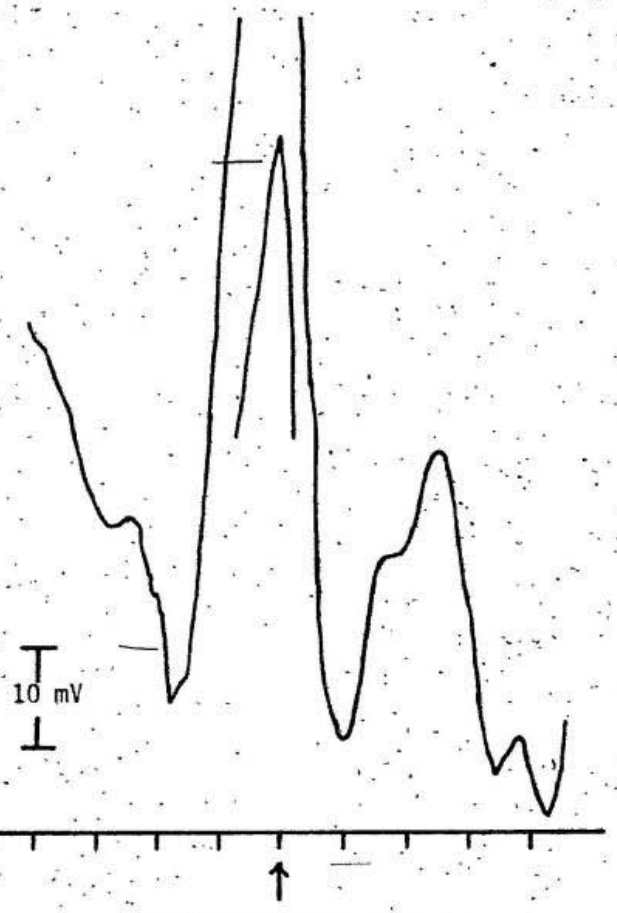

Fig. 3.5 (h)

p = 0.050 torr

I = 150 micro-amps

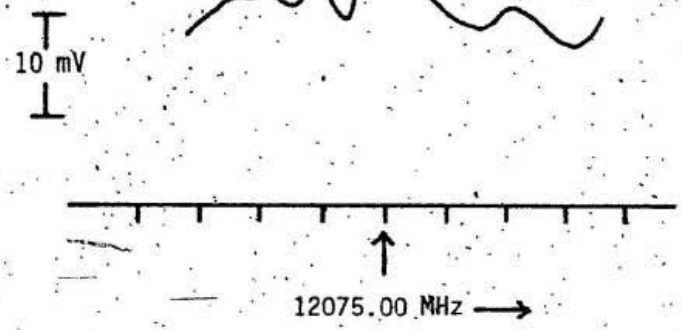

Fig. 3.5 (i)

p = 0.82 torr

I = 25 micro-amps

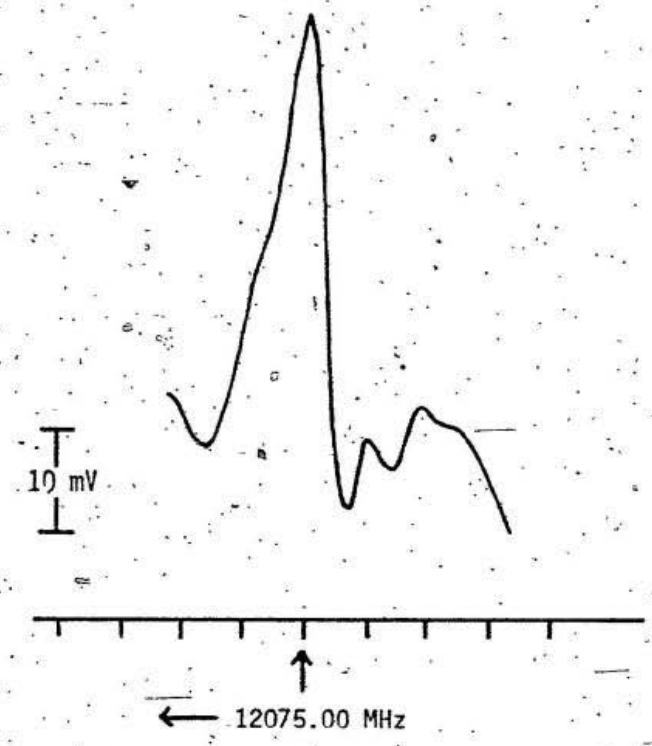

Fig. 3.5 (j)

p = 0.080 torr

I = 50 micro-amps

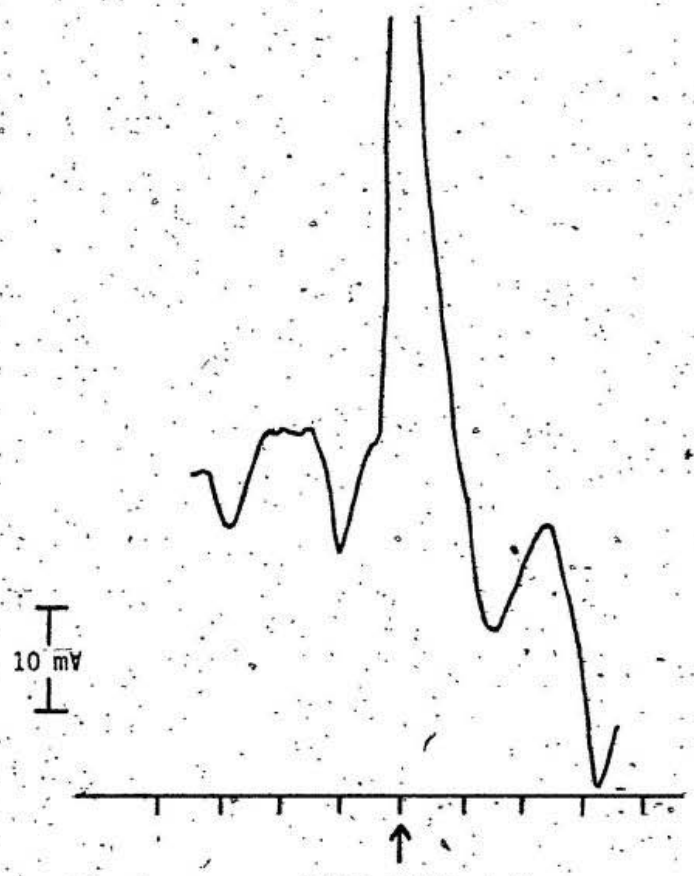

Fig. 3.5 (k)

p = 0.076 torr

I = 100 micro-amps

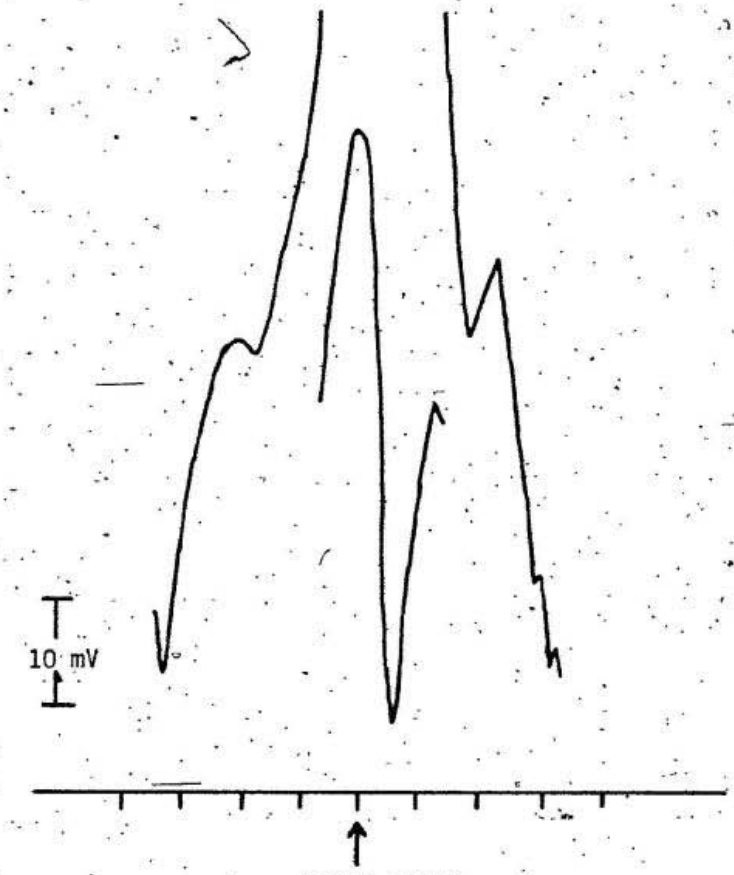

Fig. 3.5 (l)

p = 0.086 torr

I = 150 micro-amps

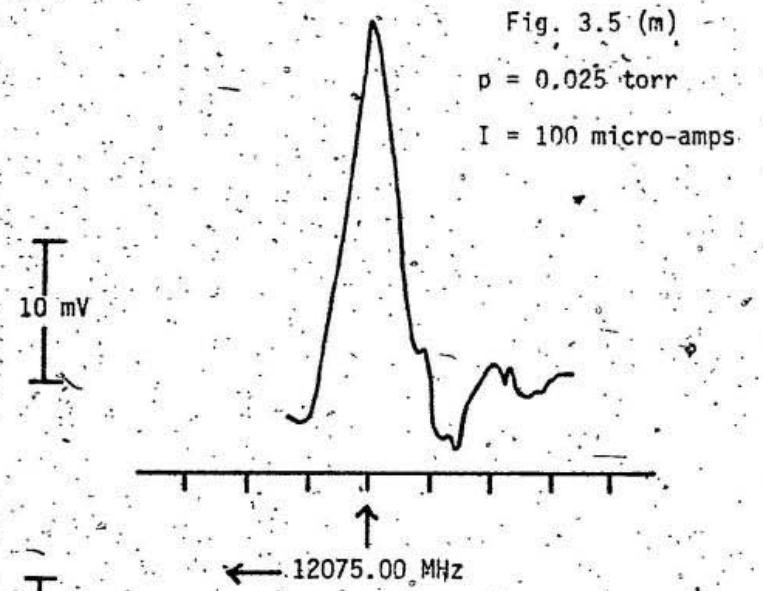

Fig. 3.5 (m)

p = 0.025 torr

I = 100 micro-amps

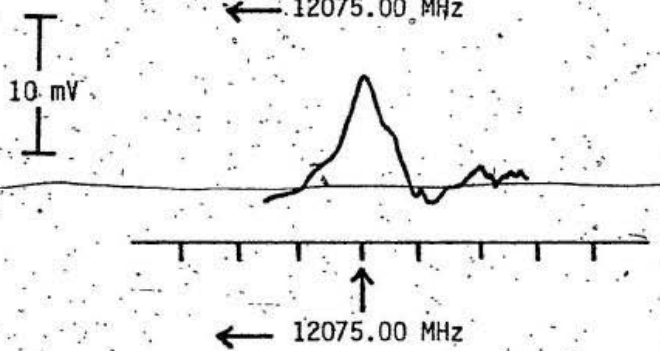

Fig. 3.5 (o)

p < 0.025 torr

I same as (n)

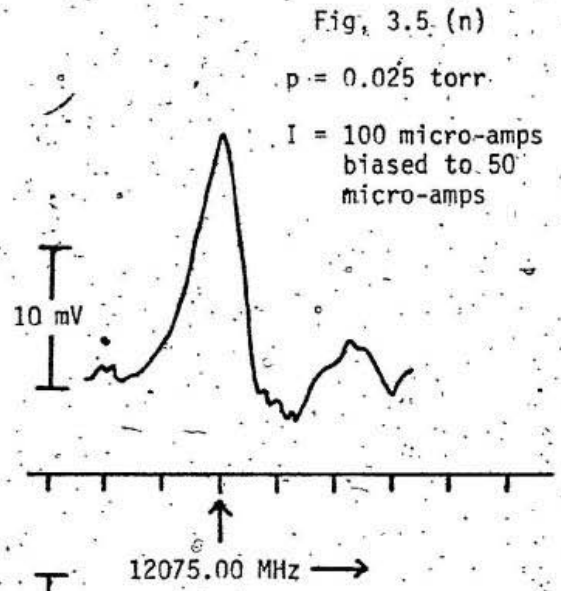

Fig. 3.5 (n)

p = 0.025 torr

I = 100 micro-amps biased to 50 micro-amps

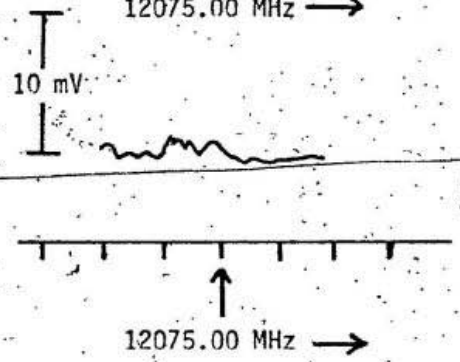

Fig. 3.5 (p)

p = 0.009 torr

I same as (n)

3.5 Method of Predicting and Analyzing the Spectra

From the rotational constants and the quadrupole coupling constants given in reference 5 for tertiary butyl chloride and tertiary butyl bromide and using the equations of Chapter 2, it was possible to calculate the expected spectra for the various transitions.

After analyzing our observed spectra we noticed slight changes in the B's and eQq's from those previously published. Hence the calculated hyperfine spectra appearing in Appendix E reflect the B's and eQq's obtained in this experiment. We note that the spectrum for $(CH_3)_3CCl^{35}$ J=1 → 2 extends from 12058.08 MHz to 12101.40 MHz, for $(CH_3)_3CCl^{37}$ J=1 → 2 from 11803.94 MHz to 11837.60 MHz, $(CH_3)_3CBr^{79}$ J=1 → 2 from 8052.00 MHz to 8306.12 MHz, $(CH_3)_3$ CBr^{79} J=1 → 3 from 12138.72 MHz to 12387.61 MHz, $(CH_3)_3$ CBr^{81} J=1 → 2 from 8008.80 MHz to 8221.54 MHz, and $(CH_3)_3CBr^{81}$ J=1 → 3 from 12063.56 MHz to 12272.20 MHz. All calculations included both the first- and second-order nuclear quadrupole correction energies. The theoretical intensities of the components varied from 1.000% to 40.000% for the J=1 → 2 transitions and from 0.204% to 35.714% for the J=2 → 3 transitions. The intensities refer only to that particular K level. Figures showing the theoretical spectra appear on the pages following Section 4.1.

The analysis of the spectra proved more difficult than earlier anticipated. A comparison was made with the theoretical spectra and this method proved quite good. The molecules were assumed to be in the ground vibrational states and weaker vibrational satellites from other vibrational states often complicated the identification of the weaker lines. In

addition, the Stark components, although in opposite phase to the 'main' lines, often complicated matters.

3.6 Observing the Spectra

From the results of Section 3.4 it was decided to use a sample vapor pressure of 0.040 to 0.050 torr with a power level converted to a slightly negative biased crystal current of 50 to 80 micro-amps.

The experimental setup and components were discussed in Section 3.2. It suffices to add that for the work on tertiary butyl chloride and tertiary butyl bromide the 10-second time constant was used. Using the motor drive mechanism the sweeping rate was .1 to .4 MHz per minute. No apparent frequency shift was discerned when observations were taken on sweeping high to low frequencies and then from low to high frequencies. Any apparent frequency shifts were much less than other errors, e.g. in frequency markings, interpolation of readings, etc. Thus it was not found necessary to sweep in both directions. The temperature of the absorption cell and enclosed vapor was maintained at or near the dry ice temperature of $-78^{\circ}C$ by filling the wooden box enclosing the cell with dry ice. The observations tabulated had Stark voltages ranging from 100 V to 500 V. Observations were taken at other Stark voltages but are not reported here.

CHAPTER 4

RESULTS AND DISCUSSION

The methods of evaluation of the rotational constants, the unsplit frequencies, quadrupole coupling constants, etc., outlined in this chapter apply specifically to the symmetric-top molecules tertiary butyl chloride and tertiary butyl bromide. As mentioned previously some work was performed on several other chemical compounds. One of these other compounds is discussed in Section 4.6 - Miscellaneous Results.

4.1 Method of Evaluating eQq, ν_o, and B_o, and Results

The rotational frequencies of a symmetric-top molecule with quadrupole coupling may be written as

$$\nu = \nu_o + eQq \left[\frac{3K^2}{J(J+1)} - 1\right]\left[Y(J+1,I,F') - Y(J,I,F)\right] \quad . \qquad (2.17)$$

Equation 2.17 only includes the first-order quadrupole energy. To it we may add a usually much smaller second-order quadrupole energy. Rewriting we have

$$\nu = \nu_o + F_1(eQq) + F_2\left[(eQq)^2\right] \quad . \qquad (4.1)$$

If we subtract the quadrupole energy contributions from Eq. 4.1 we can evaluate ν_o and hence determine the distortion constants D_{JK} and D_J as well as the rotational constant B by using Eq. 2.6

$$\nu = 2B(J+1) - 4D_J(J+1)^3 - 2D_{JK}(J+1)K^2 \quad . \qquad (2.6)$$

It is obvious that D_J must be evaluated before an exact measurement of B can be made, for even the lowest J transition $0 \rightarrow 1$ the first centrifugal stretching term does not vanish entirely.

In this experiment the theory was employed in the following manner: For each individual K level of each J transition of both molecules only those components with a theoretical intensity* greater than 8.0% were used in the calculations. (Note that the intensities considered are relative to that particular K level only.) Positive identification of components with intensities less than 8.0% were assumed to be practically impossible in this experiment.

These observed line frequencies were then written in the form of Eq. 4.1. Since $F_1\ (eQq) >> F_2[(eQq)^2]$, it was decided to approximate the $F_2[(eQq)^2]$ contribution and hence we were left with a set of first-order equations in eQq,

$$\nu = \nu_o + F_1(eQq) + F_2\ (\text{approx.}) \quad . \qquad (4.2)$$

Tables for evaluating the first- and second-order quadrupole energies are given in Appendices B and C, respectively. To approximate $F_2[(eQq)^2]$ in Eq. 4.1 the value of eQq used was that obtained from the literature, or otherwise, as outlined in Chapter 1.

Hence, if there were five observations for a given K level and a given J transition, there would be five equations of the form 4.2. By using all possible subtractions of these equations we would obtain a number of values for eQq. These values are tabulated in Appendix D. Arbitrarily accepting only those components which were separated by greater than

*The relative intensities of individual lines have been given as a percentage of the intensity of the entire $J \rightarrow J+1$, $K \rightarrow K$ transition.

10.0 MHz for tertiary butyl chloride and greater than 30.0 MHz for tertiary butyl bromide an average eQq was obtained for each K level. These eQq's are tabulated in Table 4.7

Using the average value of eQq obtained above we calculate the ν_o for each of the five equations of form 4.2. These ν_o's are then averaged to obtain an average ν_o for each K level. These values are tabulated in 4.7.

Using the value of ν_o for each K level obtained above and substituting it into Eq. 2.6 an attempt was made to evaluate the distortion constants D_J and D_{JK}. However, since the ν_o's for the K levels were so close together, no reliable determination of these distortion constants could be made, except that they were very small, and hence ignored. This was expected for such large and fairly heavy molecules. The B's were then directly evaluated and are tabulated in Table 4.7 for each K level.

SAMPLE CALCULATION

For the J = 1 → 2 rotational transition of $(C^{12}H_3)_3C^{12}Cl^{35}$, there are six suitable observed lines for the K = 1 level. They are:

F Transition	ν observed MHz	Intensity %
1/2 ← 1/2	12087.90 ± .05	8.333
3/2 ← 1/2	12079.30 ± .10	8.333
7/2 ← 5/2	12075.05 ± .05	40.000
5/2 ← 5/2	12066.50 ± .05	9.000
3/2 ← 3/2	12064.30 ± .05	10.667
5/2 ← 3/2	12057.90 ± .10	21.000

Errors in the observations are those obtained by estimating the recording and reading of the observation.

In the format of Eq. 4.1 these observations may be written as:

$$12087.90 \pm .05 = \nu_0 - 0.250000\ eQq + 0.04 \quad \text{(i)}$$

$$12079.30 \pm .10 = \nu_0 - 0.125000\ eQq + 0.03 \quad \text{(ii)}$$

$$12075.05 \pm .05 = \nu_0 - 0.060715\ eQq + 0.01 \quad \text{(iii)}$$

$$12066.50 \pm .05 = \nu_0 + 0.064286\ eQq + 0.02 \quad \text{(iv)}$$

$$12064.30 \pm .05 = \nu_0 + 0.100000\ eQq + 0.02 \quad \text{(v)}$$

$$12057.90 \pm .10 = \nu_0 + 0.189286\ eQq + 0.02 \quad \text{(vi)}$$

The errors in the second-order quadrupole energies are correspondingly very small and hence neglected.

From all possible subtractions of these equations satisfying the criteria that the separation of the components involved by greater than 10.0 MHz, nine measurements of eQq were obtained. They were:

- 66.95 ± .44 MHz	- 67.43 ± .20	- 68.06 ± .45
- 68.64 ± .44	- 66.62 ± .49	- 68.09 ± .22
- 67.83 ± .37	- 68.29 ± .25	- 67.57 ± .58

The errors in these measurements of eQq were obtained as the square root of the sum of the squares of the errors in the two observations involved.

From the above nine measurements the average value of eQq for the K=1 level would be -67.72 MHz. The deviation of each of the nine measurements from the mean value of -67.72 MHz would be 0.77, 0.99, 0.11, 0.29, 1.10, 0.57, 0.34, 0.37, and 0.15 MHz, respectively, leading to an average deviation of 0.51 MHz. Meanwhile the average error in eQq due to

the error in reading the observations is 0.38 MHz. By combining these errors by the square root of the sum of the squares method we arrive at the error in the average eQq as 0.63 MHz, i.e. eQq = - 67.72 ± .63 MHz.

Substituting the above average value of eQq in equations (i) to (vi), six values of ν_o were obtained. They were:

12070.93 ± .17 MHz	12070.93 ± .07	12071.05 ± .08
12070.80 ± .18	12070.87 ± .07	12070.70 ± .16

The errors in these measurements of ν_o were obtained as the square root of the sum of the squares of the errors in reading the observations and the error in eQq.

From the above six measurements the average value of ν_o for the K=1 level would be 12070.88 MHz. The deviations of each of the six measurements from the mean value of 12070.88 MHz would be 0.05, 0.08, 0.05, 0.01, 0.17, and 0.18 MHz, respectively, leading to an average deviation of 0.09 MHz. Meanwhile the average error in ν_o due to the error in reading the observation and the error in eQq was 0.12 MHz. By combining both these errors by the square root of the sum of the squares method, we arrive at the error in the average ν_o as 0.15 MHz, i.e. ν_o = 12070.88 ± .15 MHz.

This 'averaging' method of evaluating eQq and subsequently ν_o and B was considered more appropriate in this experiment than the 'least squares fit' method. This is so mainly because greatest weight should be given to the more widely-spaced components of a given hyperfine multiplet in evaluating eQq. However, as a test, the 'least squares fit' method was also used in a number of cases and the results are given in Table 4.7a. Figs. 4:1 to 4:8 and Tables 4:1 to 4:8 show the observations and results as discussed in this chapter.

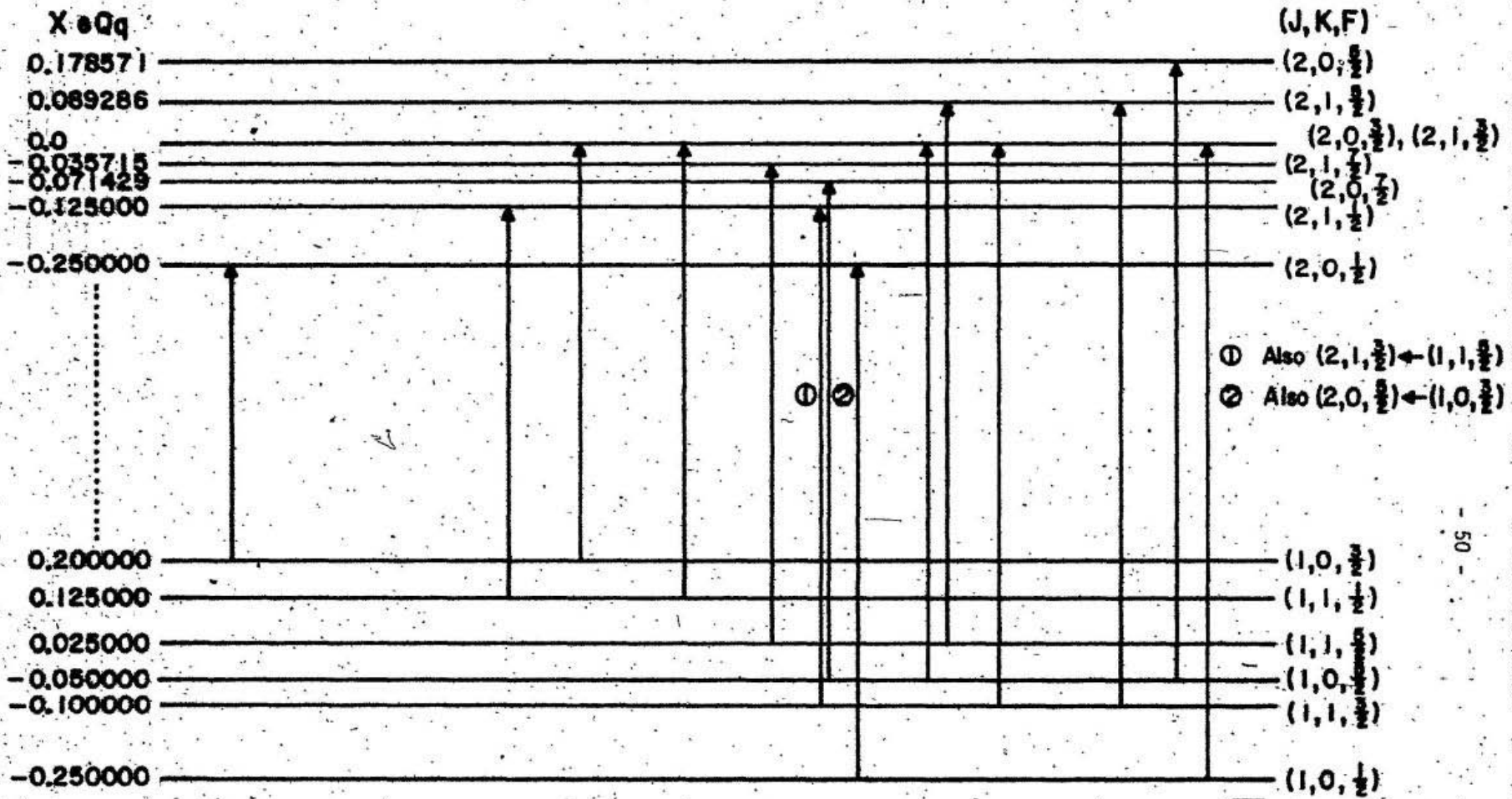

Fig. 4.1. Energy level diagram and calculated nuclear quadrupole hyperfine structure for the J=1 → 2 rotational transition of a symmetric-top molecule with a single coupling nucleus having a spin of 3/2. Only the first-order quadrupole correction energies are used.

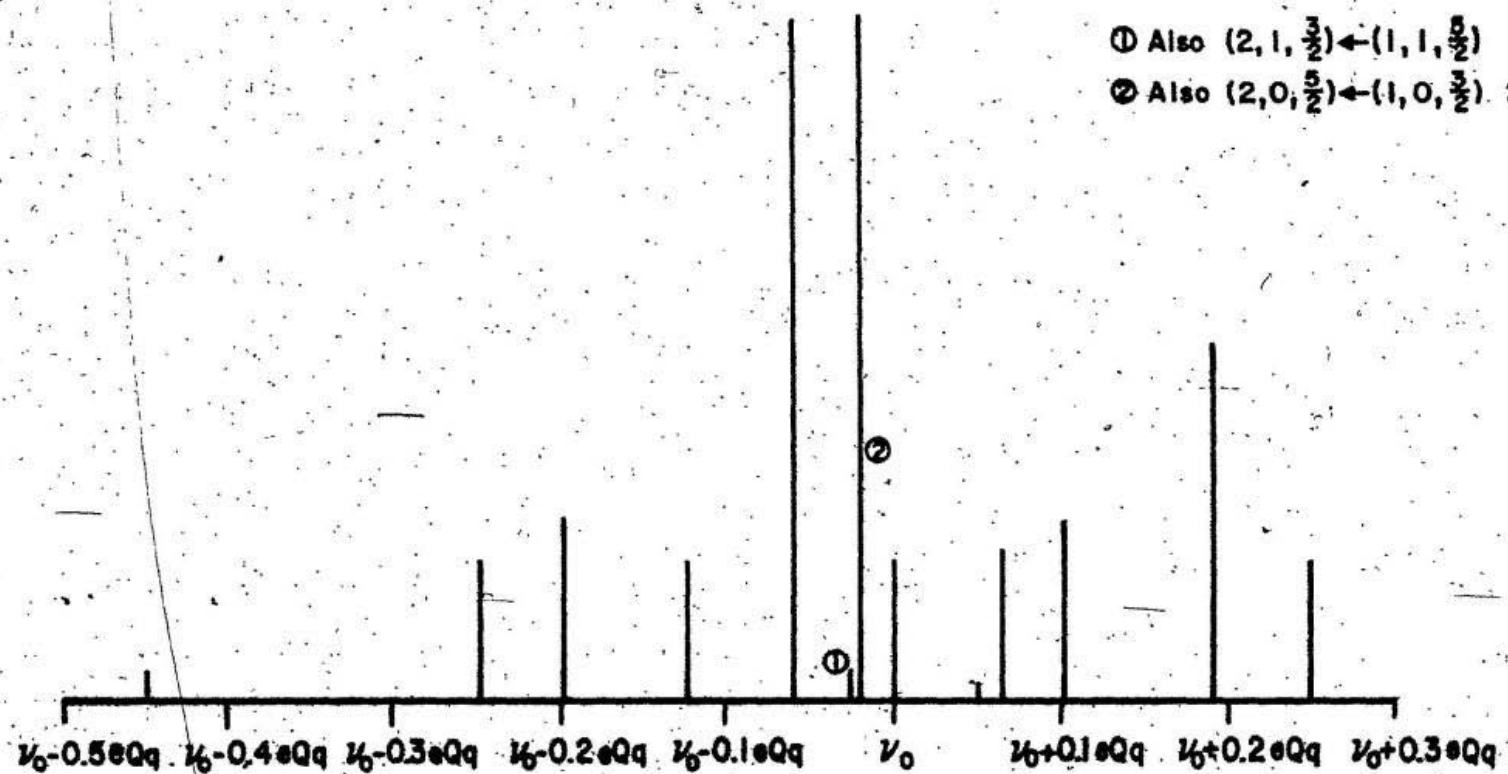

Fig. 4.2. Theoretical nuclear quadrupole hyperfine spectrum for the J=1 → 2 rotational transition of a symmetric-top molecule with a single coupling nucleus having a spin of 3/2. This figure follows from Fig. 4.1.

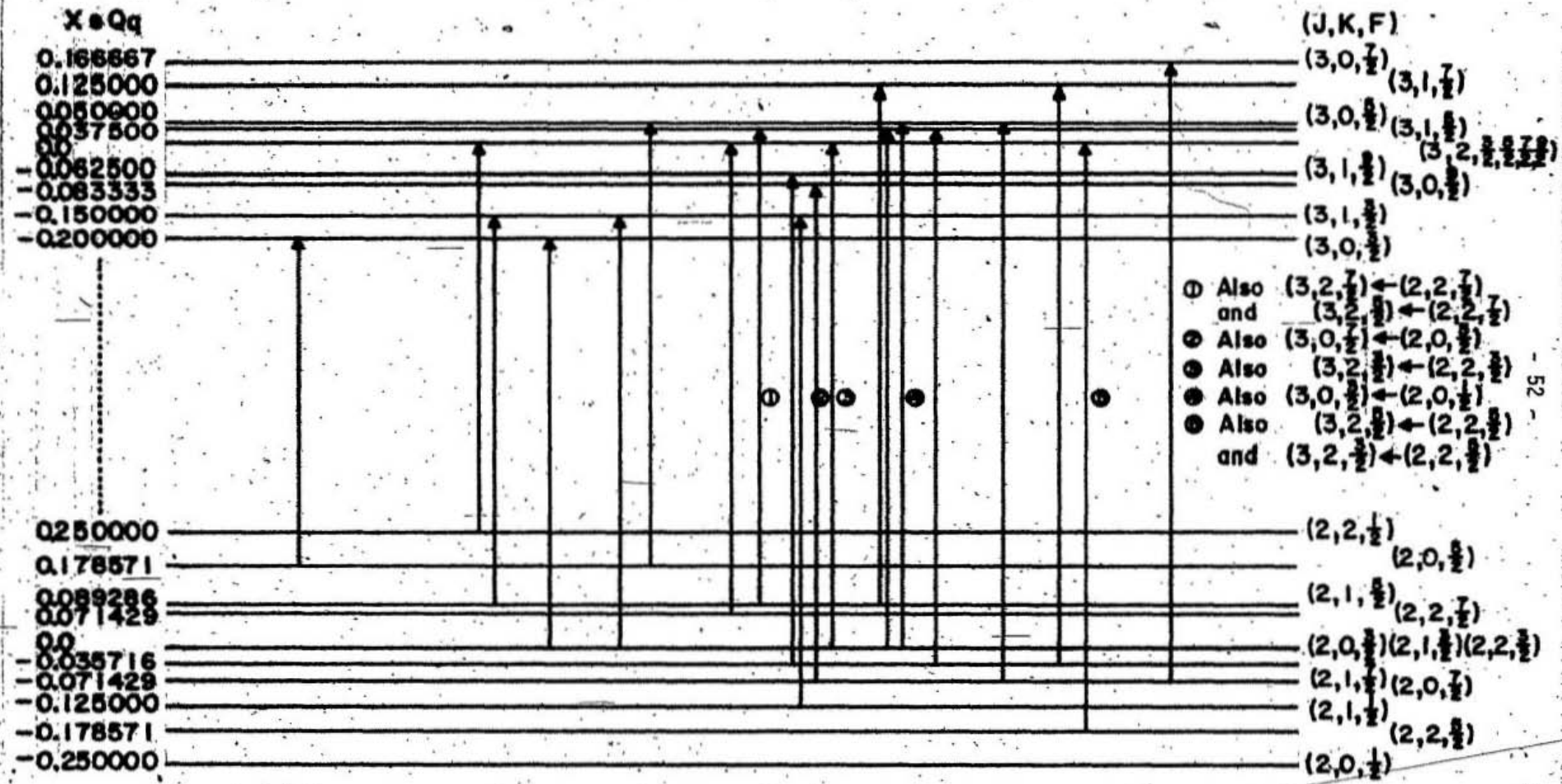

Fig. 4.3. Energy level diagram and calculated nuclear quadrupole hyperfine structure for the J=2 → 3 rotational transition of a symmetric-top molecule with a single coupling nucleus having a spin of 3/2. Only the first-order quadrupole correction energies are used.

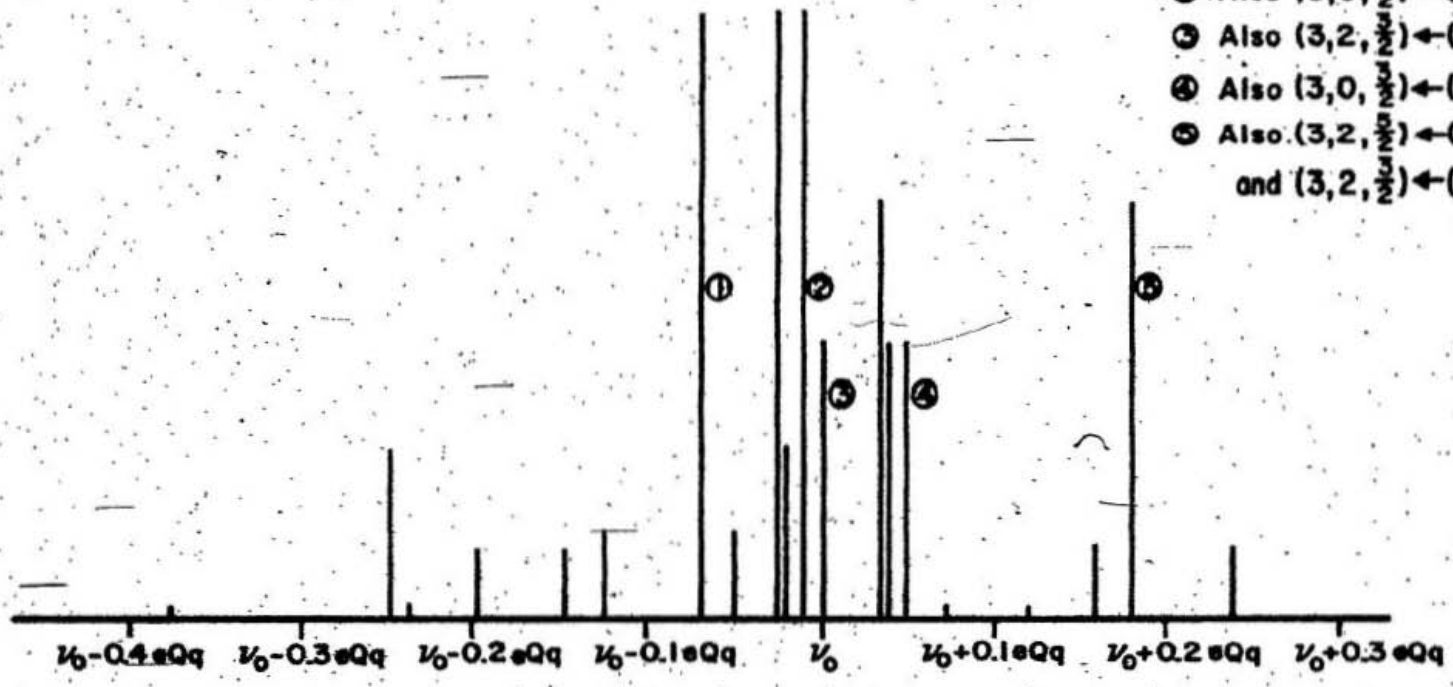

Fig. 4.4. Theoretical nuclear quadrupole hyperfine spectrum for the J=2 → 3 rotational transition of a symmetric-top molecule with a single coupling nucleus having a spin of 3/2. This figure follows from Fig. 4.3.

TABLE 4.1. The hyperfine structure of the J = 1 → 2 rotational transition for $(CH_3)_3CCl^{35}$.

K Transition	F Transition	ν (observed) MHz	ν (calculated) MHz	$\nu_{obs} - \nu_{calc}$ MHz
0	1/2 ← 3/2		12101.40	
0	3/2 ← 3/2	12084.35 ± .10	12084.49	-.14
0	7/2 ← 5/2	12072.50 ± .05	12072.38	+.12
0	5/2 ← 3/2	12072.50 ± .05	12072.38	+.12
0	1/2 ← 1/2	12071.05 ± .05	12070.93	+.12
0	3/2 ← 5/2		12067.56	
0	5/2 ← 5/2	12055.25 ± .05	12055.46	-.21
0	3/2 ← 1/2		12054.02	
1	1/2 ← 1/2	12087.90 ± .05	12087.85	+.05
1	3/2 ← 1/2	12079.30 ± .10	12079.38	+.08
1	7/2 ← 5/2	12075.05 ± .05	12075.00	+.05
1	3/2 ← 5/2		12072.59	
1	1/2 ← 3/2		12072.60	
1	5/2 ← 5/2	12066.50 ± .05	12066.55	-.05
1	3/2 ← 3/2	12064.30 ± .05	12064.13	+.17
1	5/2 ← 3/2	12057.90 ± .10	12058.08	-.18

TABLE 4.2. The hyperfine structure of the J = 1 → 2 rotational transition for $(CH_3)_3CCl^{37}$

K Transition	F Transition	ν (observed) MHz	ν (calculated) MHz	$\nu_{obs} - \nu_{calc}$ MHz
0	1/2 ← 3/2		11837.60	
0	3/2 ← 3/2	11824.50 ± .10	11824.54	-.04
0	7/2 ← 5/2	11815.60 ± .05	11815.19	+.41
0	5/2 ← 3/2	11815.60 ± .05	11815.19	+.41
0	1/2 ← 1/2	11814.03 ± .10	11814.07	-.04
0	3/2 ← 5/2		11811.47	
0	5/2 ← 5/2		11802.12	
0	3/2 ← 1/2	11800.25 ± .10	11801.01	-.76
1	1/2 ← 1/2	11826.65 ± .15	11826.92	-.27
1	3/2 ← 1/2	11820.12 ± .05	11820.39	-.27
1	7/2 ← 5/2	11817.50 ± .10	11817.00	+.50
1	3/2 ← 5/2		11815.15	
1	1/2 ← 3/2		11815.16	
1	5/2 ← 5/2		11810.48	
1	3/2 ← 3/2		11808.61	
1	5/2 ← 3/2	11804.00 ± .10	11803.94	+.06

TABLE 4.3. The hyperfine structure of the J = 1 ← 2 rotational transition for $(CH_3)_3CBr^{79}$

K Transition	F Transition	ν (observed) MHz	ν (calculated) MHz	$\nu_{obs} - \nu_{calc}$ MHz
0	3/2 ← 1/2		8306.12	
0	5/2 ← 5/2		8294.29	
0	3/2 ← 5/2		8204.43	
0	1/2 ← 1/2	8176.40 ± .05	8176.70	-.30
0	7/2 ← 5/2	8166.03 ± .05	8165.96	+.07
0	5/2 ← 3/2	8166.03 ± .05	8165.73	+.30
0	3/2 ← 3/2	8076.10 ± .20	8075.86	+.24
0	1/2 ← 3/2		7946.44	
1	5/2 ← 3/2	8275.69 ± .05	8275.76	-.07
1	3/2 ← 3/2	8230.40 ± .05	8230.36	+.04
1	5/2 ← 5/2	8211.57 ± .05	8211.54	+.03
1	1/2 ← 3/2		8167.16	
1	3/2 ← 5/2		8166.14	
1	7/2 ← 5/2	8146.47 ± .10	8146.45	+.02
1	3/2 ← 1/2	8115.15 ± .15	8155.20	-.05
1	1/2 ← 1/2	8052.00 ± .15	8052.00	0.0

TABLE 4.4. The hyperfine structure of the J = 2 → 3 rotational transition for $(CH_3)_3CBr^{79}$

K Transition	F Transition	ν (observed) MHz	ν (calculated) MHz	$\nu_{obs} - \nu_{calc}$ MHz
0	7/2 ← 7/2		12387.61	
0	5/2 ← 7/2		12328.85	
0	3/2 ← 1/2	12290.85 ± .10	12291.26	-.41
0	5/2 ← 3/2	12290.85 ± .10	12290.40	+.45
0	7/2 ← 5/2	12259.33 ± .15	12259.28	-.13
0	9/2 ← 7/2	12259.33 ± .15	12259.38	-.23
0	5/2 ← 5/2		12200.53	
0	3/2 ← 3/2	12161.75 ± .10	12161.83	-.08
0	3/2 ← 5/2		12071.97	
1	7/2 ← 7/2		12348.46	
1	5/2 ← 7/2		12304.05	
1	5/2 ← 3/2	12283.48 ± .05	12284.35	-.85
1	7/2 ← 5/2	12283.48 ± .05	12283.38	+.10
1	3/2 ← 1/2	12252.10 ± .05	12251.78	+.32
1	9/2 ← 7/2	12252.10 ± .05	12251.88	+.22
1	5/2 ← 5/2	12239.50 ± .05	12238.97	+.53
1	3/2 ← 3/2	12188.20 ± .20	12188.58	-.38
1	3/2 ← 5/2		12143.19	
2	3/2 ← 5/2		12358.79	
2	5/2 ← 5/2		12357.12	
2	7/2 ← 5/2	12357.89 ± .10	12357.90	-.01
2	3/2 ← 3/2		12268.14	
2	5/2 ← 3/2		12266.47	
2	5/2 ← 7/2		12229.47	
2	7/2 ← 7/2	12230.80 ± .20	12230.25	+.55
2	9/2 ← 7/2	12229.14 ± .10	12229.11	-.01
2	3/2 ← 1/2	12138.70 ± .15	12138.72	-.02

TABLE 4.5. The hyperfine structure of the J = 1 → 2 rotational transition for $(CH_3)_3CBr^{81}$

K Transition	F Transition	ν (observed) MHz	ν (calculated) MHz	$\nu_{obs} - \nu_{calc}$ MHz
0	3/2 ← 1/2	8221.97 ± .10	8221.54	+.43
0	5/2 ← 5/2	8211.57 ± .05	8211.76	-.21
0	3/2 ← 5/2		8136.43	
0	1/2 ← 1/2		8113.54	
0	7/2 ← 5/2	8104.50 ± .05	8104.53	-.03
0	5/2 ← 3/2	8104.50 ± .05	8104.37	+.13
0	3/2 ← 3/2	8028.85 ± .20	8029.05	-.20
0	1/2 ← 3/2		7921.04	
1	5/2 ← 3/2	8195.90 ± .10	8196.01	-.11
1	3/2 ← 3/2	8158.07 ± .05	8158.01	+.06
1	5/2 ← 5/2		8142.35	
1	1/2 ← 3/2		8105.07	
1	3/2 ← 5/2		8104.36	
1	7/2 ← 5/2	8087.90 ± .10	8088.09	-.19
1	3/2 ← 1/2	8061.70 ± .20	8061.74	-.04
1	1/2 ← 1/2	8009.20 ± .20	8008.80	+.40

TABLE 4.6. The hyperfine structure of the J = 2 ← 3 rotational transition for $(CH_3)_3CBr^{81}$

K Transition	F Transition	ν (observed) MHz	ν (calculated) MHz	$\nu_{obs} - \nu_{calc}$ MHz
0	7/2 ← 7/2	12272.30 ± .15	12272.20	+.10
0	5/2 ← 7/2		12222.96	
0	3/2 ← 1/2	12191.35 ± .10	12191.65	-.30
0	5/2 ← 3/2	12191.35 ± .10	12191.05	+.30
0	7/2 ← 5/2		12164.96	
0	9/2 ← 7/2		12165.04	
0	5/2 ← 5/2		12115.72	
0	3/2 ← 3/2		12083.66	
0	3/2 ← 5/2		12008.33	
1	7/2 ← 7/2	12239.50 ± .05	12239.32	+.18
1	5/2 ← 7/2		12204.14	
1	5/2 ← 3/2	12185.55 ± .05	12185.87	-.32
1	7/2 ← 5/2	12184.90 ± .10	12185.04	-.14
1	3/2 ← 1/2	12158.85 ± .10	12158.71	+.14
1	9/2 ← 7/2	12158.85 ± .10	12158.66	+.19
1	5/2 ← 5/2	12147.80 ± .10	12147.88	-.08
1	3/2 ← 3/2	12105.40 ± .20	12105.78	-.38
1	3/2 ← 5/2		12067.79	
2	3/2 ← 5/2		12247.45	
2	5/2 ← 5/2	12247.00 ± .05	12246.27	+.73
2	7/2 ← 5/2	12247.00 ± .05	12246.82	+.18
2	3/2 ← 3/2	12171.00 ± .10	12171.57	-.57
2	5/2 ← 3/2	12171.00 ± .10	12170.39	+.61
2	5/2 ← 7/2		12139.51	
2	7/2 ← 7/2	12140.80 ± .10	12140.07	+.73
2	9/2 ← 7/2	12138.70 ± .15	12139.26	-.56
2	3/2 ← 1/2	12063.20 ± .20	12063.56	-.36

TABLE 4.7. The hypothetical unsplit rotational frequency ν_o, the rotational constants B_o, and the quadrupole coupling constants eQq in tertiary butyl chloride and tertiary butyl bromide

Molecule	J Transition	K Transition		Values in MHz
$(CH_3)_3CCl^{35}$	1 → 2	0	ν_o	12070.93 ± .21
			B_o	3017.73 ± .05
			eQq	- 67.16 ± 1.14
$(CH_3)_3CCl^{35}$	1 → 2	1	ν_o	12070.88 ± .15
			B_o	3017.72 ± .04
			eQq	- 67.72 ± .63
$(CH_3)_3CCl^{37}$	1 → 2	0	ν_o	11814.07 ± .34
			B_o	2953.52 ± .09
			eQq	- 54.91 ± 1.53
$(CH_3)_3CCl^{37}$	1 → 2	1	ν_o	11813.84 ± .36
			B_o	2953.46 ± .09
			eQq	- 52.28 ± 1.25
$(CH_3)_3CBr^{79}$	1 → 2	0	ν_o	8176.71 ± .21
			B_o	2044.18 ± .05
			eQq	511.24 ± 1.49
$(CH_3)_3CBr^{79}$	1 → 2	1	ν_o	8177.07 ± .17
			B_o	2044.27 ± .04
			eQq	512.29 ± .95

TABLE 4.7, continued

Molecule	J Transition	K Transition		Values in MHz
$(CH_3)_3CBr^{79}$	2 → 3	0	ν_o	12265.35 ± .38
			B_o	2044.23 ± .10
			eQq	512.73 ± 7.54
$(CH_3)_3CBr^{79}$	2 → 3	1	ν_o	12265.37 ± .37
			B_o	2044.23 ± .09
			eQq	501.94 ± 7.73
$(CH_3)_3CBr^{79}$	2 → 3	2	ν_o	12265.47 ± .17
			B_o	2044.25 ± .04
			eQq	512.38 ± .67
$(CH_3)_3CBr^{81}$	1 → 2	0	ν_o	8113.54 ± .26
			B_o	2028.39 ± .07
			eQq	428.86 ± 1.11
$(CH_3)_3CBr^{81}$	1 → 2	1	ν_o	8113.73 ± .32
			B_o	2028.43 ± .08
			eQq	427.29 ± 1.61
$(CH_3)_3CBr^{81}$	2 → 3	0	ν_o	12170.04 ± .34
			B_o	2028.34 ± .06
			eQq	n.a.
$(CH_3)_3CBr^{81}$	2 → 3	1	ν_o	12169.97 ± .13
			B_o	2028.33 ± .02
			eQq	421.95 ± 2.40
$(CH_3)_3CBr^{81}$	2 → 3	2	ν_o	12169.68 ± .46
			B_o	2028.28 ± .08
			eQq	429.15 ± 2.28

TABLE 4.7a. ν_o, B_o, and eQq obtained by a least squares fit method (for comparison purposes only)

Molecule	J Transition	K Transition		Values in MHz
$(CH_3)_3CCl^{35}$	1 → 2	1	ν_o	12070.87
			B_o	3017.72
			eQq	- 67.88
$(CH_3)_3CCl^{37}$	1 → 2	1	ν_o	11813.96
			B_o	2953.49
			eQq	- 52.16
$(CH_3)_3CBr^{79}$	1 → 2	1	ν_o	8177.05
			B_o	2044.26
			eQq	512.14
$(CH_3)_3CBr^{79}$	2 → 3	2,1	ν_o	12265.37
			B_o	2044.23
			eQq	511.69
$(CH_3)_3CBr^{81}$	1 → 2	1	ν_o	8113.77
			B_o	2028.44
			eQq	428.34
$(CH_3)_3CBr^{81}$	2 → 3	2,1	ν_o	12169.77
			B_o	2028.29
			eQq	428.95

TABLE 4.8. Observed spectral constants in tertiary butyl chloride and tertiary butyl bromide

Molecule	J Transition		Previous Values* MHZ	New Values MHZ
$(CH_3)_3CCl^{35}$	1 → 2	B	3017.69 ± .02	3017.72 ± .04
		eQq	- 66.9 ± 1.5	- 67.72 ± .63
$(CH_3)_3CCl^{37}$	1 → 2	B	2953.54 ± .02	2953.46 ± .09
		eQq	not obtained	- 52.28 ± 1.25
$(CH_3)_3CBr^{79}$	1 → 2	B	2044.22 ± .05	2044.27 ± .04
		eQq	511.6 ± 5	512.29 ± .95
$(CH_3)_3CBr^{79}$	2 → 3	B	2044.22 ± .05	2044.25 ± .04
		eQq	511.6 ± 5	512.38 ± .67
$(CH_3)_3CBr^{81}$	1 → 2	B	2028.34 ± .05	2028.43 ± .08
		eQq	427.4 ± 4	427.29 ± 1.61
$(CH_3)_3CBr^{81}$	2 → 3	B	2028.34 ± .05	2028.28 ± .08
		eQq	427.4 ± 4	429.15 ± 2.28

*As can be seen from sections 1.2 and 4.7, the previous values of the spectral constants were obtained from higher rotational transitions than those used in this work. Lide and Jen[1] obtained the rotational constants of tertiary butyl chloride from the J=4 → 5 and J=5 → 6 transitions, and the quadrupole coupling constant of $(CH_3)_3CCl^{35}$ from the J=2 → 3 transition, while the constants of tertiary butyl bromide were found by Zeil, Winnewisser and Huttner[6] from the J=4 → 5 transition.

Fig. 4.5. Trace of the quadrupole hyperfine spectra of the rotational transition J=1 → 2 of tertiary butyl chloride - $(C^{12}H_3)_3C^{12}Cl^{35}$ and $(C^{12}H_3)_3C^{12}Cl^{37}$. The transition was swept at a rate of about 0.5 MHz per minute using a forty-second time constant. The horizontal scale is frequency in MHz with spot frequencies indicated by vertical 'up' arrows. The frequency marks occur every 5.0 MHz. The Stark voltage was 120 volts. The cell pressure was about 0.070 torr. The zero field transitions (up) are partially obscured by the Stark components (down). Fig. 4.5 (a), showing the Cl^{35} isotopic species, and Fig. 4.5 (b), showing the Cl^{37} isotopic species, are drawn to the same vertical (intensity) scale.

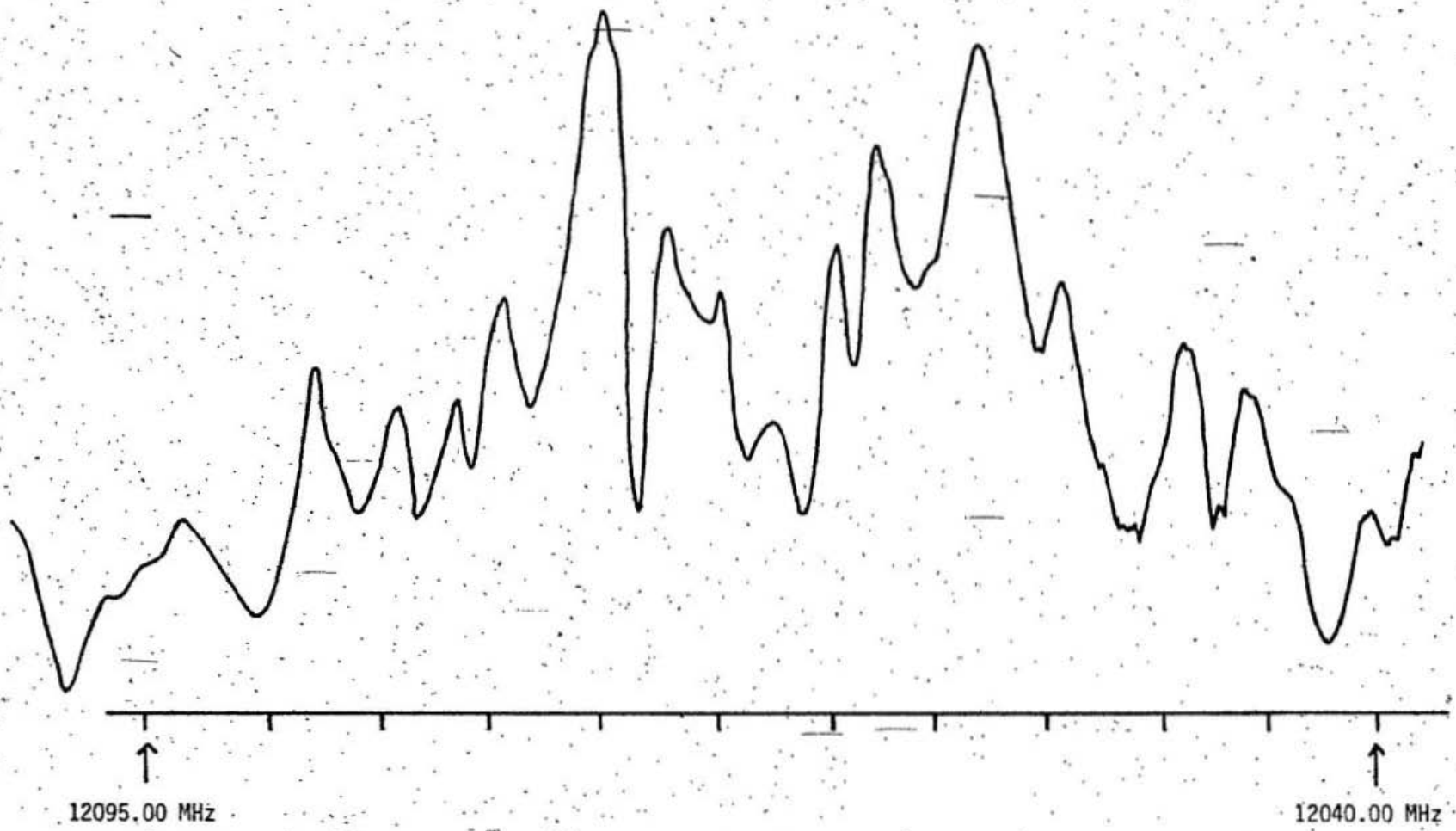

Fig. 4.5 (a). Cl^{35} isotopic species

11850.00 MHz

11785.00 MHz

Fig. 4.5 (b). Cl^{37} isotopic species

Fig. 4.6. Trace of several quadrupole components belonging to the rotational transition J=1 → 2 of tertiary butyl chloride - $(C^{12}H_3)_3C^{12}Cl^{35}$. The transition was swept at a rate of about 0.15 MHz per minute using a ten-second time constant. The horizontal scale is frequency in MHz with a spot frequency indicated by a vertical 'up' arrow. The direction of increasing frequency is indicated by the horizontal arrow. The frequency marks occur every 1.0 MHz. The Stark voltage, V_s, is as shown on each individual figure. The cell pressure was 0.050 to 0.060 torr. A vertical scale in milli-volts is shown on each figure to aid in the comparison of intensities. The hyperfine transition and observed frequency are shown above the trace with a vertical 'down' arrow pointing to the selected frequency of the component. The zero field transitions (up) are sometimes partially obscured by the Stark components (down).

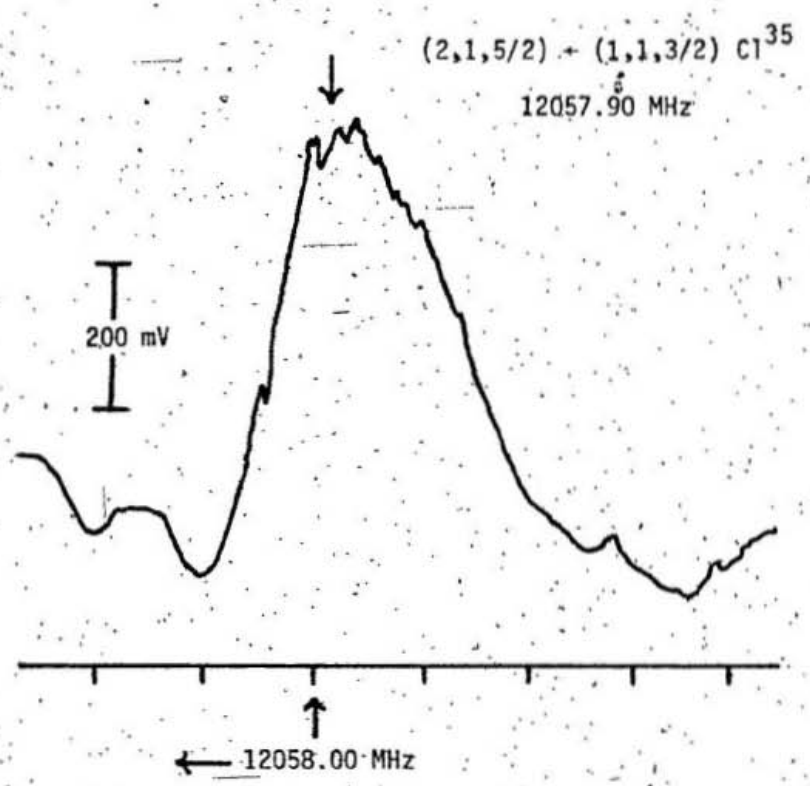

Fig. 4.6 (a). V_s = 100 volts.

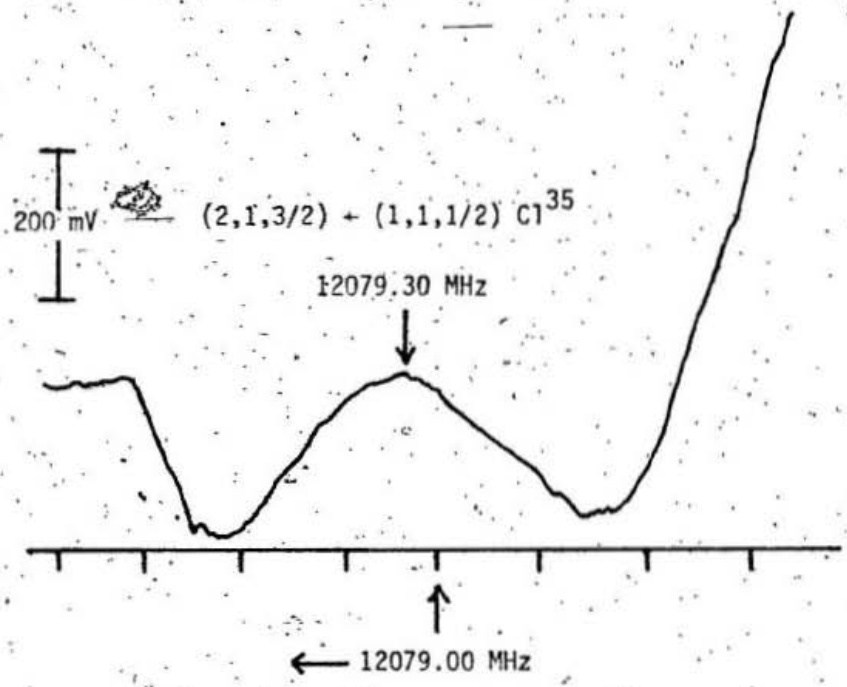

Fig. 4.6 (b). V_s = 200 volts.

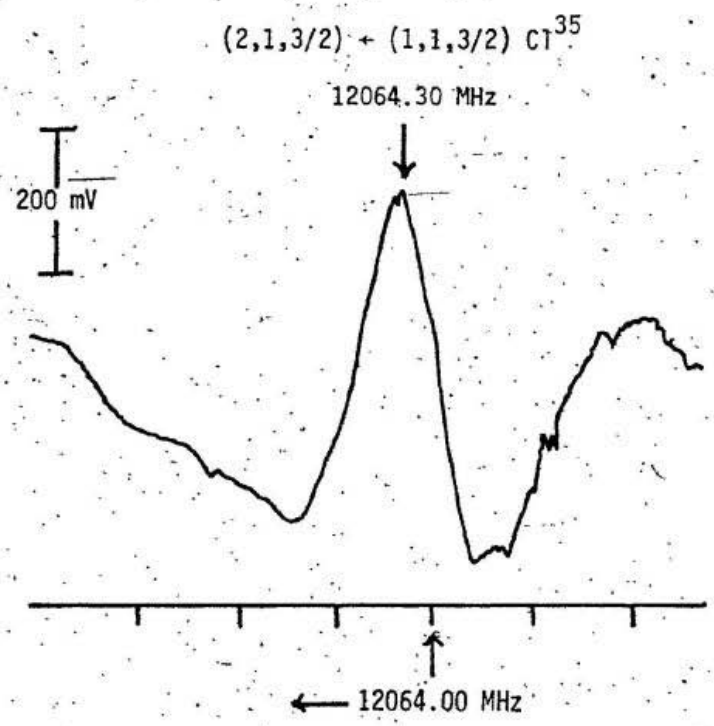

Fig. 4.6 (c). V_s = 200 volts.

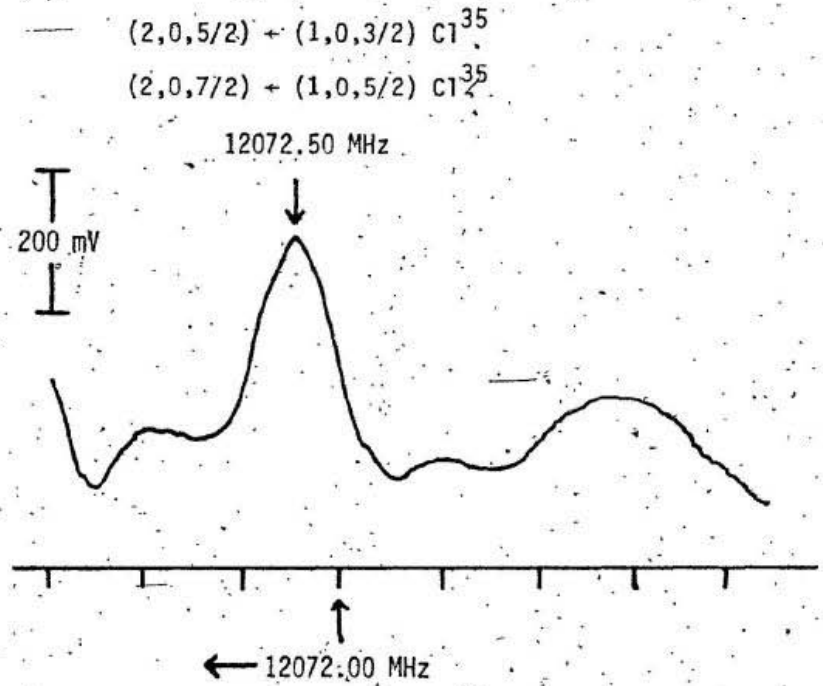

Fig. 4.6 (d). V_s = 400 volts.

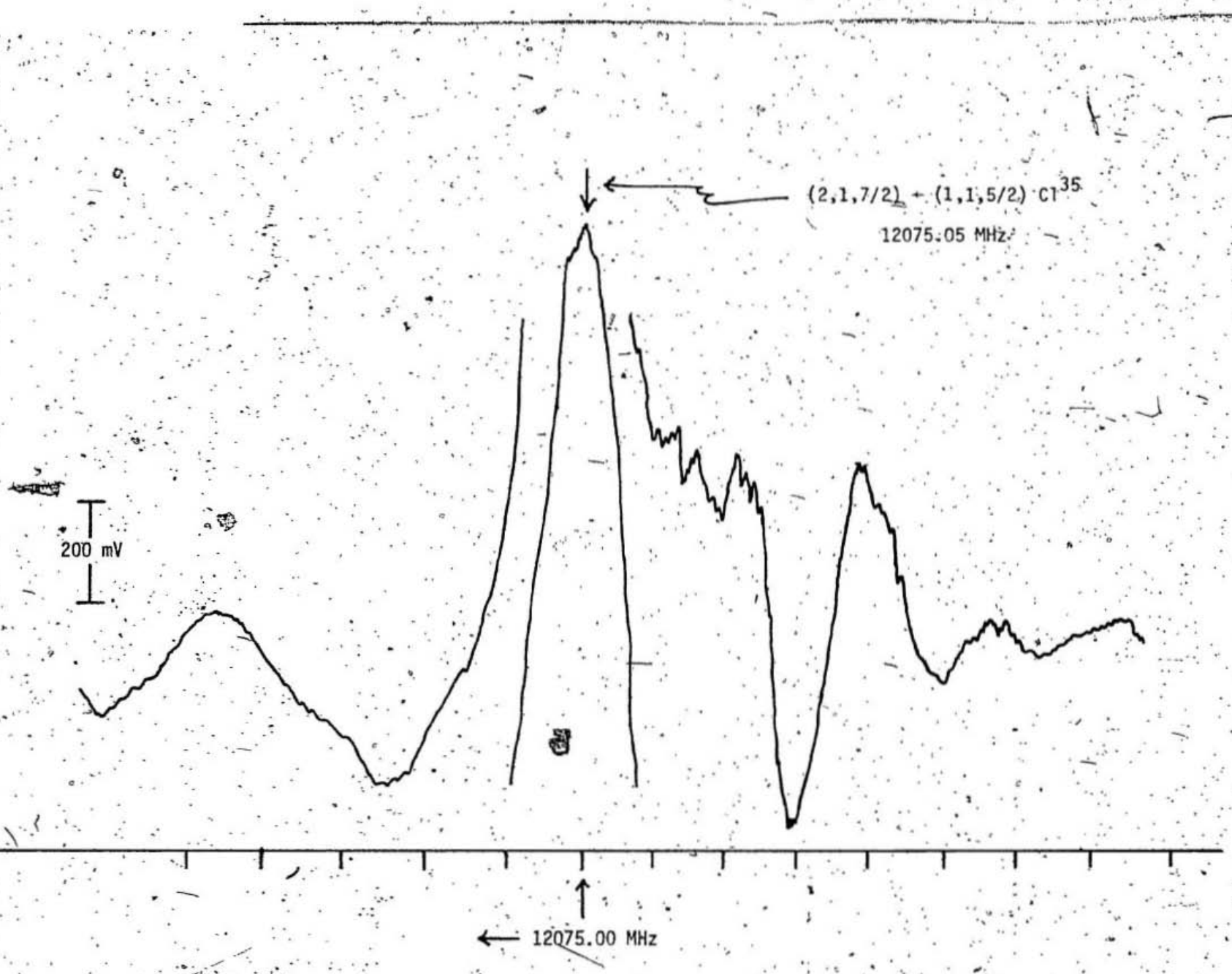

Fig. 4.6 (e). V_s = 100 volts.

Fig. 4.7. Trace of several quadrupole components belonging to the rotational transition J=1 → 2 of tertiary butyl bromide - $(C^{12}H_3)_3C^{12}Br^{79}$ and $(C^{12}H_3)_3C^{12}Br^{81}$. The transition was swept at a rate of about 0.42 MHz per minute for (a) and (b) and a rate of about 0.18 MHz per minute for (c) and (d) using a ten-second time constant. The horizontal scale is frequency in MHz with a spot frequency indicated by a vertical 'up' arrow. The direction of increasing frequency is indicated by the horizontal arrow. The frequency marks occur every 1.0 MHz. The Stark voltage, V_s, is as shown on each individual figure. The cell pressure was 0.050 to 0.060 torr. A vertical scale in milli-volts is shown on each figure to aid in the comparison of intensities. The hyperfine transition and observed frequency are shown above the trace with a vertical 'down' arrow pointing to the selected frequency of the component. The zero field transitions (up) are sometimes partially obscured by the Stark components (down).

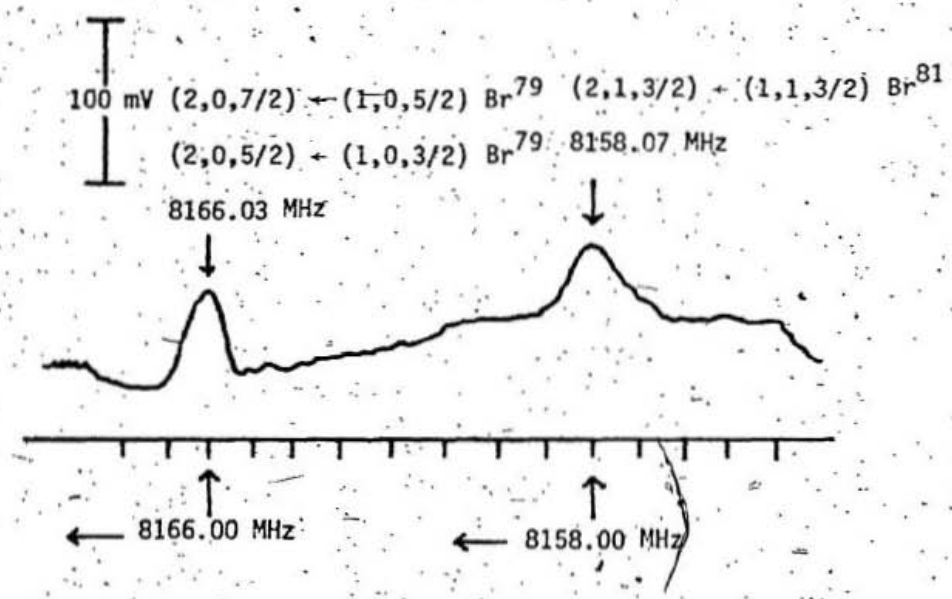

Fig. 4.7 (a). V_s = [illegible] volts.

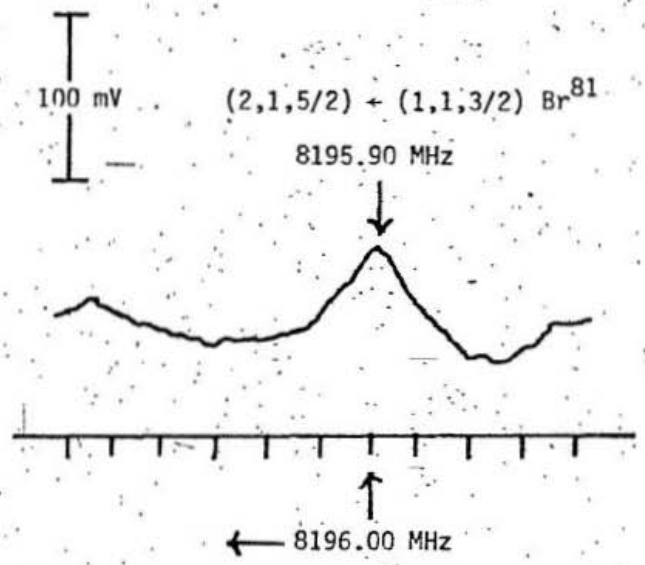

Fig. 4.7 (b). V_s = 250 volts

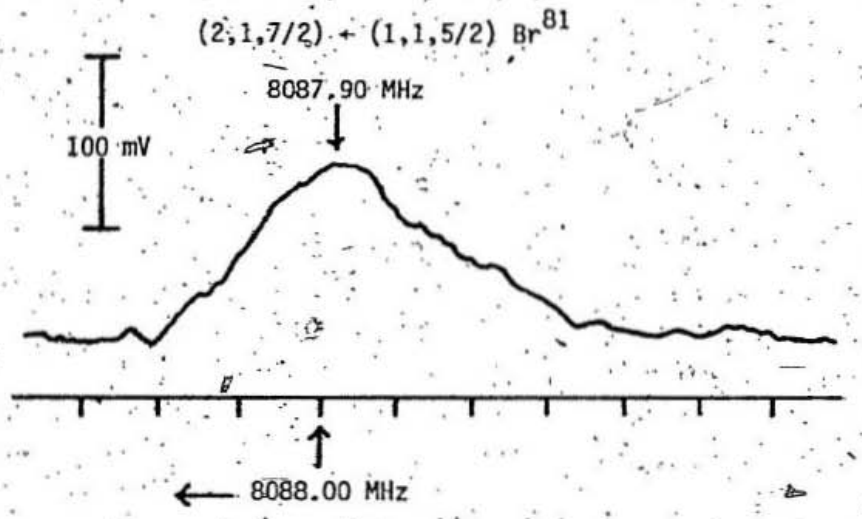

Fig. 4.7 (c). V_s = 250 volts.

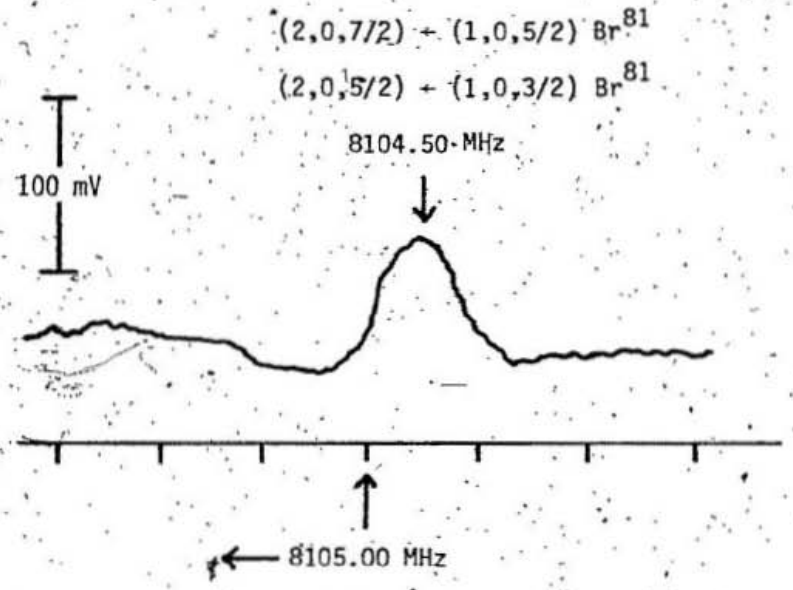

Fig. 4.7 (d). V_s = 250 volts.

Fig. 4.8. Trace of several quadrupole components belonging to the rotational transition J=2 → 3 of tertiary butyl bromide - $(C^{12}H_3)_3C^{12}Br^{79}$ and $(C^{12}H_3)_3C^{12}Br^{81}$. The transition was swept at a rate of about 0.16 MHz per minute using a ten-second time constant. The horizontal scale is frequency in MHz with a spot frequency indicated by the vertical 'up' arrow. The direction of increasing frequency is indicated by the horizontal arrow. The frequency marks occur every 1.0 MHz. The Stark voltage, V_s, is as indicated on each individual figure. The cell pressure was about 0.050 torr. A vertical scale in milli-volts is shown on each figure to aid in the comparison of intensities. The hyperfine transition and observed frequencies are shown above the trace with a vertical 'down' arrow pointing to the selected frequency of the component. The zero field (up) transitions are sometimes partially obscured by the Stark components (down).

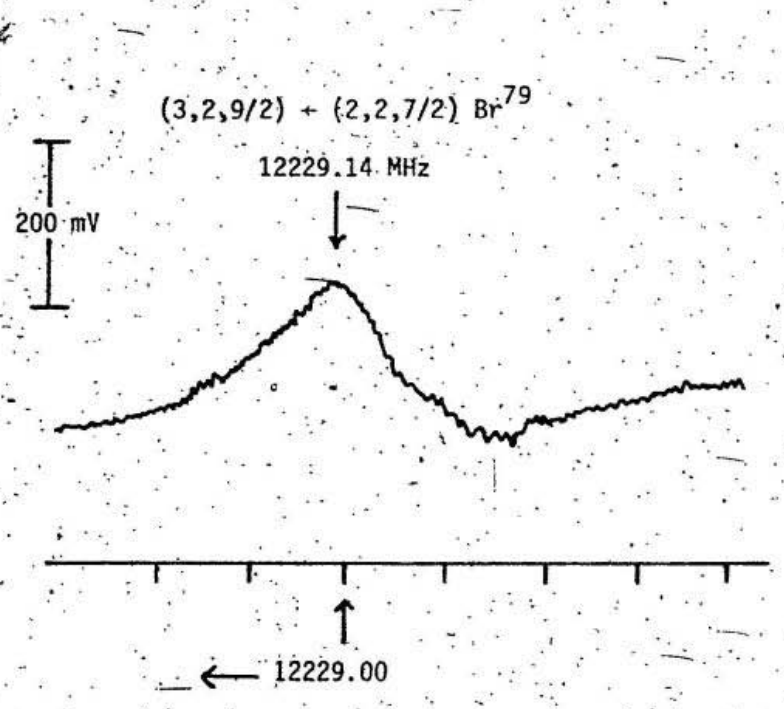

Fig. 4.8 (a). V_s = 500 volts.

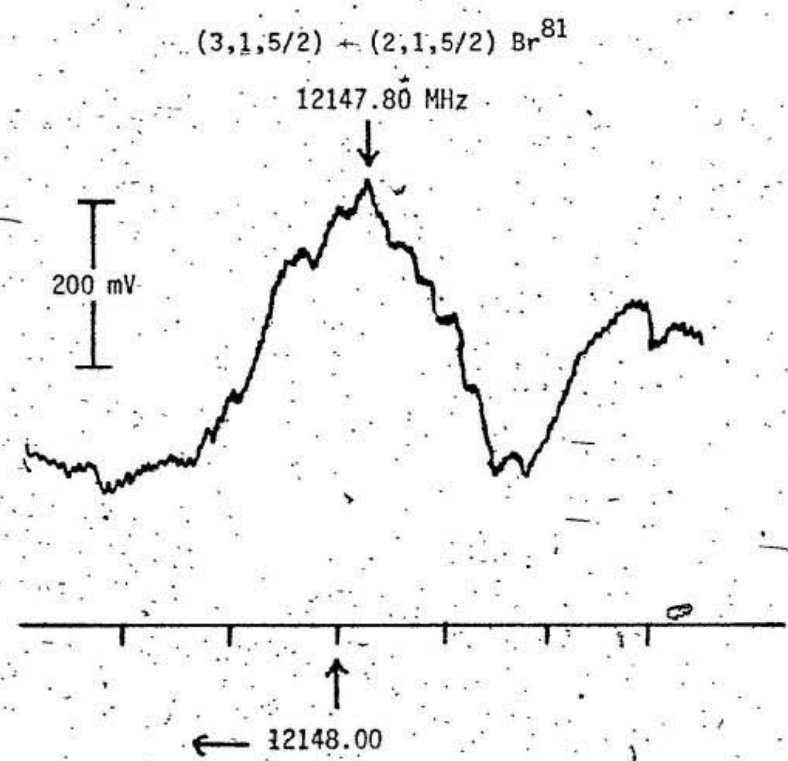

Fig. 4.8 (b). V_s = 500 volts.

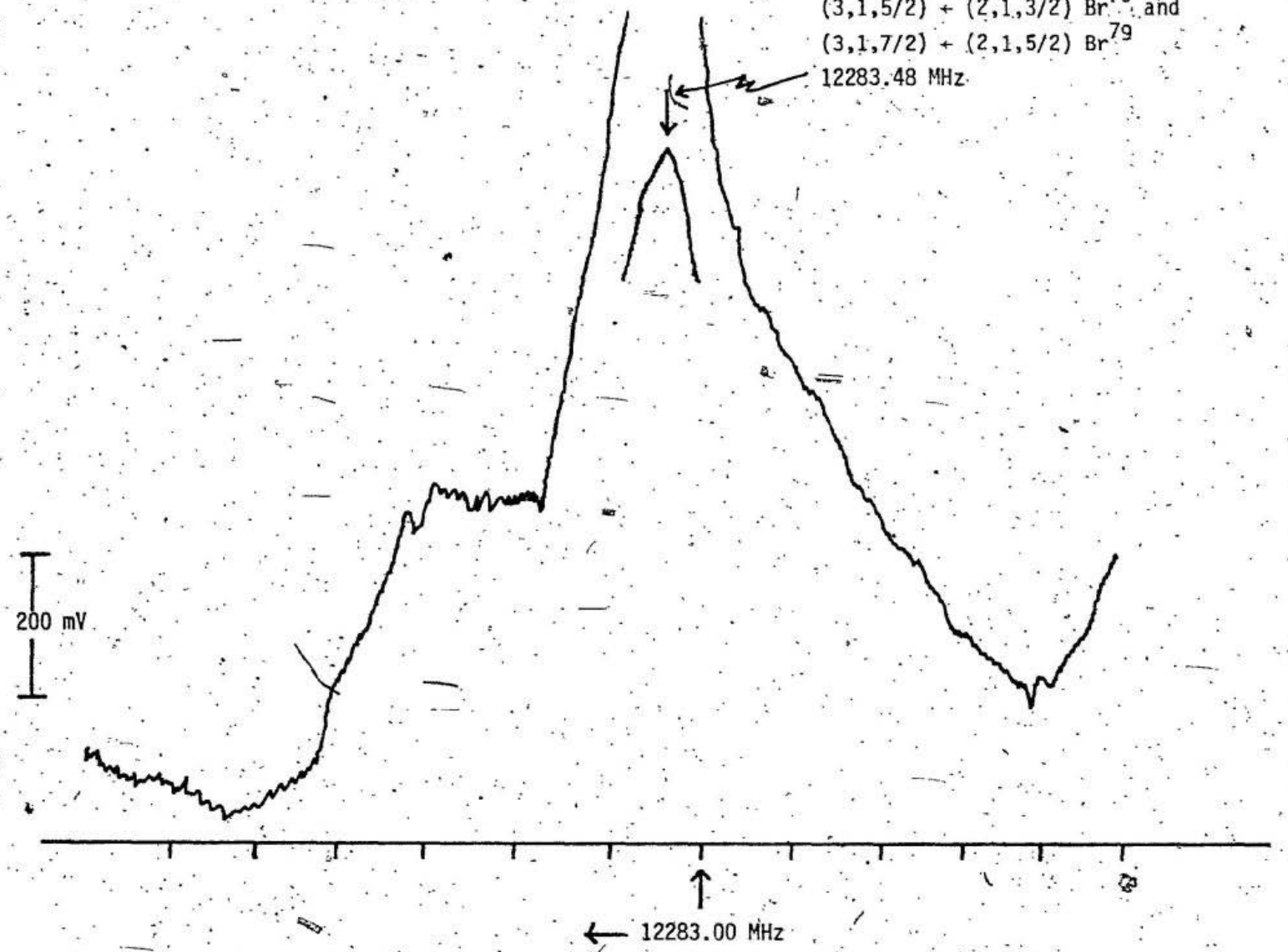

Fig. 4.8 (c). V_s = 500 volts.

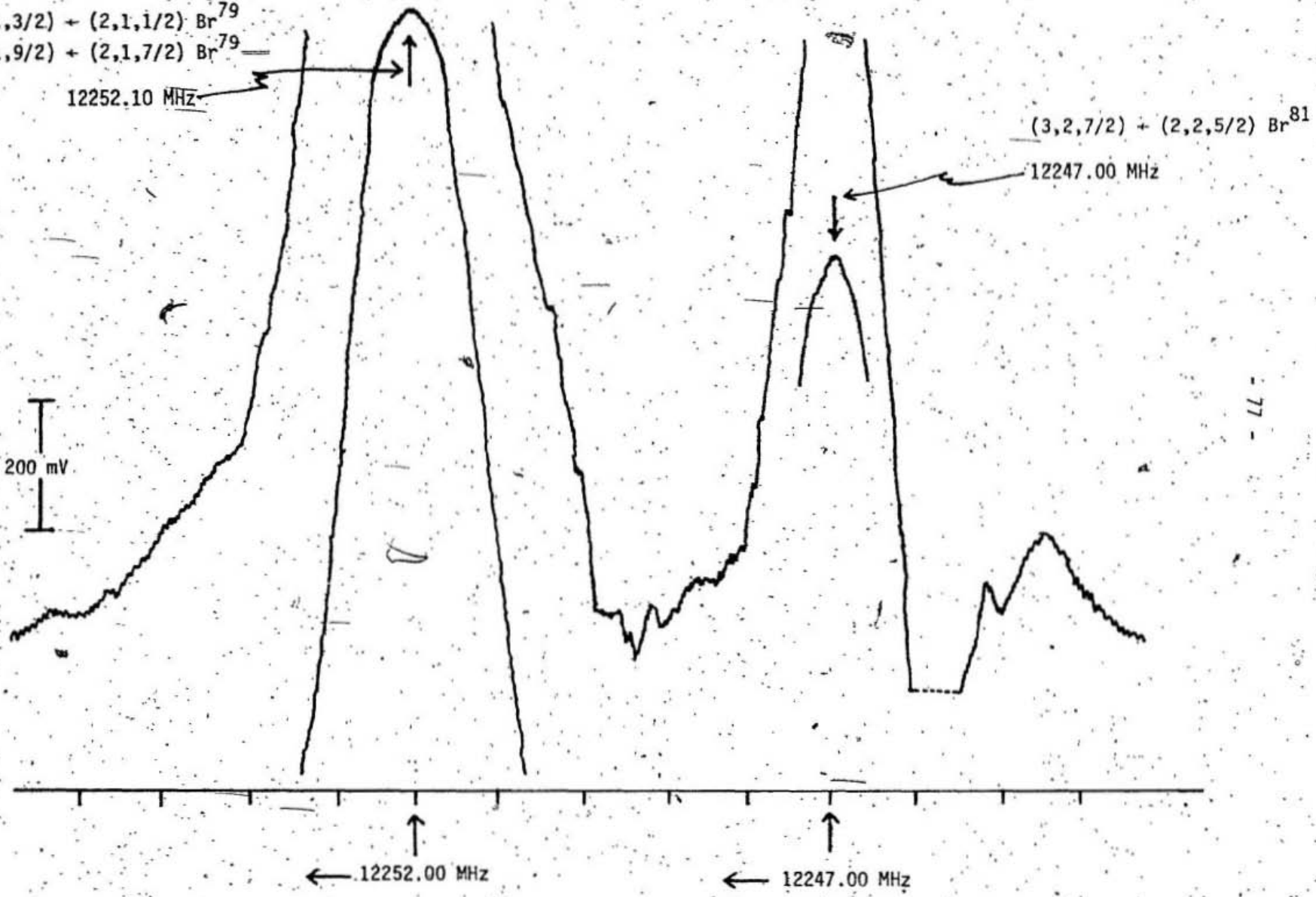

Fig. 4.8 (d): V_s = 500 volts.

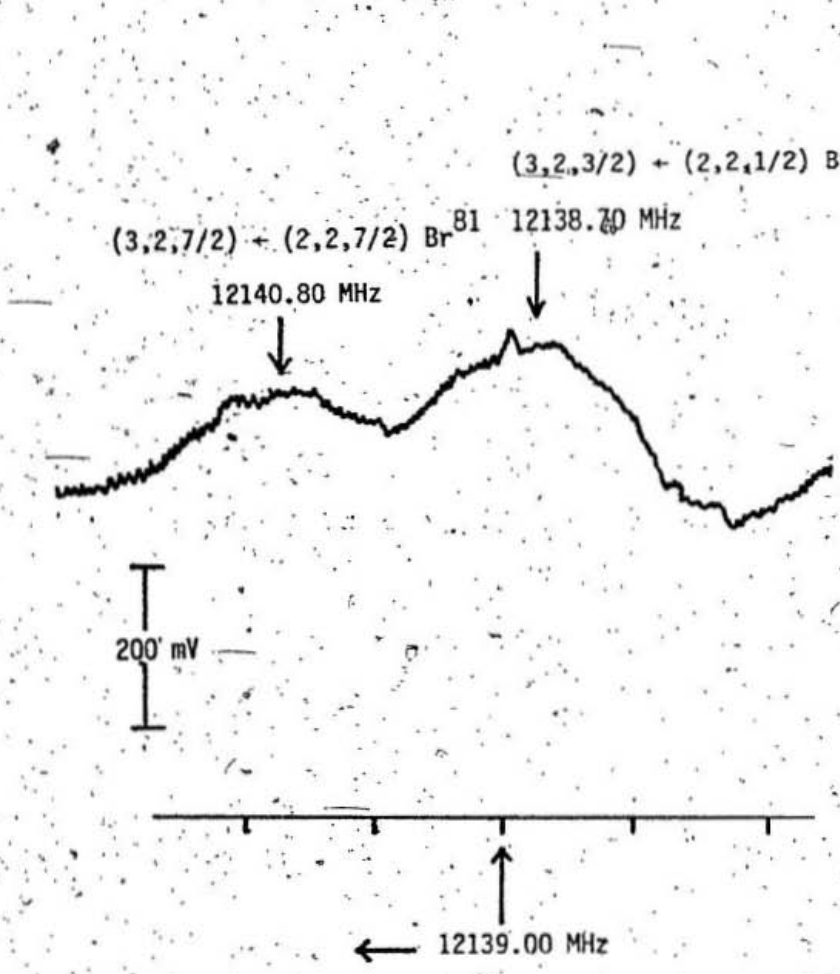

Fig. 4.8 (e). V_s = 500 volts.

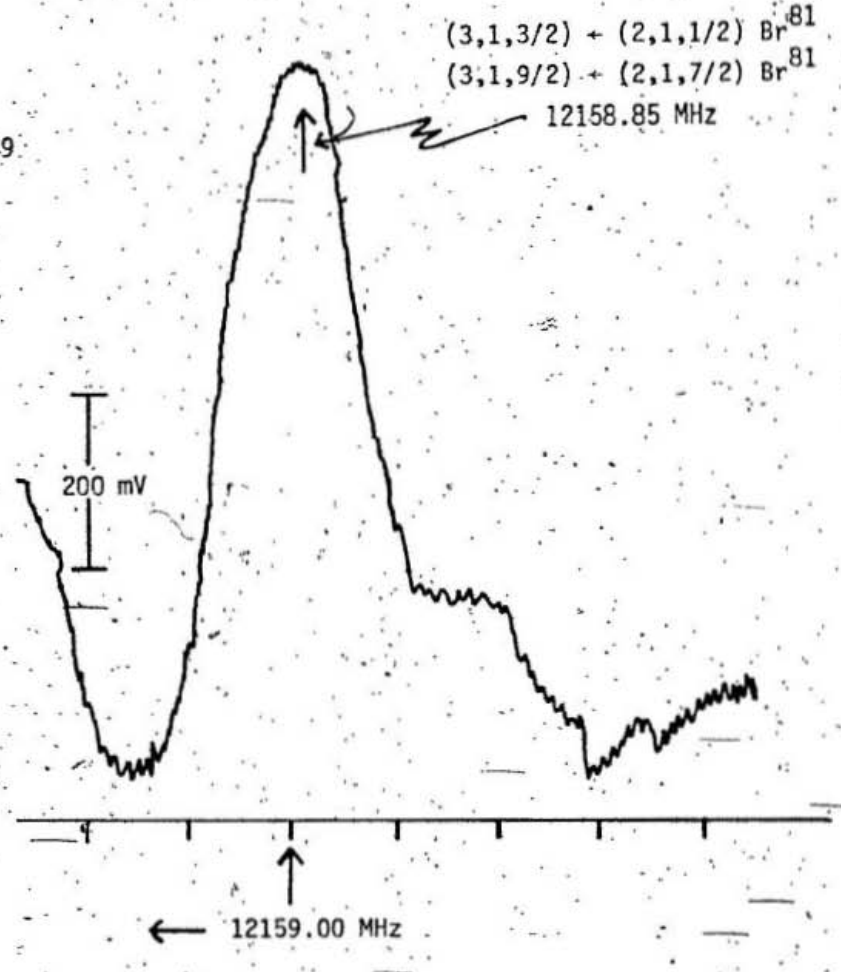

Fig. 4.8 (f). V_s = 500 volts.

Similarly the 'least squares fit' method used only lines with intensities greater than 8.000%. The results of both methods were very similar.

Calculations for each individual K level for each J transition for both molecules were performed in a similar manner to the above sample calculation.

4.2 Calibration of the Frequency Meter

As previously mentioned, the HP Electronic Counter and HP Frequency Converter were factory calibrated by the Hewlett-Packard Company but as a check we used OCS (carbonyl sulfide) as a frequency standard and observed the following results:

TABLE 4.9. Frequency calibration using the J=1 ← 0 lines of carbonyl sulfide, $O^{16}C^{12}S^{32}$

Number of Samples	MHz	Accepted Frequency*	Ratio Acc./Obs.
43	12162.973_0	12162.979_6	1.0000005
185	12162.948_5	12162.979_6	1.0000026
Mean	12162.953_1	—	1.0000022

From the above results we get a weighted average for frequency accepted: frequency observed as 1.0000022.

Hence, for this experiment, the frequencies observed would have to be corrected by multiplying by 1.0000022, a negligible correction in most cases.

*The "accepted" value was calculated by using Costain's value of 36488.8128 MHz for the J=3 ← 2 line of OCS, and the Landholdt-Bornstein value for D of 1.31×10^{-3} MHz (18).

4.3 Quadrupole Coupling Constants' Ratios

From Fuller and Cohen[14], we have the following results obtained from microwave spectroscopy:

$\frac{eQq \text{ of } Cl^{35}}{eQq \text{ of } Cl^{37}}$:

FCl	1.2704
BrCl	1.2768
GeH_3Cl	1.2670
ClCN	1.2682
CH_3Cl	1.2691
Average	1.2703

and,

$\frac{eQq \text{ of } Br^{79}}{eQq \text{ of } Br^{81}}$:

BrCN	1.197
CH_3Br	1.197
BrCl	1.1963
PBr_2	1.19711
Average	1.197

From our experiment we have the following values:

$$\frac{eQq \text{ of } Cl^{35}}{eQq \text{ of } Cl^{37}} = \frac{-67.72 \pm .63}{-52.28 \pm 1.25} = 1.295 \pm .033$$

$$\frac{eQq \text{ of } Br^{79}}{eQq \text{ of } Br^{81}} = \frac{512.34 \pm .81}{428.22 \pm 1.95} = 1.196 \pm .006$$

The results of this experiment compare favorably with those previously observed.

4.4 The Effect of Small Changes in eQq

It is useful to examine the effect that a small change in the quadrupole coupling constants would have on the first- and second-order

quadrupole coupling corrections and hence the determination of the rotational constant., This is also important in the calculations since the second-order quadrupole coupling correction was arbitrarily subtracted and thus reducing the equations 4.1 to 4.2 from second order in eQq to first order in eQq.

For the J=1 → 2 transition of tertiary butyl chloride a change in the eQq of 1 MHz would cause a maximum change in the first-order and second-order nuclear quadrupole correction energies of 0.45 MHz and 0.001 MHz, respectively. Similarly for the J=1 → 2 transition of tertiary butyl bromide we have 0.45 MHz and 0.01 MHz. Similarly for the J=2 → 3 transition of tertiary butyl bromide we have 0.38 MHz and 0.01 MHz.

Thus the manner in which the second-order nuclear quadrupole correction energy has been treated in section 4.1 is reasonable and entirely justified in this experiment.

4.5 Some Experimental Problems and Their Solutions

The vacuum system: It was very difficult to achieve a high vacuum, that is less than 0.001 torr. This was partially due to the large volume of the absorption cell and glassware and the number of potential trouble spots. However, sufficiently good vacuums were maintained to perform this research, as discussed in Section 3.3.

Frequency stabilization, voltage fluctuations, etc.: The electronic equipment was very vulnerable to fluctuations in the power mains caused by such things as start-up of heavy equipment in the vicinity, times of high power consumption, etc. This was manifested in instability in the

frequency readings, noise on the tracings. This was partially eliminated by placing isolation transformers between the equipment and the mains. Another solution was to operate the equipment during the evenings or nights when interference was at a minimum.

Stark measurements: Due to the nature of the compounds it was found difficult to measure any Stark components. It was obvious that they were present but their numbers were too great and sometimes too weak for reliable determination. For qualitative pubposes, Figure 4.9 shows the second-order Stark pattern of a linear molecule.

Temperature measurement: All observations on tertiary butyl chloride and tertiary butyl bromide were taken at the dry ice temperature. As a check on the temperature of the absorption cell, thermocouples were fastened to its outside and voltages measured by a differential voltmeter. These temperature observations were not reported here, but it suffices to say all were within two to three degrees of the dry ice temperature after the box enclosing the cell had been filled with dry ice for one-half to one hour.

These are just a few of the problems encountered but may be considered representative. Other problems encountered and partially solved would include: the motor drive mechanism to achieve a slow sweep rate; the filter change in the receiver to give larger time constants; the need for crystal elements with very high signal to noise ratios; reflections in the guide; breakdown at high voltages; phasing of signals for the phase sensitive detector; adjusting the pre-amplifier for maximum

Fig. 4.9. Trace of the rotational transition J=2 → 3 of an unidentified linear molecule. The transition was swept at a rate of about 5 MHz per minute using a ten-second time constant. The horizontal scale is frequency in MHz with a spot frequency indicated by a vertical 'up' arrow. The direction of increasing frequency is indicated by the horizontal arrow. The frequency marks occur every 0.5 MHz. The Stark voltage, V_S, and temperature, T, are indicated on each individual figure. The cell pressure was about 0.020 torr. A vertical scale in milli-volts is shown on each figure to aid in the comparison of intensities.

Note: Traces of this and all other observed transitions were also produced at much slower sweep rates and show correspondingly more detail. The example here is merely illustrative.

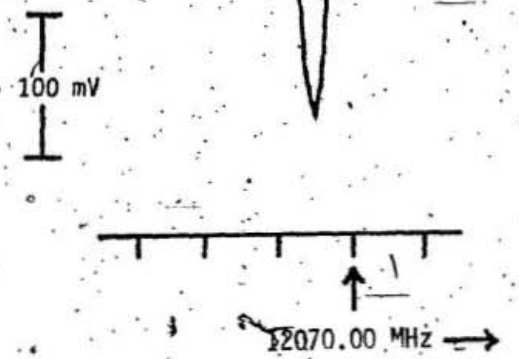

Fig. 4.9 (a)

V_s = 100 volts

T = 88°C

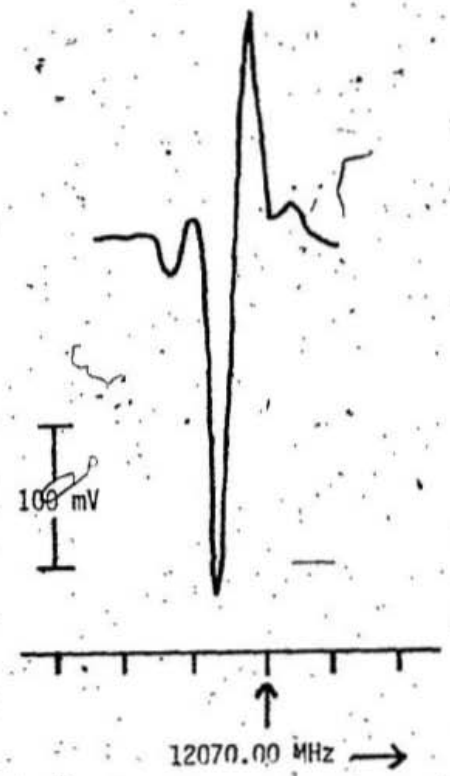

Fig. 4.9 (b)

V_s = 200 volts

T = 88°C

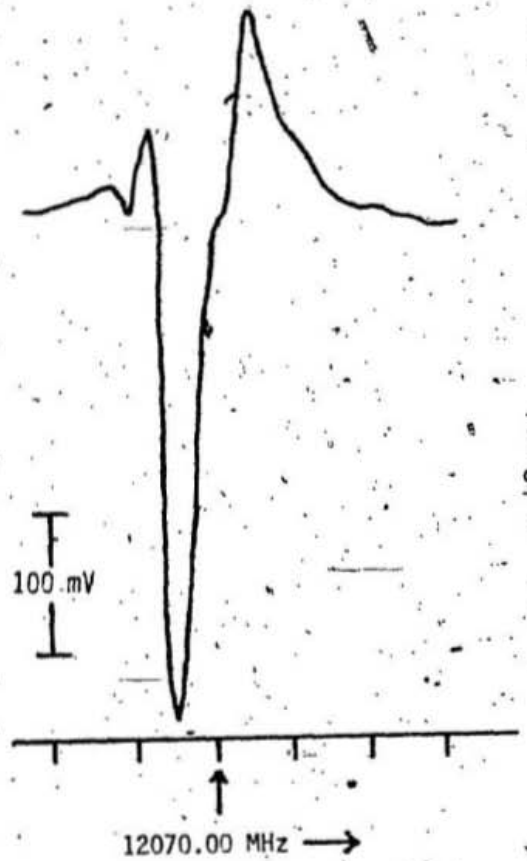

Fig. 4.9 (c)

V_s = 300 volts

T = 89°C

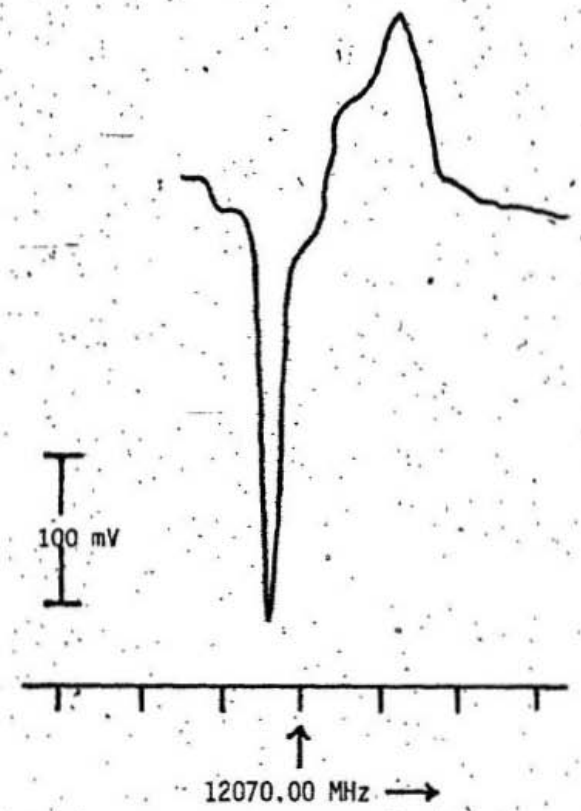

Fig. 4.9 (d)

V_s = 400 volts

T = 89°C

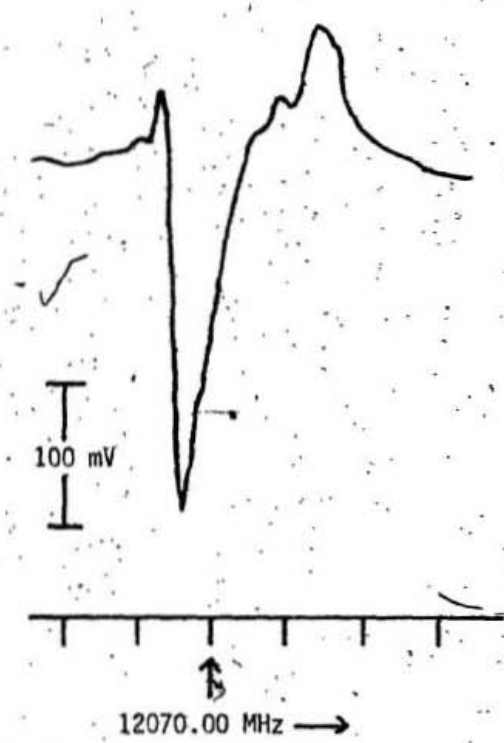

Fig. 4.9 (e)

V_s = 500 volts

T = 90°C

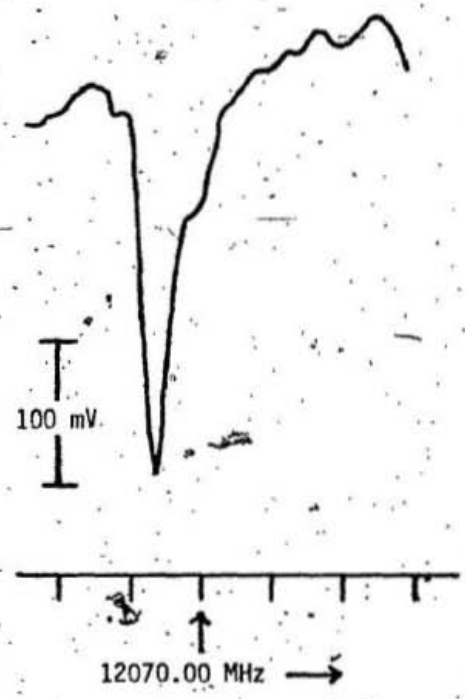

Fig. 4.9 (f)

V_s = 600 volts

T = 91°C

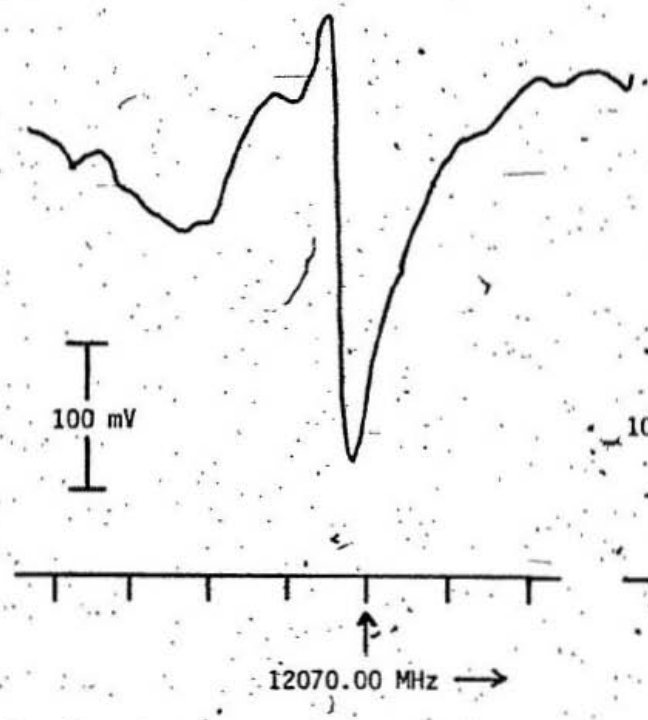

Fig. 4.9 (g)

V_s = 700 volts

T = 91°C

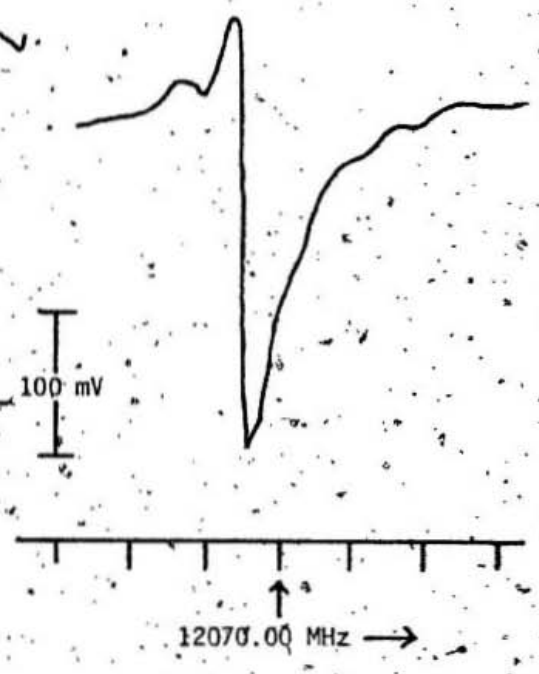

Fig. 4.9 (h)

V_s = 800 volts

T = 92°C

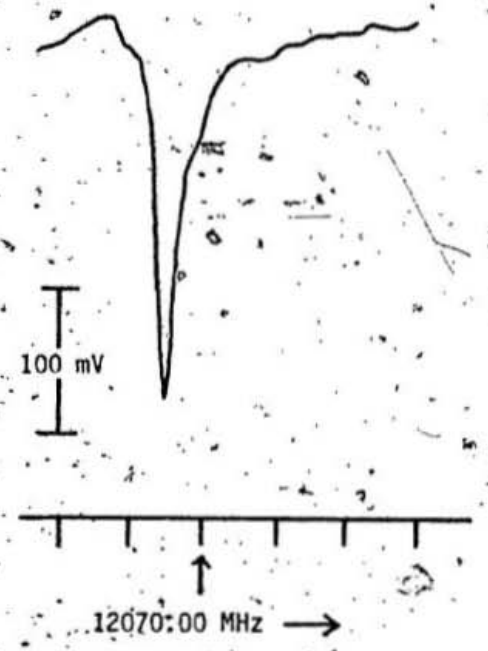

Fig. 4.9 (i)

V_s = 900 volts

T = 92°C

results; grounding problems; maintaining a balanced receiver; presence of ammonia in the guide; inability to detect the tri-methyltin bromide spectrum.

4.6 Miscellaneous Results - Ammonia

During the early stages of the experimental portion of this thesis we were examining the ammonia spectrum in an effort to look at previously identified lines and to discover new lines. This was part of the 'setting up' of the microwave spectroscopy lab. This eventually led to some computational work on the anomalous K=3 inversion lines of $N^{14}H_3$ which is reported below:

The normal inversion lines of $N^{14}H_3$ can be predicted as $\nu_{calc}(J,K)$ by using an empirical formula such as Costain's[15] for all pairs of J,K values except those with K=3. In the K=3 case, Nielson and Dennison[16,17] have shown that the frequencies of these lines can be computed from

$$\nu(J,3) = \nu_{calc}(J,3) + (-1)^J A_J J(J+1)[J(J+1) - 2][J(J+1) - 6] \qquad (4.4)$$

according to Townes and Schawlow[9] where $A_J = 3.5 \times 10^{-4}$. This formula gives good results for $J \leq 7$, but the error grows rapidly to 384 MHz at J=14. The frequencies of these K=3 lines are reported in the N.B.S. Microwave Spectral Tables[5] for all J values from 3 to 14 with the exception of J=13.

The quantity A_J was computed by using the difference between the observed and calculated frequencies ($\nu_{obs} - \nu_{calc}$) and was found to drop very linearly with increasing values of J(J+1).

ν_{calc} was computed from a revised form of Costain's formula fitted to forty-five lines from the Microwave Spectral Tables with frequencies below 16 GHz. Costain's formula is essentially

$$\nu = \nu_0 \exp S_n \qquad (4.5)$$

where S_n is a polynomial of degree n in J(J+1) and K^2. We used as ν_{calc} the

TABLE 4.10. The uncorrected, corrected and observed frequencies of certain $N^{14}H_3$ lines with K=3

J	7	8	9	10	11
ν_{calc} (uncorrected)	18072.9	16342.3	14600.2	12887.6	11239.7
$\nu(J,3)$ (computed)	18020.9	16455.4	14377.0	13296.5	10535.7
$\nu(J,3)$ (observed)	18017.42	16455.13	14376.56	13296.37	10536.30
	12	13	14	15	16
ν_{calc} (uncorrected)	9684.8	8245.1	6936.3	5768.2	4744.6
$\nu(J,3)$ (computed)	10837.2	6437.7	9669.2	1766.1	10442.4
$\nu(J,3)$ (observed)	10836.10	—	9670.78	—	—

average of the results from polynomials of the 4th, 5th, and 6th degrees in $J(J+1)$ and K^2. The resulting values of A_J plotted against $J(J+1)$ produced a line of negative slope that is very nearly straight up to J=14 which by a least squares fit can be represented as

$$A_J = 3.57582 \times 10^{-4} [1 - J(J+1)/1475.63] \text{ MHz} \qquad (4.6)$$

with an R.M.S. error of 0.61 MHz over the range J = 7, 8, 9, 10, 11, 12, and 14.

The frequencies predicted using eq. 4.6 have an R.M.S. error of 2.3 MHz compared to an R.M.S. error of 404 MHz obtained when A_J has the constant value 3.5×10^{-4}.

4.7 Summary of Results

Table 4.8 gives a summary of the spectral constants in tertiary butyl chloride and tertiary butyl bromide. Our results are in good agreement with the previously determined values. However this experiment has added the following:

$(C^{12}H_3)_3C^{12}Cl^{35}$:

Previously the spectrum had been observed in the region 18 GHz to 42 GHz or from J=2 → 3 to J=6 → 7. A partial resolution of the hyperfine structure of the J=2 → 3 transition was achieved; for the remaining rotational transitions no hyperfine structure was resolved. We have extended that coverage by including the J=1 → 2 transition in the 12 GHz region with a partial resolution of the hyperfine structure. Our observation of the eQq agrees with that previously reported.

$(C^{12}H_3)_3C^{12}Cl^{37}$:

Previously the spectrum of this less dominant (25%) species of tertiary butyl chloride had been observed in the region 23 GHz to 41 GHz or from J=4 → 5 to J = 6 → 7. No quadrupole hyperfine structure was resolved. We have extended that coverage by including the J=1 → 2 transition in the 11 GHz region with a partial resolution of the hyperfine structure. From the hyperfine structure we have determined a value for the quadrupole coupling constant eQq.

$(C^{12}H_3)_3C^{12}Br^{79}$:

Previously the spectrum has been observed in the region 20 GHz to 40 GHz or from J=4 → 5 to J=9 → 10. A partial resolution of the hyperfine structure of the J=4 → 5 transition was achieved; for the remaining rotational transitions no hyperfine structure was resolved. We have extended that coverage by including the J=1 → 2 and J=2 → 3 transitions in the 8 GHz and 12 GHz regions, respectively. A partial resolution of the hyperfine structure of both those transitions was achieved. Our observations of the eQq's agree with those previously reported.

$(C^{12}H_3)_3C^{12}Br^{81}$:

Previously the spectrum had been observed in the region 20 GHz to 40 GHz or from J=4 → 5 to J=9 → 10. A partial resolution of the hyperfine structure of the J=4 → 5 transition was reported; for the remaining transitions no hyperfine structure was resolved. We have extended that coverage by including the J=1 → 2 and J=2 → 3 transitions in the 8 GHz and 12 GHz regions, respectively. A partial resolution of the hyperfine

structure of both those transitions was achieved. Our observations of the eQq's agree with those previously reported.

LIST OF REFERENCES

1. D.R. Lide Jr. and M. Jen, J. Chem. Phys. 38, 1504 (1963).
2. J.Q. Williams and W. Gordy, J. Chem. Phys. 18, 994 (1950).
3. W. Zeil, M. Winnewisser and K. Muller, Z. Naturforsch. 16a, 1250 (1961).
4. B. Starck, Molecular constants from Microwave Spectroscopy, Vol. 4, Group II, Atomic and Molecular Physics, Numerical Data and Functional Relationships in Science and Technology; Landolt Bornstein.
5. Microwave Spectral Tables, Monograph 70, Vols. I to V; National Bureau of Standards.
6. W. Zeil, M. Winnewisser and W. Huttner, Z. Naturforsch. 16a, 1248 (1961).
7. W. Gordy and R.L. Cook, Microwave Molecular Spectra, Vol. IX, Chemical Applications of Spectroscopy, Part II; Interscience (1970).
8. W. Gordy, W.V. Smith and R.F. Trambarulo, Microwave Spectroscopy; Wiley (1953).
9. C.H. Townes and A.L. Schawlow, Microwave Spectroscopy; McGraw-Hill (1955).
10. J.E. Wollrab, Rotational Spectra and Molecular Structure; Academic Press (1967).
11. T.M. Sudgen and C.N. Kenney, Microwave Spectroscopy of Gases; Van Nostrand (1965).
12. F.A. Cotton, Chemical Applications of Group Theory; Wiley - Interscience (1963).
13. M. Orchin and H.H. Jaffe, Symmetry, Orbitals and Spectra; Wiley (1971).

14. G.H. Fuller and V.W. Cohen, Nuclear Data Tables A, Vol. 5, Nos. 5-6, 479 (1969).

15. C.C. Costain, Phys. Rev, 82, 108 (1951).

16. H.H. Nielson and D.M. Dennison, Phys. Rev. 72, 86 (1947).

17. H.H. Nielson and D.M. Dennison, Phys. Rev. 72, 1101 (1947).

18. C.C. Costain, Can. J. Phys. 47, 2431 (1969).

APPENDIX A

TABLE A-1. Isotopic Data

Z	Isotope*	% Natural Abundance	Atomic Mass
H	H		1.00797
1	$_1H$	99.985	1.007825
	$_1H^2$	0.015	2.0140
C			12.01115
6	$_6C^{12}$	98.89	12.0000
	$_6C^{13}$	1.11	13.00335
Cl			35.453
17	$_{17}Cl^{35}$	75.53	34.96885
	$_{17}Cl^{37}$	24.47	36.96589
Br			79.909
35	$_{35}Br^{79}$	50.54	78.9183
	$_{35}Br^{81}$	49.46	80.9163

*Only those isotopes with measurable abundance and occurring in the natural state are given here.

APPENDIX B

ENERGIES AND RELATIVE INTENSITIES OF NUCLEAR QUADRUPOLE HYPERFINE STRUCTURE

The function Y(J,I,F) and the relative intensities are tabulated for nuclear spin 3/2 and the J values 0, 1, 2 and 3.

$$Y(J,I,F) = \frac{3/4\,C(C+1) - I(I+1)J(J+1)}{2(2J+3)(2J-1)I(2I-1)}$$

where $C = F(F+1) - I(I+1) - J(J+1)$ and F takes the values J+I, J+I-1, ..., J-I.

The quadrupole energies are given by

$$E_Q = \frac{eQq_J\,(2J+3)}{J}\,Y(J,I,F)$$

The appropriate q_J for a linear, symmetric or asymmetric rotor must be used. The relative intensities have been normalized such that the sum of the intensities of the various hyperfine components of a transition is 100. The intensities for the J+1 → J transitions are obtained by reversal of the arrows in the entries for J → J+1. Thus the entries for F → F+1 correspond to F+1 → F and those for F → F-1 to F-1 → F.

TABLE B.1. Energies and relative intensities of nuclear quadrupole hyperfine structure

			Relative Intensities		
			J → J+1		
J	F	Y(J,I,F)	F → F+1	F → F	F → F-1
0	3/2	0.0	50.000	33.333	16.667
1	5/2	0.050000	40.000	9.000	1.000
1	3/2	-0.200000	21.000	10.667	1.667
1	1/2	0.250000	8.333	8.333	0.0
2	7/2	0.071429	35.714	4.082	0.204
2	5/2	-0.178571	24.490	5.224	0.286
2	3/2	0.0	16.000	4.000	0.0
2	1/2	0.250000	10.000	0.0	0.0
3	9/2	0.083333	33.333	2.315	0.066
3	7/2	-0.166667	25.463	3.023	0.085
3	5/2	0.050000	19.133	2.296	0.0
3	3/2	0.200000	14.286	0.0	0.0

APPENDIX C

NUCLEAR QUADRUPOLE SECOND-ORDER CORRECTION ENERGIES FOR LINEAR OR SYMMETRIC-TOP MOLECULES

To obtain $E_Q^{(2)}$ the entries given below are to be multiplied by the factor $\frac{(eQq)^2}{B} \times 10^{-3}$.

TABLE C.1. For I = 3/2, nuclear quadrupole second-order correction energies for linear or symmetric-top molecules

J	F	K = 0	K = 1	K = 2	K = 3
0	3/2	-10.4167			
1	5/2	- 6.0000	- 9.4688		
1	3/2	- 2.2500	-10.8750		
1	1/2	0.0000	-11.7188		
2	7/2	- 4.0999	- 5.6487	- 7.2855	
2	5/2	2.1866	2.4561	- 3.8875	
2	3/2	10.4167	5.2082	-10.4170	
2	1/2	0.0000	11.7188	0.0000	
3	9/2	3.0864	- 3.8520	- 5.3818	-5.3858
3	7/2	- 1.9290	0.2170	3.4721	1.7119
3	5/2	6.0000	3.4466	- 2.6042	-7.3244
3	3/2	2.2500	5.6668	10.4170	0.0000

APPENDIX D

OBSERVATIONS USED TO CALCULATE THE MOLECULAR PARAMETERS eQq, B_o, AND ν_o

The tables on the following pages of this Appendix contain the observations and related calculations used to calculate the molecular parameters eQq, B_o, and ν_o for the J=1 → 2 rotational transitions of $(C^{12}H_3)_3C^{12}Cl^{35}$, $(C^{12}H_3)_3C^{12}Cl^{37}$, $(C^{12}H_3)_3C^{12}Br^{79}$ and $(C^{12}H_3)_3C^{12}Br^{81}$, and the J=2 → 3 rotational transitions of $(C^{12}H_3)_3C^{12}Br^{79}$ and $(C^{12}H_3)_3C^{12}Br^{81}$. F_2 and F_1 are observed hyperfine components of a given K multiplet. The intensities given are relative to that particular K level only and follow from Table B.1. $\Delta\nu$ is the frequency difference in MHz between the F_2 and F_1 components. Using the appropriate factors from Table B.1 the indfvidual eQq's were computed. Further and complete details on the method of calculation of the molecular parameters may be found in Section 4.1. The relative intensities have been normalized so that the sum of the intensities of the various hyperfine components of a transition is 100.

TABLE D.1. Observations used to calculate the parameters eQq, B_o, and ν_o of the J = 1 → 2 rotational transition of $(CH_3)_3CCl^{35}$

K Transition	F_2 Transition	F_1 Transition	Intensity F_2	Intensity F_1	Δν MHz	eQq MHz
0	3/2 ← 3/2	7/2 ← 5/2	10.667	40.000	-11.83±.11	-66.25±.62
0	3/2 ← 3/2	5/2 ← 3/2	10.667	21.000	-11.83±.11	-66.25±.62
0	3/2 ← 3/2	1/2 ← 1/2	10.667	8.333	-13.28±.11	-66.40±.55
0	3/2 ← 3/2	5/2 ← 5/2	10.667	9.000	-29.09±.11	-67.88±.26
0	7/2 ← 5/2	5/2 ← 3/2	40.000	21.000	0.0 ±.07	
0	7/2 ← 5/2	1/2 ← 1/2	40.000	8.333	- 1.45±.07	-67.67±3.27
0	7/2 ← 5/2	5/2 ← 5/2	40.000	9.000	-17.26±.07	-69.04±.28
0	5/2 ← 3/2	1/2 ← 1/2	21.000	8.333	- 1.45±.07	-67.67±2.27
0	5/2 ← 3/2	5/2 ← 5/2	21.000	9.000	-17.26±.07	-69.04±.28
0	1/2 ← 1/2	5/2 ← 5/2	8.333	9.000	-15.81±.07	-69.17±.31
1	7/2 ← 5/2	3/2 ← 3/2	40.000	10.667	-10.76±.07	-66.95±.44
1	7/2 ← 5/2	5/2 ← 3/2	40.000	21.000	-17.16±.11	-68.64±.44
1	7/2 ← 5/2	1/2 ← 1/2	40.000	8.333	-12.84±.07	-67.83±.37
1	7/2 ← 5/2	3/2 ← 1/2	40.000	8.333	- 4.23±.11	-65.60±1.71
1	7/2 ← 5/2	5/2 ← 5/2	40.000	9.000	- 8.56±.07	-68.48±.56
1	3/2 ← 3/2	5/2 ← 3/2	10.667	21.000	- 6.40±.11	-71.68±1.23
1	3/2 ← 3/2	1/2 ← 1/2	10.667	8.333	-23.60±.07	-67.43±.20
1	3/2 ← 3/2	3/2 ← 1/2	10.667	8.333	-14.99±.11	-66.62±.49
1	3/2 ← 3/2	5/2 ← 5/2	10.667	9.000	- 2.20±.07	-61.60±1.96
1	5/2 ← 3/2	1/2 ← 1/2	21.000	8.333	-30.00±.11	-68.29±.25
1	5/2 ← 3/2	3/2 ← 1/2	21.000	8.333	-21.39±.14	-68.06±.45
1	5/2 ← 3/2	5/2 ← 5/2	21.000	9.000	- 8.90±.11	-71.20±.88
1	1/2 ← 1/2	3/2 ← 1/2	8.333	8.333	- 8.61±.11	-68.88±.88
1	3/2 ← 1/2	5/2 ← 5/2	8.333	9.000	-21.40±.07	-68.09±.22
1	3/2 ← 1/2	5/2 ← 5/2	8.333	9.000	-12.79±.11	-67.57±.58

TABLE D.2. Observations used to calculate the parameters eQq, B_o, and ν_o of the J = 1 ← 2 rotational transition of $(CH_3)_3CCl^{37}$

K Transition	F_2 Transition	F_1 Transition	Intensity F_2	Intensity F_1	Δν MHz	eQq MHz
0	3/2 ← 3/2	7/2 ← 5/2	10.667	40.000	- 8.89±.11	-49.78±.62
0	3/2 ← 3/2	5/2 ← 3/2	10.667	21.000	- 8.89±.11	-49.78±.62
0	3/2 ← 3/2	1/2 ← 1/2	10.667	8.333	-10.46±.14	-52.30±.70
0	3/2 ← 3/2	3/2 ← 1/2	10.667	8.333	-24.25±.14	-53.89±.31
0	7/2 ← 5/2	5/2 ← 3/2	40.000	21.000	0.0 ±.07	
0	7/2 ← 5/2	1/2 ← 1/2	40.000	8.333	- 1.57±.11	-73.27±5.13
0	7/2 ← 5/2	3/2 ← 1/2	40.000	8.333	-15.36±.11	-56.59±.41
0	5/2 ← 3/2	1/2 ← 1/2	21.000	8.333	- 1.57±.11	-73.27±5.13
0	5/2 ← 3/2	3/2 ← 1/2	21.000	8.333	-15.36±.11	-56.59±.41
0	1/2 ← 1/2	3/2 ← 1/2	8.333	8.333	-13.79±.14	-55.16±.56
1	7/2 ← 5/2	5/2 ← 3/2	40.000	21.000	-13.51±.14	-54.04±.56
1	7/2 ← 5/2	1/2 ← 1/2	40.000	8.333	- 9.13±.18	-48.23±.95
1	7/2 ← 5/2	3/2 ← 1/2	40.000	8.333	- 2.60±.11	-40.44±1.71
1	5/2 ← 3/2	1/2 ← 1/2	21.000	8.333	-22.64±.18	-51.54±.41
1	5/2 ← 3/2	3/2 ← 1/2	21.000	8.333	-16.11±.11	-51.26±.35
1	1/2 ← 1/2	3/2 ← 1/2	8.333	8.333	- 6.53±.16	-52.24±1.28

TABLE D.3. Observations used to calculate the parameters eQq, B_0, and ν_0 of the J = 1 ← 2 rotational transition of $(CH_3)_3CBr^{79}$

K Transition	F_2 Transition	F_1 Transition	Intensity F_2	Intensity F_1	Δν MHz	eQq MHz
0	7/2 ← 5/2	5/2 ← 3/2	40.000	21.000	0.23±.07	
0	7/2 ← 5/2	3/2 ← 3/2	40.000	10.667	91.32±.20	511.39±1.12
0	7/2 ← 5/2	1/2 ← 1/2	40.000	8.333	10.61±.07	495.12±3.27
0	5/2 ← 3/2	3/2 ← 3/2	21.000	10.667	91.55±.20	512.68±1.12
0	5/2 ← 3/2	1/2 ← 1/2	21.000	8.333	10.38±.07	484.39±3.27
0	3/2 ← 3/2	1/2 ← 1/2	10.667	8.333	101.93±.20	509.65±1.00
1	5/2 ← 3/2	3/2 ← 3/2	21.000	10.667	45.64±.07	511.17±.78
1	5/2 ← 3/2	7/2 ← 5/2	21.000	40.000	128.00±.11	512.00±.44
1	5/2 ← 3/2	5/2 ← 5/2	21.000	9.000	63.94±.07	511.52±.56
1	5/2 ← 3/2	3/2 ← 1/2	21.000	8.333	161.00±.16	512.27±.51
1	5/2 ← 3/2	1/2 ← 1/2	21.000	8.333	224.99±.16	512.17±.36
1	3/2 ← 3/2	7/2 ← 5/2	10.667	40.000	82.36±.11	512.46±.68
1	3/2 ← 3/2	5/2 ← 5/2	10.667	9.000	18.30±.07	512.40±1.96
1	3/2 ← 3/2	3/2 ← 1/2	10.667	8.333	115.36±.16	512.71±.71
1	3/2 ← 3/2	1/2 ← 1/2	10.667	8.333	179.35±.16	512.43±.46
1	7/2 ← 5/2	5/2 ← 5/2	40.000	9.000	64.06±.11	512.48±.88
1	7/2 ← 5/2	3/2 ← 1/2	40.000	8.333	33.00±.18	513.34±2.80
1	7/2 ← 5/2	1/2 ← 1/2	40.000	8.333	96.99±.18	512.40±.95
1	5/2 ← 5/2	3/2 ← 1/2	9.000	8.333	97.06±.16	512.77±.85
1	5.2 ← 5.2	1.2 ← 1.2	9.000	8.333	161.05±.16	512.43±.51
1	3/2 ← 1/2	1/2 ← 1/2	8.333	8.333	63.99±.21	511.92±1.68

TABLE D.4. Observations used to calculate the parameters eQq, B_o, and ν_o of the $J = 2 \leftarrow 3$ rotational transition of $(CH_3)_3CBr^{79}$

K Transition	F_2 Transition	F_1 Transition	Intensity F_2	Intensity F_1	$\Delta\nu$ MHz	eQq MHz
0	3/2 ← 1/2	5/2 ← 3/2	10.000	16.000	0.86±.14	
0	3/2 ← 1/2	7/2 ← 5/2	10.000	24.490	31.26±.18	504.98±2.91
0	3/2 ← 1/2	9/2 ← 7/2	10.000	35.714	31.36±.18	506.59±2.91
0	5/2 ← 3/2	7/2 ← 5/2	16.000	24.490	32.12±.18	518.87±2.91
0	5/2 ← 3/2	9/2 ← 7/2	16.000	35.714	32.22±.18	520.48±2.91
0	7/2 ← 5/2	9/2 ← 7/2	24.490	35.714	0.10±.21	
1	5/2 ← 3/2	7/2 ← 5/2	16.000	24.490	0.06±.07	
1	5/2 ← 3/2	3/2 ← 1/2	16.000	10.000	30.83±.07	493.28±1.12
1	5/2 ← 3/2	9/2 ← 7/2	16.000	35.714	31.84±.07	495.29±1.09
1	7/2 ← 5/2	3/2 ← 1/2	24.490	10.000	30.89±.07	508.77±1.15
1	7/2 ← 5/2	9/2 ← 7/2	24.490	35.714	31.90±.07	510.40±1.12
1	3/2 ← 1/2	9/2 ← 7/2	10.000	35.714	1.01±.07	
2	7/2 ← 5/2	9/2 ← 7/2	24.490	35.714	128.05±.14	512.20±.56
2	7/2 ← 5/2	3/2 ← 1/2	24.490	10.000	219.58±.18	512.36±.42
2	9/2 ← 7/2	3/2 ← 1/2	35.714	10.000	91.53±.18	512.57±1.01

TABLE D.5. Observations used to calculate the parameters eQq, B_o, and ν_o of the J = 1 → 2 rotational transition of $(CH_3)_3CBr^{81}$

K Transition	F_2 Transition	F_1 Transition	Intensity F_2	Intensity F_1	$\Delta\nu$ MHz	eQq MHz
0	7/2 → 5/2	5/2 → 3/2	40.000	21.000	0.16±.07	
0	7/2 → 5/2	3/2 → 3/2	40.000	10.667	76.63±.20	429.13±1.12
0	7/2 → 5/2	3/2 → 1/2	40.000	8.333	116.70±.11	429.95±.41
0	7/2 → 5/2	5/2 → 5/2	40.000	9.000	106.90±.07	427.60±.28
0	5/2 → 3/2	3/2 → 3/2	21.000	10.667	76.79±.20	430.03±1.12
0	5/2 → 3/2	3/2 → 1/2	21.000	8.333	116.54±.11	429.36±.41
0	5/2 → 3/2	5/2 → 5/2	21.000	9.000	106.74±.07	426.96±.28
0	3/2 → 3/2	3/2 → 1/2	10.667	8.333	193.33±.22	429.62±.49
0	3/2 → 3/2	5/2 → 5/2	10.667	9.000	183.53±.20	428.24±.47
0	3/2 → 1/2	5/2 → 5/2	8.333	9.000	9.80±.11	457.32±5.13
1	5/2 → 3/2	3/2 → 3/2	21.000	10.667	38.07±.11	426.38±1.23
1	5/2 → 3/2	7/2 → 5/2	21.000	40.000	107.14±.14	428.56±.56
1	5/2 → 3/2	3/2 → 1/2	21.000	8.333	134.52±.22	428.02±.70
1	5/2 → 3/2	1/2 → 1/2	21.000	8.333	187.61±.22	427.08±.50
1	3/2 → 3/2	7/2 → 5/2	10.667	40.000	69.07±.11	429.76±.68
1	3/2 → 3/2	3/2 → 1/2	10.667	8.333	96.45±.20	428.67±.89
1	3/2 → 3/2	1/2 → 1/2	10.667	8.333	149.54±.20	427.26±.57
1	7/2 → 5/2	3/2 → 1/2	40.000	8.333	27.38±.22	425.92±3.42
1	7/2 → 5/2	1/2 → 1/2	40.000	8.333	80.47±.22	425.13±1.16
1	3/2 → 1/2	1/2 → 1/2	8.333	8.333	53.09±.28	424.72±2.24

TABLE D.6. Observations used to calculate the parameters eQq, B_o, and ν_o of the J = 2 → 3 rotational transition of $(CH_3)_3CBr^{81}$

K Transition	F_2 Transition		F_1 Transition		Intensity F_2	Intensity F_1	Δν MHz	eQq MHz
0	3/2	1/2	5/2	3/2	10.000	16.000	0.60±.14	
1	5/2	3/2	7/2	5/2	16.000	24.490	0.59±.11	
1	5/2	3/2	3/2	1/2	16.000	10.000	26.31±.11	420.96±1.76
1	5/2	3/2	9/2	7/2	16.000	35.714	27.02±.11	420.31±1.71
1	7/2	5/2	3/2	1/2	24.490	10.000	25.72±.14	423.63±2.31
1	7/2	5/2	9/2	7/2	24.490	35.714	26.43±.14	422.88±2.24
1	3/2	1/2	9/2	7/2	10.000	35.714	0.71±.14	
2	7/2	5/2	5/2	3/2	24.490	16.000	76.04±.11	425.83±.62
2	7/2	5/2	9/2	7/2	24.490	35.714	107.80±.16	431.20±.64
2	7/2	5/2	3/2	1/2	24.490	10.000	184.07±.20	429.49±.47
2	5/2	3/2	9/2	7/2	16.000	35.714	31.76±.18	444.63±2.52
2	5/2	3/2	3/2	1/2	16.000	10.000	108.03±.22	432.12±.88
2	9/2	7/2	3/2	1/2	35.714	10.000	76.27±.25	427.12±1.40

APPENDIX E

THE CALCULATED HYPERFINE SPECTRA FOR TERTIARY BUTYL CHLORIDE AND TERTIARY BUTYL BROMIDE

The tables on the following pages of this Appendix contain the calculated nuclear quadrupole hyperfine spectra of the J=1 → 2 rotational transition for $(C^{12}H_3)_3C^{12}Cl^{35}$, $(C^{12}H_3)_3C^{12}Cl^{37}$, $(C^{12}H_3)_3C^{12}Br^{79}$ and $(C^{12}H_3)_3C^{12}Br^{81}$, and the J=2 → 3 rotational transitions for $(C^{12}H_3)_3C^{12}Br^{79}$ and $(C^{12}H_3)_3C^{12}Br^{81}$. K and F have their usual meanings in microwave spectroscopy. The intensities given are relative to that particular K level only and follow from Table B.1. Using Eq. 2.17 and Table B.1 to find ν_0 plus the first-order correction and Table B.2 to find the second-order correction, the spectra were calculated. Further and complete details on the molecular theory used in this portion may be found in Chapter 2. In calculating the hyperfine spectra, the ν_Q's and B_0's used are those tabulated in Table 4.7 with the following important considerations on the eQq's:

for $(C^{12}H_3)_3C^{12}Cl^{35}$ eQq = -67.72 ± 0.63 MHz throughout;

for $(C^{12}H_3)_3C^{12}Cl^{37}$ eQq = -52.28 ± 1.25 MHz throughout;

for $(C^{12}H_3)_3C^{12}Br^{79}$ eQq = 512.33 ± 1.16 MHz throughout; and

for $(C^{12}H_3)_3C^{12}Br^{81}$ eQq = 428.22 ± 2.79 MHz throughout.

TABLE E.1. The calculated hyperfine spectrum of the J = 1 → 2 rotational transition for $(CH_3)_3CCl^{35}$

K Transition	F Transition	Relative Intensity %	1st Order Correction MHz	2nd Order Correction MHz	ν_{calc} 2nd Order MHz
0	1/2 ← 3/2	1.667	30.47 ± .28	0.003	12101.40
0	3/2 ← 3/2	10.667	13.54 ± .13	0.02	12084.49
0	7/2 ← 5/2	40.000	1.45 ± .01	0.003	12072.38
0	5/2 ← 3/2	21.000	1.45 ± .01	0	12072.38
0	1/2 ← 1/2	8.333	0	0	12070.93
0	3/2 ← 5/2	1.000	- 3.39 ± .03	0.02	12067.56
0	5/2 ← 5/2	9.000	-15.48 ± .15	0.01	12055.46
0	3/2 ← 1/2	8.333	-16.93 ± .16	0.02	12054.02
1	1/2 ← 1/2	8.333	16.93 ± .16	0.04	12087.85
1	3/2 ← 1/2	8.333	8.47 ± .08	0.03	12079.38
1	7/2 ← 5/2	40.000	4.11 ± .04	0.01	12075.00
1	3/2 ← 5/2	1.000	1.69 ± .02	0.02	12072.59
1	1/2 ← 3/2	1.667	1.69 ± .02	0.03	12072.60
1	5/2 ← 5/2	9.000	- 4.35 ± .04	0.02	12066.55
1	3/2 ← 3/2	10.667	- 6.77 ± .06	0.02	12064.13
1	5/2 ← 3/2	21.000	-12.82 ± .12	0.02	12058.08

TABLE E.2. The calculated hyperfine spectrum of the J = 1 ← 2 rotational transition for $(CH_3)_3CCl^{37}$

K Transition	F Transition	Relative Intensity %	1st Order Correction MHz	2nd Order Correction MHz	ν_{calc} 2nd Order MHz
0	1/2 ← 3/2	1.667	23.53 ± .56	0.002	11837.60
0	3/2 ← 3/2	10.667	10.46 ± .25	0.01	11824.54
0	7/2 ← 5/2	40.000	1.12 ± .03	0.002	11815.19
0	5/2 ← 3/2	21.000	1.12 ± .03	~0	11815.19
0	1/2 ← 1/2	8.333	0	0	11814.07
0	3/2 ← 5/2	1.000	- 2.61 ± .06	0.01	11811.47
0	5/2 ← 5/2	9.000	-11.95 ± .29	0.003	11802.12
0	3/2 ← 1/2	8.333	-13.07 ± .31	0.01	11801.01
1	1/2 ← 1/2	8.333	13.07 ± .31	0.02	11826.92
1	3/2 ← 1/2	8.333	6.54 ± .16	0.02	11820.39
1	7/2 ← 5/2	40.000	3.17 ± .08	0.003	11817.00
1	3/2 ← 5/2	1.000	1.31 ± .03	0.01	11815.15
1	1/2 ← 3/2	1.667	1.31 ± .03	0.02	11815.16
1	5/2 ← 5/2	9.000	- 3.36 ± .08	0.01	11810.48
1	3/2 ← 3/2	10.667	- 5.23 ± .12	0.01	11808.61
1	5/2 ← 3/2	21.000	- 9.90 ± .24	0.01	11803.94

TABLE E.3. The calculated hyperfine spectrum of the $J = 1 \rightarrow 2$ rotational transition for $(CH_3)_3CBr^{79}$

K Transition	F Transition	Relative Intensity %	1st Order Correction MHz	2nd Order Correction MHz	ν_{calc} 2nd Order MHz
0	3/2 ← 1/2	8.333	128.08 ± .29	1.34	8306.12
0	5/2 ← 5/2	9.000	117.10 ± .27	0.49	8294.29
0	3/2 ← 5/2	1.000	25.62 ± .06	2.11	8204.43
0	1/2 ← 1/2	8.333	0	0	8176.70
0	7/2 ← 5/2	40.000	- 10.98 ± .03	0.24	8165.96
0	5/2 ← 3/2	21.000	- 10.98 ± .03	0.01	8165.73
0	3/2 ← 3/2	10.667	-102.47 ± .24	1.63	8075.86
0	1/2 ← 3/2	1.667	-230.55 ± .53	0.29	7946.44
1	5/2 ← 3/2	21.000	96.98 ± .22	1.71	8275.76
1	3/2 ← 3/2	10.667	51.23 ± .12	2.06	8230.36
1	5/2 ← 5/2	9.000	32.94 ± .08	1.53	8211.54
1	1/2 ← 3/2	1.667	- 12.81 ± .03	2.90	8167.16
1	3/2 ← 5/2	1.000	- 12.81 ± .03	1.88	8166.14
1	7/2 ← 5/2	40.000	- 31.11 ± .07	0.49	8146.45
1	3/2 ← 1/2	8.333	- 64.04 ± .15	2.17	8115.20
1	1/2 ← 1/2	8.333	-128.08 ± .29	3.01	8052.00

TABLE E.4. The calculated hyperfine spectrum of the J = 2 ← 3 rotational transition for $(CH_3)_3CBr^{79}$

K Transition	F Transition	Relative Intensity %	1st Order Correction MHz	2nd Order Correction MHz	ν_{calc} 2nd Order MHz
0	7/2 ← 7/2	4.082	121.98 ± .28	0.28	12387.61
0	5/2 ← 7/2	0.204	62.21 ± .14	1.29	12328.85
0	3/2 ← 1/2	10.000	25.62 ± .06	0.29	12291.26
0	5/2 ← 3/2	16.000	25.62 ± .06	-0.57	12290.40
0	7/2 ← 5/2	24.490	- 6.10 ± .01	0.03	12259.28
0	9/2 ← 7/2	35.714	- 6.10 ± .01	0.13	12259.38
0	5/2 ← 5/2	5.224	- 65.87 ± .15	1.05	12200.53
0	3/2 ← 3/2	4.000	-102.47 ± .23	-1.05	12161.84
0	3/2 ← 5/2	0.286	-193.95 ± .45	0.57	12071.97
1	7/2 ← 7/2	4.082	82.34 ± .19	0.75	12348.46
1	5/2 ← 7/2	0.204	37.51 ± .09	1.17	12304.05
1	5/2 ← 3/2	16.000	19.21 ± .04	-0.23	12284.35
1	7/2 ← 5/2	24.490	18.30 ± .04	-0.29	12283.38
1	3/2 ← 1/2	10.000	- 12.81 ± .03	-0.78	12251.78
1	9/2 ← 7/2	35.714	- 13.72 ± .03	0.23	12251.88
1	5/2 ← 5/2	5.224	- 26.53 ± .06	0.13	12238.97
1	3/2 ← 3/2	4.000	- 76.85 ± .18	0.06	12188.58
1	3/2 ← 5/2	0.286	-122.59 ± .28	0.41	12143.19
2	3/2 ← 5/2	0.286	91.49 ± .21	1.83	12358.79
2	5/2 ← 5/2	5.224	91.49 ± .21	0.16	12357.12
2	7/2 ← 5/2	24.490	91.49 ± .21	0.94	12357.90
2	3/2 ← 3/2	4.000	0	2.67	12268.14
2	5/2 ← 3/2	16.000	0	1.00	12266.47
2	5/2 ← 7/2	0.204	- 36.60 ± .08	0.60	12229.47
2	7/2 ← 7/2	4.082	- 36.60 ± .08	-1.38	12230.25
2	9/2 ← 7/2	35.714	- 36.60 ± .08	0.24	12229.11
2	3/2 ← 1/2	10.000	-128.08 ± .29	1.33	12138.72

TABLE E.5. The calculated hyperfine spectrum of the J = 1 → 2 rotational transition for $(CH_3)_3CBr^{81}$

K Transition	F Transition	Relative Intensity %	1st Order Correction MHz	2nd Order Correction MHz	ν_{calc} 2nd Order MHz
0	3/2 ← 1/2	8.333	107.06 ± .70	0.94	8221.54
0	5/2 ← 5/2	9.000	97.88 ± .64	0.34	8211.76
0	3/2 ← 5/2	1.000	21.41 ± .14	1.48	8136.43
0	1/2 ← 1/2	8.333	0	0	8113.54
0	7/2 ← 5/2	40.000	- 9.18 ± .06	0.17	8104.53
0	5/2 ← 3/2	21.000	- 9.18 ± .06	0.01	8104.37
0	3/2 ← 3/2	10.667	- 85.64 ± .56	1.15	8029.05
0	1/2 ← 3/2	1.667	-192.70 ± 1.25	0.20	7921.04
1	5/2 ← 3/2	21.000	81.06 ± .53	1.21	8196.01
1	3/2 ← 3/2	10.667	42.82 ± .28	1.45	8158.01
1	5/2 ← 5/2	9.000	27.53 ± .18	1.08	8142.35
1	1/2 ← 3/2	1.667	- 10.71 ± .08	2.04	8105.07
1	3/2 ← 5/2	1.000	- 10.71 ± .08	1.33	8104.36
1	7/2 ← 5/2	40.000	- 26.00 ± .17	0.35	8088.09
1	3/2 ← 1/2	8.333	- 53.53 ± .35	1.63	8061.74
1	1/2 ← 1/2	8.333	-107.06 ± .70	2.12	8008.80

TABLE E.6. The calculated hyperfine spectrum of the J = 2 → 3 rotational transition for $(CH_3)_3CBr^{81}$

K Transition	F Transition	Relative Intensity %	1st Order Correction MHz	2nd Order Correction MHz	ν_{calc} 2nd Order MHz
0	7/2 ← 7/2	4.082	101.96 ± .66	0.20	12272.20
0	5/2 ← 7/2	0.204	52.00 ± .34	0.92	12222.96
0	3/2 ← 1/2	10.000	21.41 ± .14	0.20	12191.65
0	5/2 ← 3/2	16.000	21.41 ± .14	-0.40	12191.05
0	7/2 ← 5/2	24.490	- 5.10 ± .03	0.02	12164.96
0	9/2 ← 7/2	35.714	- 5.10 ± .03	0.09	12165.04
0	5/2 ← 5/2	5.224	- 55.06 ± .36	0.74	12115.72
0	3/2 ← 3/2	4.000	- 85.64 ± .56	-0.74	12083.66
0	3/2 ← 5/2	0.286	-162.11 ± 1.05	0.40	12008.33
1	7/2 ← 7/2	4.082	68.82 ± .45	0.53	12239.32
1	5/2 ← 7/2	0.204	31.35 ± .20	0.82	12204.14
1	5/2 ← 3/2	16.000	16.06 ± .10	-0.16	12185.87
1	7/2 ← 5/2	24.490	15.29 ± .10	-0.22	12185.04
1	3/2 ← 1/2	10.000	- 10.71 ± .07	-0.55	12158.71
1	9/2 ← 7/2	35.714	- 11.47 ± .07	0.16	12158.61
1	5/2 ← 5/2	5.224	- 22.18 ± .14	0.09	12147.88
1	3/2 ← 3/2	4.000	- 64.23 ± .42	0.04	12105.78
1	3/2 ← 5/2	0.286	-102.47 ± .67	0.29	12067.79
2	3/2 ← 5/2	0.286	76.47 ± .50	1.30	12247.45
2	5/2 ← 5/2	5.224	76.47 ± .50	0.12	12246.27
2	7/2 ← 5/2	24.490	76.47 ± .50	0.67	12246.82
2	3/2 ← 3/2	4.000	0	1.89	12171.57
2	5/2 ← 3/2	16.000	0	0.71	12170.39
2	5/2 ← 7/2	0.204	- 30.59 ± .20	0.42	12139.51
2	7/2 ← 7/2	4.082	- 30.59 ± .20	0.98	12140.07
2	9/2 ← 7/2	35.714	- 30.58 ± .20	0.17	12139.26
2	3/2 ← 1/2	10.000	-107.06 ± .70	0.94	12063.56